INFORMATION TO USERS

This manuscript has been reproduced from the microfilm master. UMI films the text directly from the original or copy submitted. Thus, some thesis and dissertation copies are in typewriter face, while others may be from any type of computer printer.

The quality of this reproduction is dependent upon the quality of the copy submitted. Broken or indistinct print, colored or poor quality illustrations and photographs, print bleedthrough, substandard margins, and improper alignment can adversely affect reproduction.

In the unlikely event that the author did not send UMI a complete manuscript and there are missing pages, these will be noted. Also, if unauthorized copyright material had to be removed, a note will indicate the deletion.

Oversize materials (e.g., maps, drawings, charts) are reproduced by sectioning the original, beginning at the upper left-hand corner and continuing from left to right in equal sections with small overlaps. Each original is also photographed in one exposure and is included in reduced form at the back of the book.

Photographs included in the original manuscript have been reproduced xerographically in this copy. Higher quality 6" x 9" black and white photographic prints are available for any photographs or illustrations appearing in this copy for an additional charge. Contact UMI directly to order.

UMI

A Bell & Howell Information Company
300 North Zeeb Road, Ann Arbor MI 48106-1346 USA
313/761-4700 800/521-0600

SENSITIVITY ENHANCEMENT FOR CAPILLARY ZONE ELECTROPHORESIS-MASS SPECTROMETRY: DEVELOPMENTS AND APPLICATIONS

by

Kevin P. Bateman

Submitted in partial fulfillment of the requirements
for the degree of Doctor of Philosophy

at
Dalhousie University
Halifax, Nova Scotia
June, 1997

DALHOUSIE UNIVERSITY

FACULTY OF GRADUATE STUDIES

The undersigned hereby certify that they have read and recommend to the Faculty of Graduate Studies for acceptance a thesis entitled "Sensitivity Enhancement for Capillary Zone Electrophoresis-Mass Spectrometry: Developments and Applications"

by Kevin Bateman

in partial fulfillment of the requirements for the degree of Doctor of Philosophy.

Dated: August 1, 1997

External Examiner

Research Supervisor

Research Supervisor

Examining Committee

DALHOUSIE UNIVERSITY

DATE: August 1/97

AUTHOR: Kevin Bateman

TITLE: Sensitivity Enhancement for Capillary Zone Electrophoresis-Mass Spectrometry: Developments and Applications

DEPARTMENT OR SCHOOL: Chemistry

DEGREE: Ph.D. CONVOCATION: October YEAR: 1997

Permission is herewith granted to Dalhousie University to circulate and to have copied for non-commercial purposes, at its discretion, the above title upon the request of individuals or institutions.

[redacted]

Signature of Author

For Diane and Alison

and

My parents

TABLE OF CONTENTS

LIST OF FIGURES

LIST OF TABLES

LIST OF ABBREVIATIONS

APS	aminopropylsilane
BCQ	[(acryloylamino)propyl]trimethylammonium chloride
CZE	capillary zone electrophoresis
DNA	deoxyribonucleic acid
eof	electroosmotic flow
ESI	electrospray ionization
ESMS	electrospray mass spectrometry
HPLC	high performance liquid chromatography
LPA	linear polyacrylamide
MAPTAC	[(methacryloylamino)propyl]trimethylammonium chloride
MRM	multiple reaction monitoring
MS-MS	tandem mass spectrometry
nES	nanoelectrospray
nESMS	nanoelectrospray mass spectrometry
PC	preconcentration
pI	isoelectric point
QMF	quadrupole mass filter
RIE	reconstructed ion electropherogram
RSD	relative standard deviations
SIR	selected ion recording
TEMED	*N,N,N',N'*-tetramethylethylenediamine
TIE	total ion electropherogram
tris	[Tris(hydroxymethyl)aminomethane]
XIE	extracted ion electropherogram

ABSTRACT

Advances in mass spectrometry (MS), i.e., electrospray ionization and tandem mass spectrometry using triple quadrupole instruments, have greatly enhanced the analysis of biopolymers, such as proteins and glycoproteins. Electrospray ionization enables the direct coupling of liquid-based separations with mass spectrometric detection. Capillary zone electrophoresis (CZE) allows for high resolution separation of biomolecules, and its inherent low flow rate is ideally suited for coupling to electrospray mass spectrometry (ESMS). A major shortcoming of CZE is its high concentration detection limits relative to liquid chromatography. This thesis presents two approaches for the improvement of the sensitivity of CZE. These improved methods are applied to the characterization of proteins and glycoproteins by CZE-ESMS.

A nanoelectrospray mass spectrometry (nESMS) interface for CZE was constructed from metallized fused silica tips that were connected to the separation capillary. Several methods for connecting the tips to the separation capillary were evaluated. The tip geometry and capillary coating were optimized to produce a rugged and reliable interface. The optimized CZE-nESMS interface gave detection limits for peptides at least one order of magnitude lower than a conventional co-axial CZE-ESMS interface.

On-line chromatographic preconcentration was also used to enhance the sensitivity of CZE-ESMS. Several stationary phases were evaluated with respect to sample retention and elution for use in the preconcentrator. A sample loading and elution protocol for the reliable and reproducible use of the preconcentrator was developed. Detection limits were improved by a factor of 1000 (relative to a conventional coaxial interface without preconcentration) when the preconcentrator was coupled with the nanoelectrospray interface (PC-CZE-nESMS).

Several N-linked and O-linked glycoproteins were analyzed by CZE-nESMS. The high resolution separation provided by CZE gave glycoform population information, not typically generated by the more conventional HPLC analysis of glycoproteins. CZE with on-line tandem mass spectrometry was used to study the size and composition of the oligosaccharides attached to the proteins. New scanning methods were developed to investigate the peptide sequence of the glycopeptides. First generation fragment ions produced in the orifice/skimmer region of the ion source were analyzed by tandem mass spectrometry in the collision cell to provide peptide sequence ions. The sequence allowed the assignment of oligosaccharide linkage for the N-linked glycopeptides.

The PC-CZE-nESMS method was capable of analyzing a protein tryptic digest at the femtomole/μL, equivalent to approximately 5 picoomoles of protein injected. The data generated permitted the exclusive identification of the protein from the search of a database of 32000 proteins.

ACKNOWLEDGMENTS

I want to thank my supervisors, Pierre Thibault and Robert White, for setting high standards and always expecting my best effort. It is a philosophy that I will maintain for the rest of my life. Dr. Bob Boyd deserves to be mentioned with my supervisors. He is responsible for my introduction to the NRC lab and has offered guidance throughout my time as a Ph.D. student and I am grateful to him for that.

The people at the Institute for Marine Biosciences have been very good to me, both on a personal and academic level. Here goes: Steve "CZE God" Locke, Gunther "I Can Make Anything" Morstatt, Archie "The Godfather" McCulloch, Ed "Fixit" Dyer, Pearl "Information" Blay, Denise "I Need a Man" LeBlanc, Dietrich "Papers" Volmer, Kenny "I Love Preston" MacLeod, Anna "Don't Take My Books" Backman, Bill "Don't Beat Me" Hardstaff, Dave "Mr. Hockey" O'Neil. John "Young Irish" Kelly also should be mentioned in this list, a friend and former lab mate.

I must also thank my wife, Diane, for putting up with long nights spent alone, initially, and then with our daughter, Alison (I must have been home some nights!). Finally, my parents deserve thanks for believing in me, and being patient as I wandered through life to were I am now.

Chapter 1

1.0 Introduction

Instrumentation and methodologies for the analysis of biopolymers are constantly evolving, with each new development providing enhanced sensitivity and/or information content. One such development, electrospray mass spectrometry (ESMS), has led to a revolution in biochemical analysis. Electrospray ionization provides a method for coupling high performance liquid chromatography or capillary zone electrophoresis directly to a mass spectrometer and allows for the on-line detection of separated components in complex biological matrices.

Capillary zone electrophoresis (CZE), with its inherent low flow rate, is ideally suited for coupling to electrospray mass spectrometry. However, the small injection volumes (10-50 nL) required to maintain the separation efficiency of CZE provide poor concentration detection limits. Much of the work presented in this thesis deals with methods for improving the sensitivity of CZE, especially with mass spectrometric detection. A novel low-flow electrospray interface for coupling CZE with mass

spectrometry was developed, providing more than an order of magnitude enhancement of sensitivity relative to a conventional co-axial interface. An online chromatographic preconcentration method was also developed for qualitative analysis using CZE-ESMS. The combination of these two methods enabled the analysis of protein digests at the femtomol/μL level.

These new techniques were applied to the study of various glycoproteins, peptides and protein digests. Glycoproteins exhibit extraordinary complexity, and this feature is undoubtedly a required attribute for their unique biological specificity. Their structural complexity is derived not only from the various linkages between sugar monomers, but also from the composition and branching of the carbohydrate attached to the polypeptide backbone. The analysis of proteolytic digests of glycoproteins using low flow CZE-ESMS and tandem mass spectrometry (MS-MS) provided structural information about the glycoform as well as the amino acid sequence of the glycopeptide from sub-picomole quantities of original protein.

1.1 Capillary Zone Electrophoresis

CZE has evolved from a multitude of developments over the past 100 years in various separation sciences, most notably electrophoresis and chromatography. The development and application of CZE as a modern, high resolution separation technique is historically attributed to the work of Jorgenson and Lukacs, in which the theory was clarified and the potential of CZE as an analytical technique was demonstrated [1]. Since then CZE has been used in many diverse fields such as the pulp and paper industry [2], forensic science [3], toxicology [4] and the food industry [5] and applied to a wide range of compounds, including proteins and peptides [6], DNA [7], carbohydrates [8], amino acids [9], marine toxins [10], and inorganic ions [11]. A schematic of the typical instrumental requirements of CZE is shown in Figure 1.1.

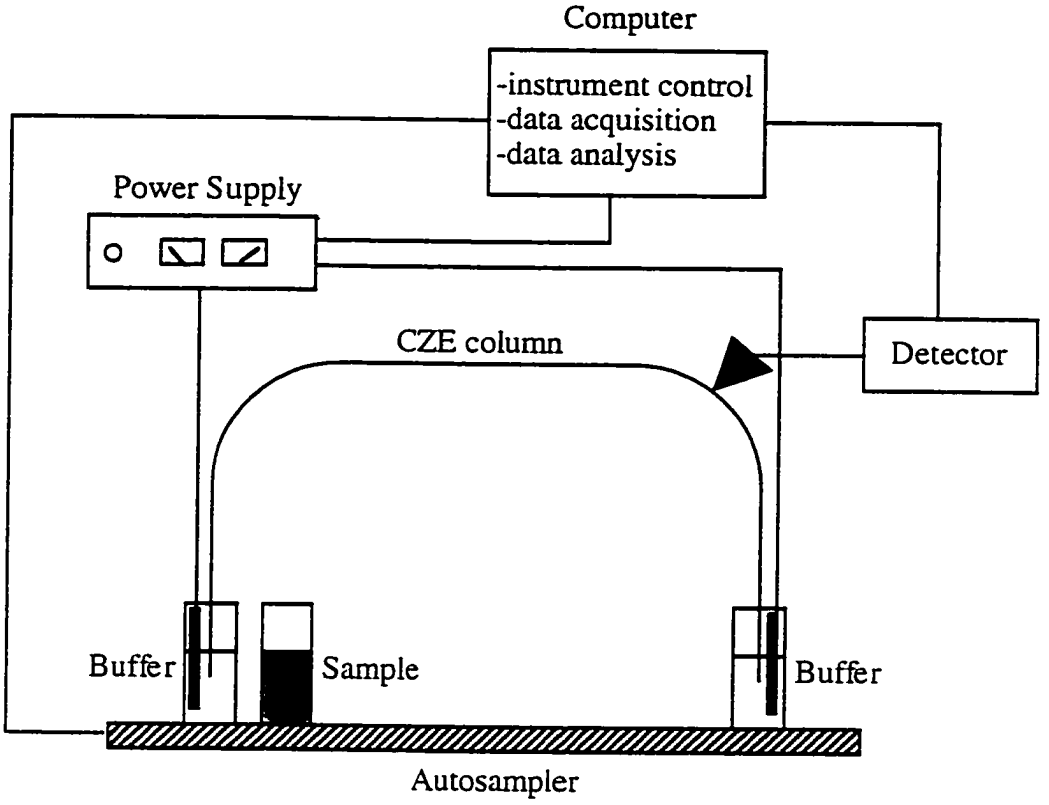

Figure 1.1 Schematic of a typical CZE instrument.

1.1.1 Electrophoretic Mobility

The basic theoretical concept of electrophoresis is relatively simple. It involves the migration of charged particles in an electrolyte solution under the influence of an electric field. The electric field (typically ±300 volts/cm) is a function of the applied voltage and capillary length. Ionic and ionizable solutes are separated due to differences in charge, size and shape. When a charged particle is placed in an electric field (E) it experiences a force which is proportional to its effective charge (q) and the electric field strength. The translational movement of the particle is opposed by a viscous drag force which is proportional to the particle velocity (v), hydrodynamic radius (r) and medium viscosity (η). When the two forces are counterbalanced the particle moves with a steady state velocity:

$$v = \mu_e E \qquad (1)$$

where μ_e, the electrophoretic mobility is given by:

$$\mu_e = \frac{q}{6\pi\eta r} \qquad (2)$$

The mobility is a constant that is a characteristic of a given ion in a particular medium. From Eq. 2 it is evident that small, highly charged species have high mobilities whereas large, minimally charged species have low mobilities.

1.1.2 Electroosmotic Flow (eof)

When the bare fused silica capillary is filled with an electrolyte, an electric double layer is always formed on the inner wall surface due to ionizable groups on the capillary wall material and/or ions adsorbed onto the capillary wall. For example, in fused silica capillaries, the ionized silanol groups present at the surface form the fixed negative region of the electric double layer, and the positive layer is formed by ions present in the solution. A fraction of the ions forming the electrolyte region of the electric double layer is always fixed by electrostatic forces near the capillary wall and forms the so-called Stern layer, the rest of the ions form the mobile diffuse double layer (Figure 1.2). The potential drop between the Stern layer and the bulk solution is called the zeta potential, ζ (in volts).

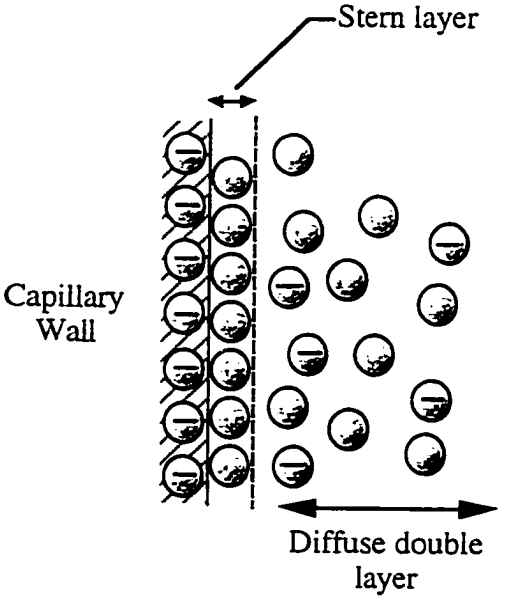

Figure 1.2 Representation of the double layer at the capillary wall.

Upon the application of an electric field across the column, the ions in the diffuse layer move towards the appropriate electrode, transporting with them solvent molecules referred to as their solvation sphere. Due to frictional forces among the solvent molecules, this movement is immediately spread over the whole liquid, and the resulting profile is almost flat. The linear velocity (v_{eof}) of this flow is given by the Helmholtz-Smoluchowski equation;

$$v_{eof} = \frac{\varepsilon\zeta}{\eta}E \qquad (3)$$

where ε is the dielectric constant of the electrolyte used. From Eq. 3 the independence of the electroosmotic velocity on the column diameter can be deduced. The term $\varepsilon\zeta/\eta$ in Eq. 3 is frequently denoted μ_{eof} and named electroosmotic mobility which is convenient for the comparison of electroosmosis and electromigration.

The zeta potential is essentially determined by the surface charge on the capillary wall. Since this charge is strongly dependent on the pH of the electrolyte, the magnitude of the electroosmotic flow (eof) is also pH-dependent. The zeta potential also depends on the ionic strength of the electrolyte, as described by double layer theory. Increased ionic strength results in double layer compression and decreased zeta potential, thereby reducing the eof. The eof is typically measured by injection of a neutral marker that has no electrophoretic mobility and whose velocity is derived from the electroosmotic flow.

1.1.3 Migration Time and Efficiency

The total mobility of a sample molecule is a result of the vectorial addition of the electrophoretic mobility and the electroosmotic mobility:

$$\mu_{tot} = \mu_e + \mu_{eof} \qquad (4)$$

and the analyte velocity, v, is dependent on μ_{tot}, the total capillary length, L_t, and the applied voltage, V, as described in (5).

$$v = \mu_{tot} E = \frac{\mu_{tot} V}{L_t} \qquad (5)$$

The time required for a solute to migrate to the point of detection is called the migration time, which corresponds to the quotient of migration distance (L_d) and velocity. The product, $L_d L_t$, can be approximated by L^2 when the detection takes place close to the end of the capillary which is the usual case.

$$t = \frac{L_d}{v} = \frac{L^2}{\mu_{tot} V} \qquad (6)$$

These equations indicate that the shortest analysis time is generated by high voltages and short capillaries.

Jorgenson and Lukacs derived the efficiency of the electrophoretic system from basic principles using the assumption that diffusion is the only source of band broadening [1]. Diffusion in liquids that leads to broadening of an initially sharp band is described by the Einstein equation, where D is the diffusion coefficient of the individual solute.

$$\sigma_L^2 = 2Dt = \frac{2DL^2}{\mu_{tot} V} \qquad (7)$$

The number of theoretical plates, N, is given by:

$$N = \frac{L^2}{\sigma_L^2} \qquad (8)$$

Substituting Eq. 7 into Eq. 8 gives an expression for the number of theoretical plates,

$$N = \frac{\mu_{tot} V}{2D} \qquad (9)$$

Some important generalizations can be made from this expression. The use of high voltage gives the greatest number of theoretical plates since the separation proceeds rapidly, minimizing the effect of diffusion. Highly mobile solutes produce high plate counts because their rapid velocity minimizes the time for diffusion. Solutes with low diffusion coefficients give high efficiency because of slow diffusional bandbroadening.

In practice, Eq. 9 is rarely used and N tends to be underestimated using the more convenient expression:

$$N = 5.54 \times \left(\frac{t_m}{w_{1/2}} \right)^2 \qquad (10)$$

This assumes the peaks to be Gaussian, where 5.54 = 8 ln 2, $w_{1/2}$ is the width at half-height, and t_m is the migration time. It is important to point out that it is misleading to discuss theoretical plates in electrophoresis. The concept is a carryover from chromatographic theory, where a true partition equilibrium between two phases is the physical basis of separation. In electrophoresis, separation of the components of a mixture is determined by their relative mobilities in the applied electric field, which is a function of their charge, mass, and shape. The theoretical plate is merely a convenient concept to describe the analyte peak shape, and to assess the factors that affect separation.

1.1.4 Resolution

Resolution of sample components is the ultimate goal in separation science. Resolution is most simply defined as:

$$R = 2\frac{(t_2 - t_1)}{w_1 + w_2} = \frac{t_2 - t_1}{4\sigma} \qquad (11)$$

where t is migration time, w is baseline peak width (in time), and σ is the temporal standard deviation. The numerator in Eq. 11 describes the separation process in terms of differential migration and the denominator represents the dispersive processes acting against it.

Separation performance in CZE is primarily driven by efficiency. Due to very sharp solute zones, small differences in analyte mobilities are often sufficient to achieve complete band resolution. The resolution of two components can also be expressed with respect to efficiency:

$$R = \frac{1}{4}\sqrt{N}\left(\frac{\Delta\mu}{\bar{\mu}}\right) \qquad (12)$$

where $\Delta\mu = \mu_2 - \mu_1$, and $\bar{\mu} = (\mu_2 - \mu_1)/2$. Substituting Eq. 9 into Eq. 12 yields a theoretical equation for resolution that does not require explicit calculation of efficiency. It also describes the effect of eof on resolution.

$$R = \left(\frac{1}{4\sqrt{2}}\right)(\Delta\mu)\sqrt{\frac{V}{D(\bar{\mu} + \mu_{eof})}} \qquad (13)$$

In contrast to efficiency, which increases linearly with applied voltage, a similar gain in resolution is not found, due to the square root relationship. The voltage must be quadrupled to double the resolution. The generation of Joule heat often limits the benefits gained from this action. It is evident from Eq. 13 that infinite resolution will be obtained when $\bar{\mu}$ and μ_{eof} are equal but of opposite sign. That is, when the ion has an electrophoretic mobility equal to the μ_{eof} but of opposite direction. In this case the analysis time approaches infinity, and the operational parameters must be controlled to balance resolution and analysis time.

1.1.5 Capillary Coatings

Interaction between the analyte and the capillary wall is detrimental to CZE, leading to peak tailing and even total adsorption of the solute. The primary causes of adsorption to the fused silica walls are ionic and hydrophobic interactions between cationic analytes and the negatively charged wall. This is especially true for peptides and proteins because these species possess numerous charged and hydrophobic moieties. Two different approaches

have been used to eliminate these interactions: (1) dynamic modification of the surface with a neutral or cationic polymer solution [12], and (2) chemical modification using a covalent attachment of a reagent to the fused silica surface [13].

Dynamic modification of the acidic-silica surfaces with the cationic polymer polybrene (hexadimethrine bromide) has been used extensively in this laboratory [14]. The polymer acts as a charge reversal agent, binding to the surface, imparting a positively charged coating on the capillary surface. The positively charged surface eliminates interaction of peptides and proteins with the surface at low pH's. However, this results in a reversal of the eof direction and the applied voltage polarity has to be adjusted accordingly.

Covalent modification of the fused silica surface with linear polyacrylamide (LPA) is a common approach used to eliminate adsorption of analyte on the capillary surface. The coating is stable over the pH range 2-10 with elimination of the eof and reduction of solute-wall interactions [15]. Similar methods have been used to covalently modify the capillary with positively charged coatings such as [(acryloylamino)propyl]trimethylammonium chloride to reverse the electroosmotic flow and prevent solute-wall interactions [16,17]. An advantage of eliminating the electroosmotic flow using polyacrylamide is the possibility of performing alternative modes of electrophoretic separations such as isotachophoresis.

1.1.6 Sensitivity Enhancement

Injection volumes in the low nanolitre range combined with a short optical path length (10-100 μm) in the detector present a major drawback in CZE as concentration detection limits are relatively high when compared with the more established method of HPLC. Increased sample loading leads to peak dispersion and loss of efficiency and resolution. Addressing this limitation has been an active pursuit of many research groups, and various approaches to enhancing the sensitivity of CZE have been developed. These

methods can be separated into two types of improvements: (1) detection and (2) sample loading.

Improvements in detection methodology include the use of increased pathlength, laser-induced fluorescence, thermo-optical absorbance, and mass spectrometry. Increased sensitivity provided by the longer optical pathlengths of rectangular capillaries has been reported [18]. However, most rectangular capillaries are made of glass, have poor optical properties and are extremely fragile. More successful uses of increased pathlength are the commercially available bubble cell (Hewlett Packard, Palo Alto, CA) and Z-cell (Perkin Elmer, ABI, Foster City, CA and LC Packings, Zurich, Switzerland) detection windows [19]. An alternative approach to increased pathlength for enhanced sensitivity was described by Xi and Yeung [20], who obtained a seven-fold improvement in sensitivity by illumination and detection along the capillary axis.

Laser-induced fluorescence produces remarkable improvements in detection limits compared with the use of conventional light sources. Both on-column and post-column fluorescence-based detectors have been described [21-25], with detection limits approaching a single molecule in favourable cases [26,27]. However, the use of fluorescence relies on the presence of a suitable fluorophore, which introduces an additional derivatization step. This may be unneccessary when an alternative method of detection is used.

Thermo-optical detection takes advantage of small refractive index changes induced by the temperature change of the analyte peak associated with absorbance of a modulated pump laser beam [28]. Separation and detection of phenylthiohydantoin amino acid derivatives has been described, and the thermo-optical detector produced detection limits two orders of magnitude better than those achieved using a conventional UV detector [29]. A major limitation of the thermo-optical technique is the requirement for ultrapure solvents and reagents to minimize background absorbance.

The mass spectrometer is potentially the most powerful of all CZE detectors, providing sensitivity, mass accuracy and structural information. Mass spectrometry is well suited to coupling with CZE, especially when using electrospray ionization. Smith *et al.* [30] were the first to describe a CZE-ESMS interface, and since then the technique has been widely used [31]. Mass spectrometry is one of the most complex and expensive detectors for CZE; however costs are decreasing and so-called "walk-up" systems that do not require a skilled operator (PE-SCIEX LC series for example) are now available. Improvements in interface design have further enhanced the sensitivity of CZE-ESMS, giving concentration detection limits approaching those of LC-MS [32-35].

Online sample concentration techniques have improved the sensitivity of CZE by increasing the amount of sample injected without compromising the separation efficiency. Sample stacking, isotachophoresis and chromatographic concentration methods have provided concentration detection limits similar to those achieved by HPLC.

Sample stacking provides increased sample loading by utilizing ionic strength differences between the sample and separation electrolyte solutions. The low ionic strength sample solution acts as a voltage divider, with most of the potential applied across the low conductivity solution. As a result, the ions in the sample solution are concentrated in the capillary until the ionic strength of the sample equals that of the separation buffer. Chien and Burgi have described conditions where the entire capillary is filled with sample and reversed polarity is used to effect sample stacking [36-38]. In this case, the eof removes the sample solvent while the analyte is focussed inside the capillary. The polarity is then switched before the analyte exits the capillary and the separation is allowed to proceed. Sensitivity enhancements of several hundred-fold over conventional zone electrophoresis have been achieved using this method.

Improvements in sample loading can also be achieved by using a discontinous buffer system to perform isotachophoretic stacking prior to zone electrophoresis, and this

technique was recently reviewed [39]. In this method, the capillary is first filled with a high mobility background electrolyte solution, followed by a lower mobility sample solution, and finally a terminating electrolyte solution with mobility lower than that of the sample solution. As a result of the discontinuous buffer system, the field strength varies along the capillary. As the components separate, the field strength within indivdual zones changes until a steady state has been reached and all zones migrate with the same velocity. At this point the terminating solution is replaced with the background electrolyte and zone electrophoresis of the analyte bands occurs. Like the sample stacking method described above, the injection volume is limited by the dimensions of the capillary.

The analysis of relatively large volumes of dilute solutions has been carried out using CZE with chromatographic preconcentration. A review of different chromatographic preconcentrators has been presented recently [40]. In this approach a small bed of reversed-phase material is packed in a column and coupled directly to the separation capillary. Despite the large increase in sample loading possible with this technique, it has not gained wide acceptance due to the degradation of CZE performance and the complexity of the instrumentation. Significant losses in separation efficiency, band broadening and column overloading often compromise the separation [40,41]. Different attempts, including the reduction of stationary phase volume and the use of discontinuous buffer systems have been proposed to alleviate these difficulties [41]. A detailed study of the mechanism of on-line solid phase extraction capillary electrophoresis with UV detection was recently published [42]. The technique also has been coupled with MS detection using both co-axial [43] and sheathless interfaces [44].

1.2 Quadrupole Mass Spectrometry

Mass spectrometers are excellent detectors for chromatography, providing both high sensitivity and structural information. Of the different types of mass analyzers, quadrupole mass filters have gained significant popularity over the past fifteen years. The

simplicity, compactness, economy, absence of magnetic fields, and electronic control of ion transmission and resolution are among the major advantages of the quadrupole mass filter (QMF). The electrode structure of the quadrupole is shown in Figure 1.3, where Φ_o is the applied electrode potential, r_o is the inscribed radius between the equally spaced electrodes, and the field-free z-axis is the direction of ion entry into the QMF.

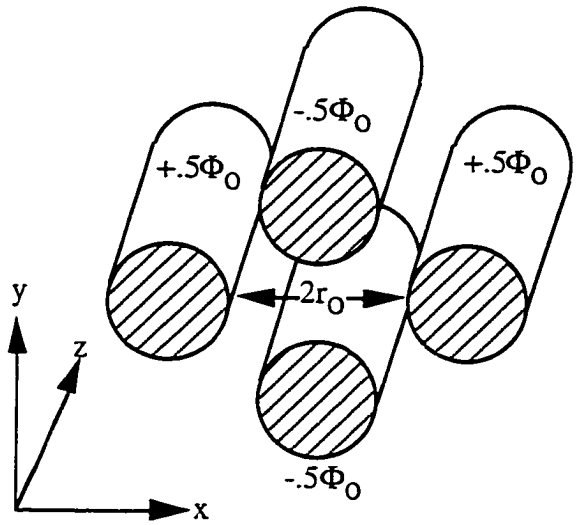

Figure 1.3 The electrode structure of the quadrupole mass filter.

For a single quadrupole lens, where Φ_o is constant, focusing takes place in one plane while defocusing occurs in the perpendicular plane. However, an interesting situation arises when the dc voltage (U) is combined with an ac voltage so that

$$\Phi_o = U + V\cos\omega t \qquad (14)$$

where V is the peak radio-frequency (rf) voltage, ω is the angular frequency $2\pi f$ (f is the rf frequency in Hertz), and t is time. The equations of motion for a ion within such a field are:

$$\left(\frac{d^2x}{dt^2}\right)+\left(\frac{e}{Mr_o^2}\right)(U - V\cos\omega t)x = 0 \qquad (15)$$

$$\left(\frac{d^2y}{dt^2}\right)+\left(\frac{e}{Mr_o^2}\right)(U-V\cos\omega t)y=0 \qquad (16)$$

Now, with the definitions

$$\frac{4eU}{M\omega^2r_o^2}=a_x=-a_y=a \qquad (17)$$

$$\frac{2eV}{M\omega^2r_o^2}=q_x=-q_y=q \qquad (18)$$

and

$$\xi=\frac{1}{2}\omega t \qquad (19)$$

these equations take the same form:

$$\frac{d^2u}{d\xi^2}+(a-2q\cos 2\xi)u=0 \qquad (20)$$

where u represents either x or y. The derivation and resulting equation is known as the Mathieu equation and describes the ion trajectories [45]. The essential feature of equation (20) is that the solution for u may be either (1) oscillatory with finite amplitudes in x and y, directing ions through the rods to the detector, or (2) exponential with amplitudes that increase rapidly with time, causing ions to impinge on the rods. These solutions are normally represented on a stability diagram (Figure 1.4). The points at which the operating line intersects the stability region determines the bandpass of the mass spectrometer.

The mass spectrum may be scanned by varying the rf and dc voltages (V and U, respectively) in such a way that ratio U/V is constant. In this case the frequency of the rf voltage is also kept constant. The resolution may be varied by an adjustment of the U/V ratio; as it is increased, the operating line in Figure 1.4 approaches the tip of the stable region. This line cuts the stability boundary at two points, corresponding to two m/z

values. All ions with m/z values between these will be transmitted by the filter and detected. The closer the line comes to the apex of the stability boundary, the greater the resolution. However, as the resolution is increased a corresponding loss in sensitivity is obtained.

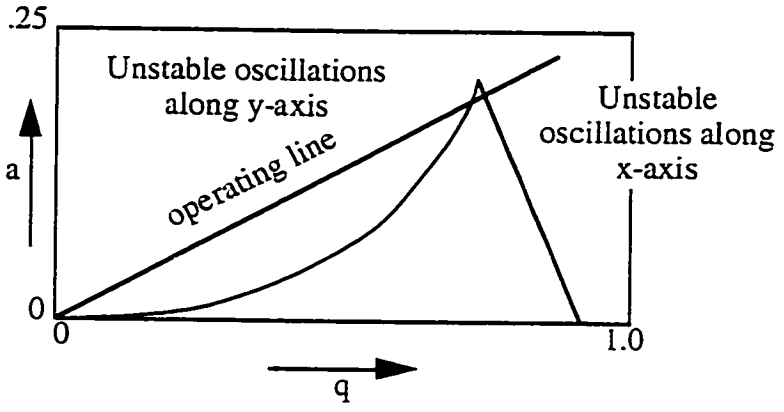

Figure 1.4 Stability diagram for the quadrupole mass filter.

1.3 Electrospray Ionization

Mass spectrometry is based on producing, differentiating, and detecting ions in the gas phase. The search for ionization sources that transfer large, thermally labile molecules (peptides and proteins, for example) into the gas phase without degradation has occupied mass spectrometrists for many years. Development of the electrospray (ESI) and closely related ionspray ionization sources [46-48] has made possible the transfer of biological molecules from solution to the gas phase as intact ions. The ability of these ionization sources to generate ions directly from liquids has allowed for direct coupling of chromatographic separations with mass spectrometric detection.

A key feature of the electrospray process is the formation of multiply (as opposed to singly) charged molecular species, if the analyte contains more than one possible site of cation attachment. In the case of peptides, the maximum number of charges observed correlates well with the number of side chain moieties that can readily accept a proton at the

low pH of the analyte stream (i.e. Arg, Lys, His, plus the free α-amino terminus). Proteins usually exhibit a coherent series of multiply charged molecular ions. The molecular mass of the protein may be calculated by deriving the charge states of any two adjacent molecular ions in the series. The mass of any multiply charged molecular ion is determined by multiplying the m/z ratio at which the ion is observed by the derived charge; this process may be done automatically using a computer algorithm.

The maximum number of charges observed for proteins does not correlate with the number of basic side chains as well as it does for peptides. This is presumably because the native folded state of the protein may make certain potential protonation sites inaccessible to solvent. Nevertheless, a rough correlation of 0.5-1.0 charge/kDa is observed for most proteins, which means that an instrumental mass-to-charge range of ≤3000 is, in most cases, sufficient. Proteins with molecular masses of up to 150 000 Da have been successfully analyzed using electrospray ionization on commercially available quadrupole instrumentation. Mass assignment accuracies of 0.01% are routine, and accuracies of 0.001% to 0.005% are achievable with appropriate curve-fitting and centroiding of the multiply charged peaks.

1.3.1 Ion Formation

The operating principle of electrospray and ionspray is the dispersion of a sample solution into an electrically charged aerosol. In the case of electrospray, nebulization takes place by exposing the liquid surface to a high electric field. A solution of the analyte is introduced into dry air or nitrogen at atmospheric pressure through a metal capillary tube held at a potential of several kV relative to the walls of the ion source. The buildup of charges at the liquid surface creates such an instability in the liquid that Coulomb repulsion forces are sufficient to overcome the surface tension so that small (<1 μm) charged droplets

are ejected from the liquid emerging from the capillary tube [49]. The technique works best with flow rates in the 1-10 μL/min range.

In the case of ionspray, the nebulizing action of the electric field is assisted by a high-velocity gas flow [47]. The ionspray interface is essentially a concentric pneumatic nebulizer, exposed to an electric field. The nebulizing capillary is usually floated at several kV relative to the sampling orifice of the ion source. The input of mechanical energy in the nebulization step enables the introduction of higher flow rates (200 μL/min) through the ion source compared to that typically obtainable with electrospray.

Irrespective of how the electrically charged aerosol is formed, solvents evaporate from the small charged droplets. As the size of the droplets decreases, the electric field at the surface of the liquid droplet increases. The exact mechanism of ion formation from these small highly charged droplets has not yet been fully elucidated. In the Iribane and Thomson model, the charged droplets are assumed to be perfect spheres for calculations of the electric fields at the liquid surface [50]. After sufficient evaporation of solvents and disintegration into smaller droplets, a stage is reached where the electric field at the surface is so high that the solute ions escape (evaporate) from the liquid phase into the gas phase [49]. The alternative model, proposed by Dole, suggests that the liquid surface becomes so unstable that the microdroplets containing a few ions, or ions with one or more shells of solvent, separate from the droplets [51]. A final desolvation of each microdroplet or solvated ion then produces sample ions. Regardless of the exact mechanism of ion formation, both electrospray and ionspray ionization coupled with HPLC or CZE have brought about a revolution in biochemical research [52].

1.3.2 Nanoelectrospray

Recently, the development of a nanoelectrospray (nES) ion source for infusion studies of analytes has provided significantly increased sensitivity over that obtained using

conventional electrospray interfaces [53,54]. Much of this work has been carried out by Mann and coworkers [55] who have developed a practical nanoelectrospray ion source from borosilicate capillaries drawn with a short taper to a fine tip of ~1-2 μm inner diameter and gold-coated by vapor deposition. With electrospray tips of such small inner diameters, the flow rate is dictated by the electrospray process itself and is typically 20-40 nL/min. The low flow rate permits the infusion analysis of purified samples and simple mixtures by providing a long measurement time with reduced sample consumption (0.2-2 μL total volume of sample solution required) [56,57]. The 1-2 μm aperture produces droplets of much smaller volume than conventional electrospray sources. These droplets desolvate more rapidly, producing a greater number of ions that can be mass analyzed and detected, leading to greater overall sensitivity. However, efficient coupling of CZE or liquid chromatography with electrospray emitters of such small diameters is difficult, and not practical in view of the likelihood of capillary tip blockage.

1.4 CZE-ESMS Interfaces

Typical flow rates from the CZE separation capillary are in the range of 100-300 nL/min. As mentioned above, electrospray interfaces operate at flowrates of 1-10 μL/min and ionspray sources are compatible with even higher flowrates, although they work well at flowrates in the 5-10 μL/min range. Interface design must therefore accommodate the low flow rates inherent to CZE and maintain the electrical continuity of the electrophoretic circuit. The first experiments in CZE-ESMS were described by Smith's group in 1987 [30]. Refinements of their initial interface led to the design of the coaxial interface arrangement depicted in Figure 1.5a [58]. The CZE column is inserted inside a stainless steel capillary, which acts as both an ionspray needle and a make-up sheath. Solvent make-up flow is introduced through the rear tee, providing for both stable ionspray and electrical continuity. Nebuliser gas is introduced through the front tee, and the snug fit of the ionspray needle with the nebuliser sheath gas capillary restricts the nebulizer gas and allows the flow to be controlled.

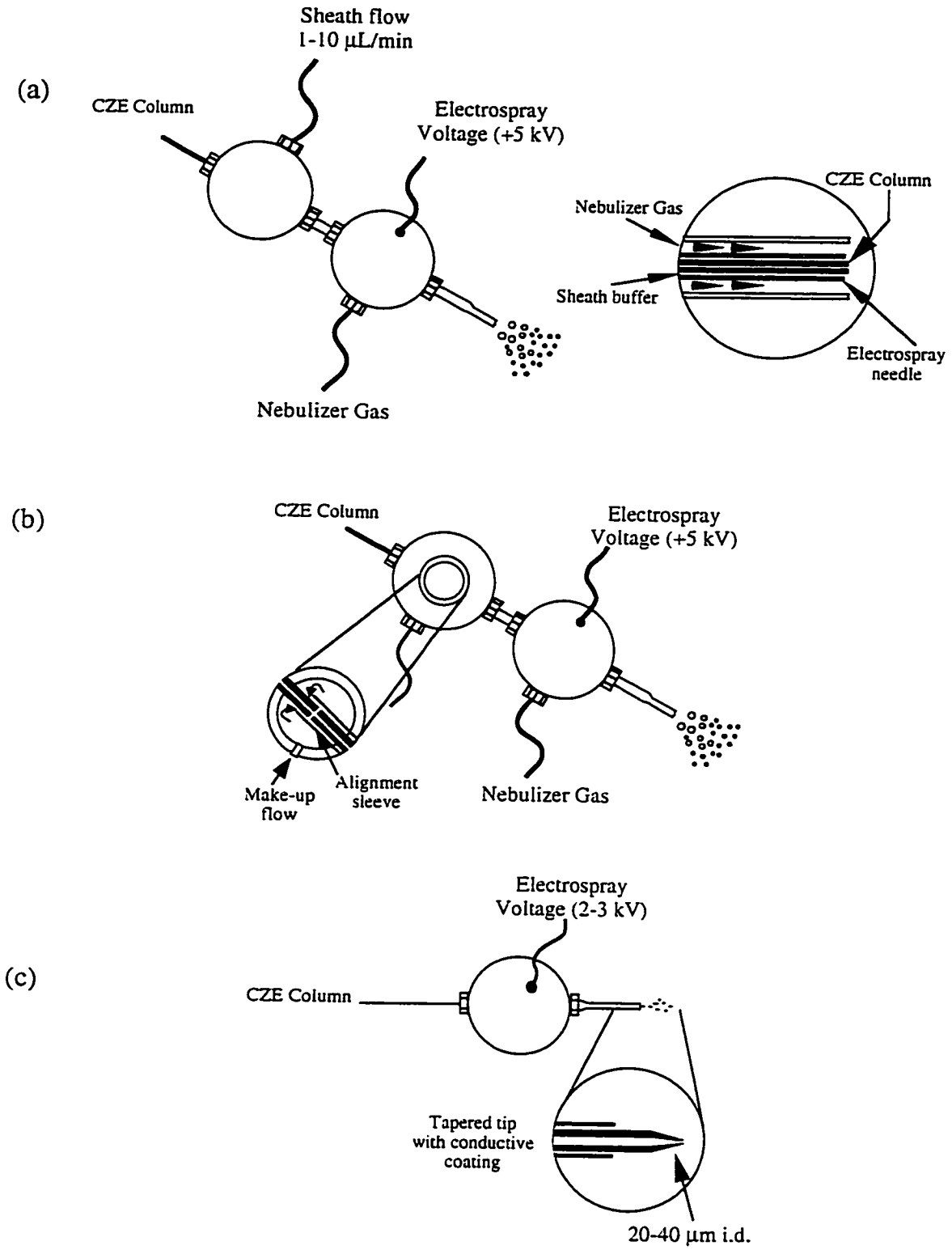

Figure 1.5 Electrospray interfaces for CZE-ESMS. (a) Co-axial interface, (b) liquid-junction interface, and (c) sheathless interface.

The liquid-junction interface for CZE-ESMS described by Henion and coworkers [59-61], differs from the co-axial interface in the configuration of the back tee (Figure 1.5b). In this arrangement, the CZE column terminates inside the liquid junction tee, approximately 10-20 μm from the transfer line or electrospray needle. The make-up fluid is supplied from a small reservoir and is drawn into the junction by a combination of gravity and Venturi vacuum due to the nebulizer gas. A comparison of the co-axial and liquid junction interfaces has been published [58], and addresses parameters such as ruggedness, ease of use, sensitivity and electrophoretic performance.

An alternative approach to interfacing CZE with ESMS involves ionization from capillaries tapered at the interface end to take advantage of the characteristics of the nanoelectrospray interface discussed above. To maintain electrical continuity and to provide a means of applying the electrospray voltage, the tip is either coated with a conductive material or a liquid junction is used [32-35,62-64]. Remarkable limits of detection, low-flow capabilities (compatible with CZE), and tolerance of a wide range of solvents have been reported [32]. It is often referred to as a 'sheathless' interface (Figure 1.5c) because there is no need for a sheath-flow of liquid to maintain electrical contact.

1.5 Tandem Mass Spectrometry

The determination of molecular structure by mass spectrometry requires that the molecule be ionized and undergo structurally informative fragmentations. Fragmentation may be induced by the ionization process itself or by some other means of excitation. Electrospray ionization does not typically impart sufficient energy to cause appreciable fragmentation of the multiply charged ions. The internal energy of the ion in these circumstances may be increased by collisional activation.

Tandem mass spectrometry (MS/MS) has emerged as the most important technique to promote the formation of fragment ions. In the case of triple quadrupole instruments the

first quadrupole (Q1) is used to select the ion of interest for structural studies. The second quadrupole (q2), operating in rf-only mode, contains an inert gas, such as argon, with which the low energy (10-50 eV) ions collides. Multiple collisions occur, increasing the internal energy of the ion, resulting in the production of fragment ions by bond cleavage. The rf-only quadrupole also acts as a focussing lens, collimating the ion beam for efficient transfer of the fragment ions to the third quadrupole. The third quadrupole (Q3) is scanned to transmit the fragment ions for detection. This method of tandem mass spectrometry is referred to as product ion scanning.

Alternative modes of tandem mass spectrometry exist and include precursor ion, multiple reaction monitoring and constant neutral loss scanning. In precursor ion scanning, all ions transmitted through Q1 which produce a specific fragment ion mass are detected. To do this, Q1 is scanned over the precursor ion mass range while Q3 transmits only the m/z value of the fragment ion of interest. Fragmentation occurs as usual in q2, the rf-only quadrupole. When an ion is detected, the point in the Q1 scan is known and converted to a m/z value. This gives the m/z value of the ion which produced the fragment ion of interest. This type of scanning is useful when studying a series of related compounds that produce the same diagnostic fragment ion, such as an oxonium ion in the analysis of glycopeptides.

Multiple reaction monitoring (MRM) is used to investigate multiple fragmentation pathways of a single compound or to select several fragmentation channels of different compounds. The m/z values selected for both Q1 and Q3 correspond to the transition of interest. When Q1 transmits the ion of interest, it undergoes collision-induced dissociation in q2, and if a fragment ion corresponding to the mass set for Q3 is produced, a signal is generated. Therefore MRM is a powerful method for compound-specific analysis using tandem mass spectrometry.

In constant neutral loss scanning, Q1 and Q3 are scanned simultaneously but with an offset equal to the mass of the neutral loss of interest. This mode of tandem mass

spectrometry is useful when compounds of interest lose a fragment that is not charged but is indicative of that class of compound.

1.6 Peptide Sequencing using Tandem Mass Spectrometry

Understanding the function of a protein at the molecular level is greatly facilitated by knowing its complete primary structure, which includes the amino acid sequence as well as the type and sites of any post-translational modifications. The determination of the amino acid sequence of proteins from increasingly available DNA sequence libraries has shifted the emphasis from primary sequence determination to identifying the functions, structure and regulation of each gene product. Tandem mass spectrometry sequencing of peptides produced by chemical or proteolytic digest of a protein provides search keys for interrogating the genomic sequence information contained in databases. Once the protein is identified, the biological function can be more easily investigated.

Collision-induced dissociation of peptides in triple quadrupole mass spectrometers has been extensively studied [65]. Under multiple, low energy collision conditions (10-50 eV), peptides fragment primarily at the amide bonds to produce a ladder of sequence ions. Depending on the gas-phase basicity of the amino acids within the sequence, the charge can be retained on the amino terminus of the ion to form an acylium ion (type b-ion, NH_2-CHR_1-CO···$NHCHR_nCO^+$) or, by H-rearrangement, on the carboxy terminus (type y-ion, NH_2-CHR_n-CO···$NHCHR_1$-CO_2H+H^+) of the ion (Figure 1.6). The mass of R depends on the amino acid and ranges from 1 (Gly) to 131 (Trp) Da (Table 1.1). A complete series of one type of fragment ions, or a complete series made of ions from both types, allows the amino acid sequence to be deduced by subtracting the masses of adjacent ions in the sequence ladder.

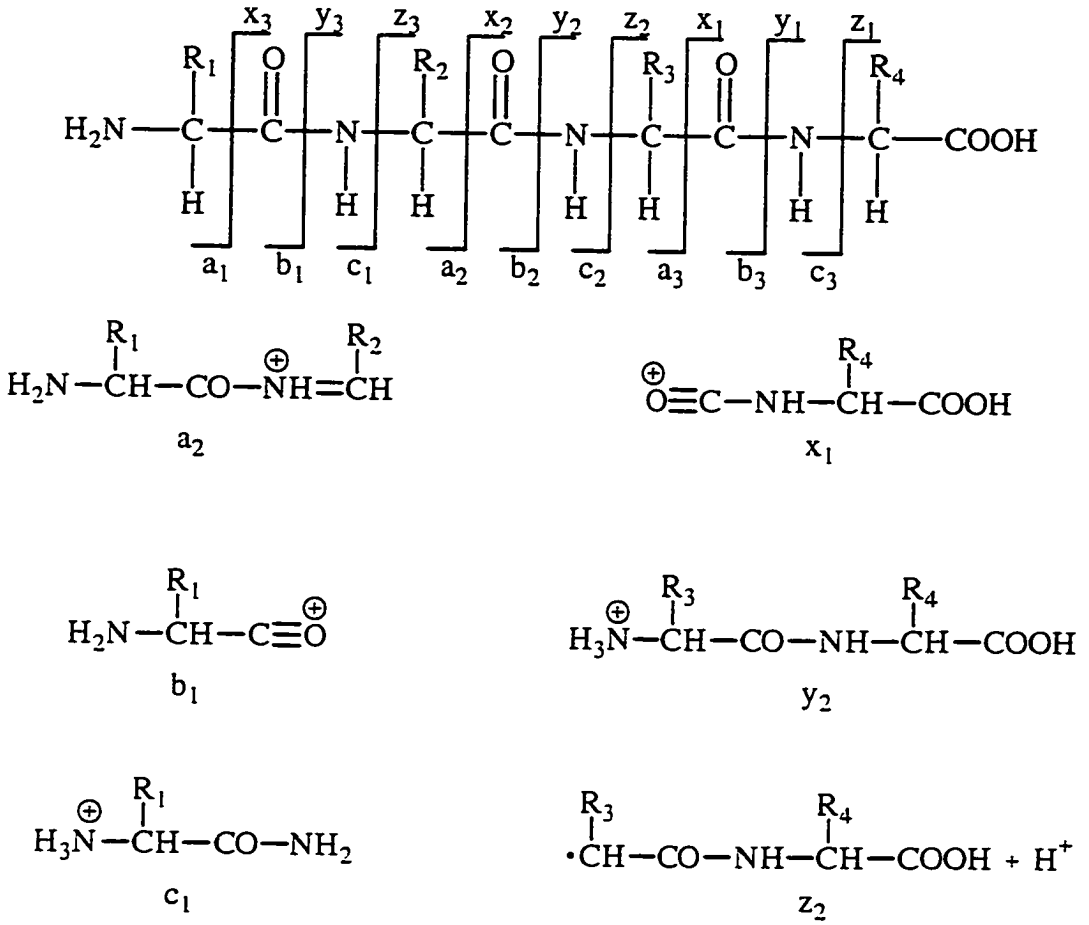

Figure 1.6 Characteristic fragment ions observed in tandem MS of peptides.

1.7 Database Searching

The analysis of proteins using mass spectrometry and tandem mass spectrometry generates a wealth of data. Interpretation of these data to extract information about the identity of the protein is a time consuming task. The advent of large scale genome sequencing projects combined with previously known protein sequences have led to the compilation of amino acid sequences of proteins in databases . The interfacing of LC or CZE-ESMS and MS-MS analyses of protein digests with these databases has provided a means for the rapid identification of proteins.

Table 1.1 The masses and compositions of the twenty commonly occurring amino acid residues.

Symbols	Name and Composition	Side Chain Structure	Average Mass	Side Chain Mass
Ala A	Alanine C_3H_5NO	$-CH_3$	71.0788	15.0348
Arg R	Arginine $C_6H_{12}N_4O$	$-CH_2-(CH_2)_2-NH-\underset{\underset{NH}{\|}}{C}-NH_2$	156.1876	100.1436
Asn N	Asparagine $C_4H_6N_2O_2$	$-CH_2-CONH_2$	114.1039	58.0599
Asp D	Aspartic Acid $C_4H_5NO_3$	$-CH_2-COOH$	115.0886	59.0446
Cys C	Cysteine C_3H_5NOS	$-CH_2-SH$	103.1448	47.1008
Glu E	Glutamic Acid $C_5H_7NO_3$	$-CH_2-CH_2-COOH$	129.1155	73.0715
Gln Q	Glutamine $C_5H_8N_2O_2$	$-CH_2-CH_2-CONH_2$	128.1308	72.0868
Gly G	Glycine C_2H_3NO	$-H$	57.0520	1.0080
His H	Histidine $C_6H_7N_3O$	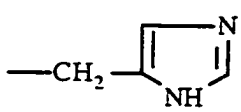	137.1412	81.0972
Ile I	Isoleucine $C_6H_{11}NO$	$-CH(CH_3)CH_2-CH_3$	113.1595	57.1155
Leu L	Leucine $C_6H_{11}NO$	$-CH_2CH(CH_3)_2$	113.1595	57.1155
Lys K	Lysine $C_6H_{12}N_2O$	$-CH_2-(CH_2)_3-NH_2$	128.1742	72.1302
Met M	Methionine C_5H_9NOS	$-CH_2-CH_2-S-CH_3$	131.1986	75.1546
Phe F	Phenylalanine C_9H_9NO	$-CH_2-Ph$	147.1766	91.1326
Pro P	Proline C_5H_7NO	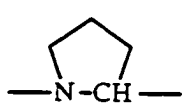	97.1167	41.0727
Ser S	Serine $C_3H_5NO_2$	$-CH_2-OH$	87.0782	31.0342
Thr T	Threonine $C_4H_7NO_2$	$-CH(OH)CH_3$	101.1051	45.0611
Trp W	Tryptophan $C_{11}H_{10}N_2O$	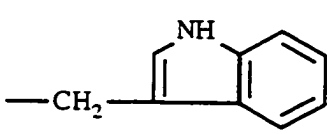	186.2133	130.1693
Tyr Y	Tyrosine $C_9H_9NO_2$	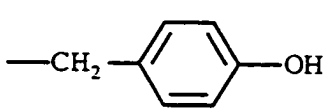	163.1760	107.1320
Val V	Valine C_5H_9NO	$-CH(CH_3)_2$	99.1326	43.0886

Several groups have published various approaches for the interrogation of protein databases using mass spectral data [66-73], and commercial software is available [74,75]. Databases of gene sequences are rapidly expanding and efforts to correlate proteins with specific genes will rely on these techniques. An important attribute of some of these programs is their ability to tolerate "errors" in predicted masses due to post-translational modification of proteins [66,68,75].

1.8 Glycoproteins

The covalent attachment of oligosaccharides to given amino acid residues of proteins is one of the most common post-translational modifications of these biomolecules. Glycoproteins are fundamental to many important biological processes including fertilization, immune defense, viral replication, parasitic infection, cell growth, cell-cell adhesion, degradation of blood clots, and inflammation [76]. These biomolecules contain oligosaccharides attached to a protein at the hydroxyl group of a serine or threonine residue (O-linked) or to the amide sidechain of an asparagine residue (N-linked). Variable oligosaccharide structures are found at each linkage site, and further complexity arises from partial occupancy at each glycosylation site. The consequence of this microheterogeniety is that a glycoprotein is seldom represented by a single structural entity, but rather as a set of glycosylated variants (referred to as glycoforms) of a common protein [77].

The N-linked oligosaccharides can be divided into three main categories: high-mannose, hybrid, and complex (Figure 1.7a). All three share a common pentasaccharide core: $Man_3GlcNAc_2$ (Man: mannose, GlcNAc: *N*-acetylglucosamine). Attachment at the asparagine residue of the polypeptide chain is via the reducing end GlcNAc, which originates from a common precursor oligosaccharide, $Glc_3Man_9GlcNAc_2$ (Glc: glucose), for all N-linked oligosaccharides [78,79]. This oligosaccharide is first assembled in the endoplasmic reticulum on an isoprenoid lipid, dolicholpyrophosphate, and is then transferred to the growing polypeptide chain. Trimming of the non-reducing end

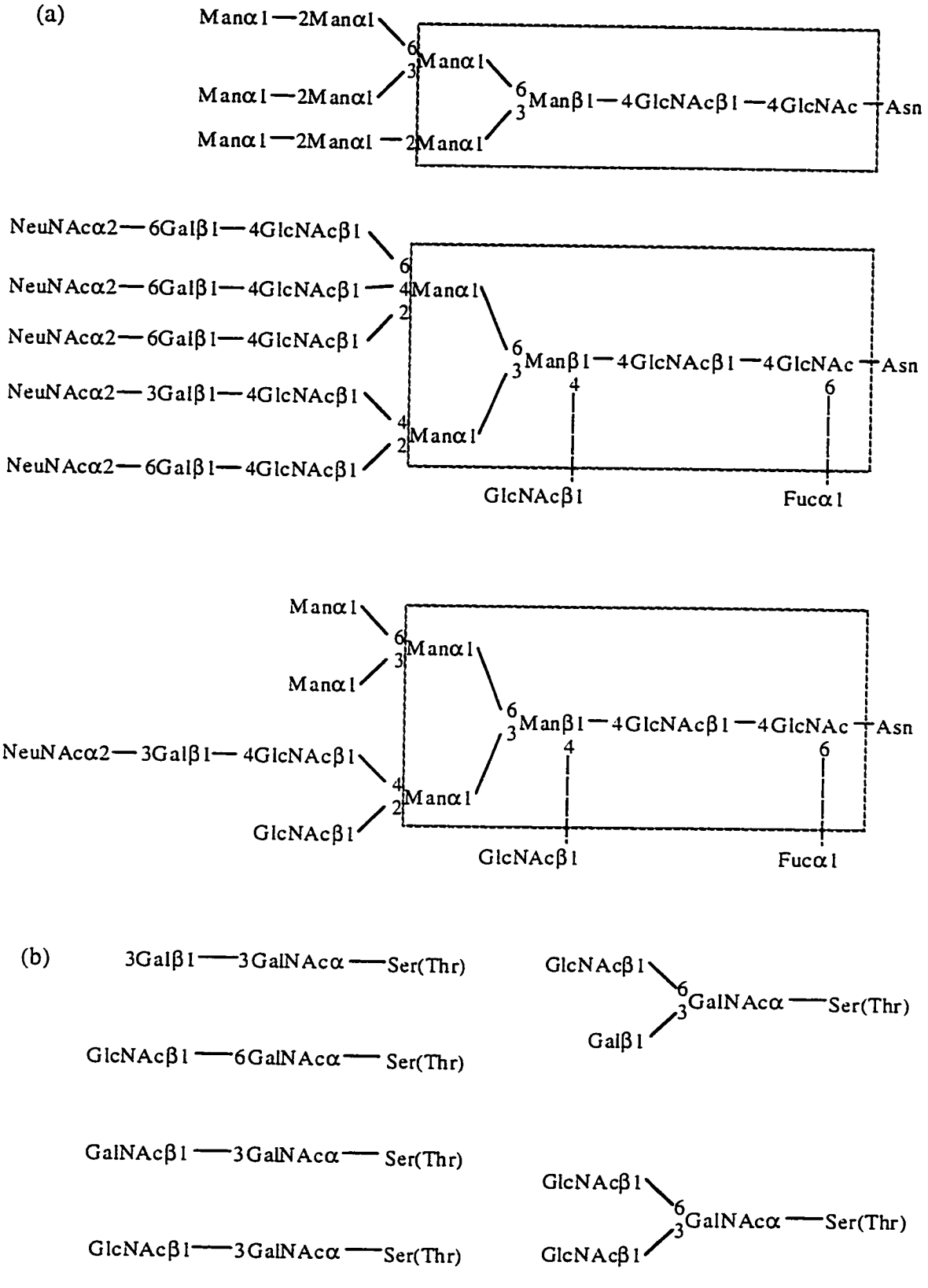

Figure 1.7 Core structures for (a) N-linked and (b) O-linked oligosaccharides [76].

saccharide residues results in the formation of high-mannose type oligosaccharides. The complex oligosaccharides are produced by further trimming of the precursor oligosaccharide to leave the pentasaccharide core, followed by addition of various saccharides such as galactose (Gal), glucose, GlcNAc, sialic acid (Neu5Ac) and fucose (fuc). This process occurs as the glycoprotein travels through the various compartments of the Golgi complex [78,79]. Hybrid oligosaccharides encompass features of both high-mannose and complex types. N-Linked glycosylation generally occurs at the sequon Asn-X-Ser or Asn-X-Thr, where X is any amino acid except proline [80-82]. Recently, it has been shown the the amino acid at the X position plays a role in glycosylation efficiency at that sequon [83].

In contrast, O-linked glycoproteins do not share a common core structure; at least six different core structures are known [76] (Figure 1.7b). Although the glycans are most often linked to serine or threonine residues through GalNAc (N-acetylgalactosamine), the linkages may also be through other residues. The synthesis of O-linked oligosaccharides is entirely a post-translational event with a series of enzymes acting sequentially on the fully folded protein. Unlike N-linked glycosylation, no signal sequon has yet been found for O-linked glycosylation. Since all hydroxyamino acids are not O-glycosylated, signals must exist to specify which Ser and Thr residues acquire O-glycans. Charged amino acids in the proximity of the site of glycosylation appear to play an important role in signaling this post-translational modification [84].

The complexity of glycoproteins provides a truly challenging analytical problem. Various approaches have been developed for the characterization of both the carbohydrate structure and the sequence of the protein. Typical methods for the analysis of N- or O-linked glycoproteins are illustrated in Figure 1.8. All carbohydrates appended to the protein can be removed chemically or enzymatically and collected as a pool of mixed oligosaccharides. These are then analyzed by various methods including NMR, enzymatic

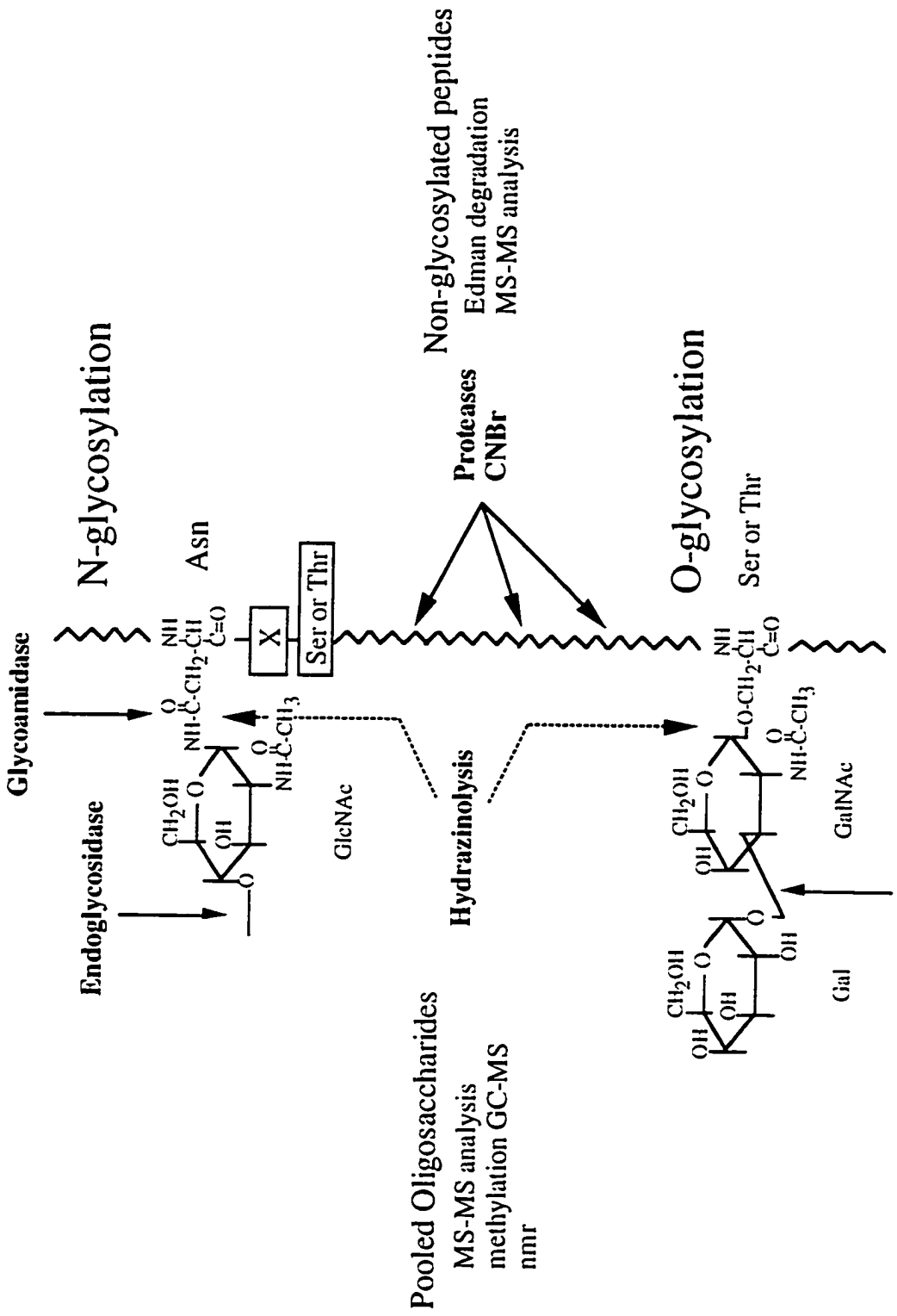

Figure 1.8 Summary of methods used for glycoprotein analysis.

digestion, chemical cleavage, and methylation followed by GC-MS [85]. These analyses provide information on the specific structures and linkages (the glycomer [86]) of the various sugars present in the oligosaccharide. Mass spectrometry of the intact oligosaccharide provides molecular weight information, and high-energy tandem MS studies, after appropriate derivatization, can be used to assign the structure and linkages of the oligosaccharide [87].

The analysis of the protein after removal of the attached carbohydrates provides the primary structure of the original glycoprotein. For N-linked glycoproteins, identification of the potential sites of glycosylation can be made based on the consensus sequon, although further confirmation is required. For unequivocal determination of the site of linkage, the glycoproteins are typically digested using proteolytic enzymes followed by endoglycosidases, and the digests are analyzed by LC-UV or LC-MS before and after removal of the glycans [88,89]. The peaks that disappear in the second analysis correspond to glycopeptides, and can be collected from the analysis of the original glycoprotein digest for further characterization using Edman sequencing. The amino acid linked to carbohydrates would typically be lost in the washing cycle, thereby resulting in a blank during sequence analysis. This can be further confirmed by conducting the Edman degradation of the glycopeptide after chemical or enzymatic removal of the carbohydrate.

Mass spectrometry has played a valuable role in the elucidation of glycoprotein structure, including carbohydrate structure and primary sequence determination. Recently, several MS techniques have been reported for glycoproteins permitting the specific location and analysis of glycopeptides in digests of glycoproteins [90,91]. These methods make use of fragmentation in the orifice/skimmer region of the mass spectrometer to produce ions characteristic for specific classes of carbohydates (Table 1.2). The mass spectrometer is scanned over the region corresponding to these oxonium fragment ions using a high orifice/skimmer voltage to promote their formation prior to mass spectral analysis. The

potential drop in this region is then reduced to acquire the multiply-protonated ions of the intact peptides and glycopeptides. Using this mixed-scan acquisition function the location of the glycopeptides in the total ion chromatogram can be determined. Once the glycopeptides have been identified the relevant precursor ions can be subjected to LC-MS-MS analysis and further structural information on the glycoform can be obtained. Low energy collision activation of glycopeptides typically results in cleavage of the labile glycosidic bonds while the amide peptide linkages do not normally undergo dissociation under these collision conditions. Although tandem mass spectra of glycopeptides provide important structural features of the type of oligosaccharide appended to the peptide, the technique is of limited practical value for sequencing the peptide backbone.

Table 1.2 Diagnostic oxonium ions for glycopeptides.

m/z	Sugar
133	Pentose (arabinose Ara, ribose Rib, xylose Xyl)
147	Deoxyhexose (fucose Fuc)
162	Hexosamine (galactosamine GalN, glucosamine GlcN)
163	Hexose (glucose Glu, galactose Gal, mannose Man)
204	N-acetylhexosamine (N-acetylgalactosamine GalNAc, N-acetylglucosamine GlcNAc)
274	N-acetylneuramic acid - H_20 (Neu5Ac- H_20)
292	N-acetylneuramic acid (Neu5Ac)
366	HexNAc-Hex
407	HexNAc-HexNAc

Another shortcoming of the LC-MS techniques described above is the limited resolution obtained for glycopeptides present in digests of glycoproteins. The glycopeptides tend to be present as broad peaks in the tryptic map, indicating the microheterogeneity of these molecules [91]. Capillary zone electrophoresis has greatly enhanced resolving power relative to HPLC, and this attribute has been used in the study of glycoproteins and carbohydrates [92, and references therein].

1.9 Summary

Developments in mass spectrometry and separation science are providing the tools necessary for the investigation of biochemical processes. Capillary zone electrophoresis interfaced with electrospray mass spectrometry is one such tool. Developments in CZE-ESMS are ongoing and this thesis presents improved methods aimed at aiding researchers using CZE-ESMS to investigate the structures and functions of proteins and peptides. Methods presented in subsequent chapters enhance the sensitivity of CZE-ESMS through the development of a nanoelectrospray interface and a chromatographic preconcentration method for the analysis of large (μL) sample volumes. Application of these techniques to the analysis of peptides and protein digests at the attomole to femtomole level is presented. Protein database searching using data generated at these low levels is illustrated with a commercially available program. The study of glycoproteins using CZE-ESMS and higher orders of MS is also presented. New scanning methods for maximizing the information gained from the study of these biomolecules were developed and provided valuable structural information, from oligosaccharide composition to peptide sequence.

Chapter 2

2.0 Experimental

2.1 Reagents and Materials

All fused silica capillaries were purchased from Polymicro Technologies (Phoenix, AZ). Teflon tubing and the capillary column butt connector (Part #2-3796) were obtained from Supelco (Oakville, ONT). Formic acid (99%), ammonium persulfate (98%), peptide standards and lectins were obtained from Sigma Chemical Co. (St. Louis, MO) and used without further purification. The α-amylase inhibitor was a gift from Dr. Marteen Chrispeels (Dept. of Biology, University of California, San Diego) and was further purified using reverse phase C_8 HPLC to isolate the 11.5 kDa α-chain glycopeptide prior to mild acid cleavage. The κ-casein was prepared according to the method of Zittle and Custer [93] with the exception that the final purification with ethanol was omitted. A 1% w/v solution of κ-casein in tris citrate (50 mM, pH 6.6) was treated with rennin (1 μg rennin/mg of κ-casein) for 15 min at 35 °C. The pH of the solution was adjusted to 4.6 and the para-κ-casein was precipitated. The supernatant solution containing

the soluble rennin fragment was dialyzed at 4 °C overnight and freeze-dried prior to proteolytic digestion. Sequencing grade TPCK-trypsin and endoproteinase Glu-C were purchased from Boehringer Mannheim (Montréal, QUE). All organic solvents as well as NaOH were purchased from BDH Inc. (Toronto, ONT). 7-Oct-1-enyltrimethoxysilane was purchased from Hüls America Inc. (Bristol, PA). For modification of the capillary surface, hexadimethrine bromide (Polybrene®) and [3-(methacryloylamino)propyl]trimethylammonium chloride (MAPTAC) were obtained from Aldrich Chemical Company Inc. (Milwaukee, WI). [(Acryloylamino)propyl]trimethylammonium chloride (called BCQ by the manufacturer) was supplied by Chemische Fabrik Stockhausen (Krefeld, Germany), and (3-aminopropyl)trimethoxysilane was from Sigma. *N,N,N'N'*-Tetramethylethylenediamine (TEMED) was purchased from International Biotechnologies Inc. (New Haven, CT). Sal Hyde 24K bright English gold plating salts (Mr. Clock, Halifax, NS) were used to prepare the gold plating solution, and the silver conductive paint was purchased at a local General Motors automobile dealership. The preconcentrator was constructed from the following stationary phase material: 40 µm aminopropyl (Varian, Palo Alto, CA), 40 µm C18 (Supelco) and 5 µm C18 (POROS R1, Perseptive Biosystems, Farmingham, MA).

2.2 Glycoprotein Digests

Both proteolytic and chemical digestion of proteins were used to generate peptides for analysis by CZE-ESMS. The methods used are described below.

2.2.1 Tryptic Digestion

Lectins from *Phaseolus vulgaris* (0.9 mg), *Glycine max* (1.1 mg) and *Tetragonolobus purpureas* (0.98 mg) were dissolved in 0.2 M ammonium bicarbonate. Tryptic digestion was carried out for 24 h at 37 °C using a 30:1 mass ratio of substrate to enzyme. The solutions were evaporated to dryness and dissolved in deionized water to

final concentrations of 4.5, 4.4 and 4.9 mg/mL, respectively, calculated in terms of the original mass of glycoprotein.

2.2.2 Endoproteinase Glu-C Digests

Kappa-casein renin fragment (2.7 mg) was dissolved in 0.2 M ammonium bicarbonate. Glu-C digestion was carried out for 5 h at 37 °C using a 50:1 mass ratio of substrate to enzyme. The solution was evaporated to dryness, and the residue was dissolved in deionized water to a final concentration of 10 mg/mL, calculated in terms of the original mass of glycoprotein.

2.2.3 Mild Acid Cleavage

The α-chain of α-amylase inhibitor 1 (~0.5 mg) was dissolved in acetic acid (0.25 M) and incubated at 115°C for 8 h to favour cleavage at the aspartic acid residues. The digested protein solution was evaporated to dryness, and the residue was redissolved in deionized water to a final concentration of 1.0 mg/mL.

2.3 Nanosprayer Tip Construction

Fused silica capillary (bare or coated) was cut to a length of 1.1 m for the one-piece columns, or to ~10 cm for the butted tips, and tapered by suspending a metal weight (15 g) from one end of the capillary and melting the fused silica with the flame from a microwelding torch. The thinnest portion of the tapered column (up to 10 cm long and 2-5 μm o.d.) was trimmed to 2-3 cm, inserted into a larger i.d. capillary, and bent until the tapered end snapped. The i.d. of the larger capillary used as the cutting tool dictated the dimensions of the tapered tip. For example, a 100 μm i.d. cutting capillary produced a tapered capillary of 100 μm o.d. and ~14 μm i.d. from original dimensions of 360 μm o.d. and 50 μm i.d.. The tapered end was further sharpened by etching in a stirred solution of 48% HF for 15-30 min. During this process the capillary was rinsed with water (6

μL/min) to prevent the acid from etching the inner surface. After etching, the capillary surface was rinsed with water and purged with N_2 to remove any traces of HF.

The gold coating was applied by winding the tapered column around a ring support (5 cm in diameter). About 5 cm of the tapered end was left exposed, and the rest of the column was covered with aluminum foil to prevent gold deposition. The short tapered tips were inserted into a 1.5 cm thick piece of foam rubber at a 45° angle. The support foam was positioned 5 cm from the gold target electrode on the stage of an Edwards 306A high vacuum coater. The exposed portion was sputter-coated with gold for 15-20 min by maintaining a voltage and current across the electrodes of 1.5 kV and 20 mA, respectively. The best results were achieved when a vacuum of $\leq 1 \times 10^{-5}$ Torr was obtained prior to coating. Typically, four one-piece columns or 20-30 tips were sputter-coated at one time.

After sputter-coating, the gold coating on the tips was thickened by electroplating. The gold-coated portion of the tip was covered with silver conductive paint to within 1 cm of the tapered tip to prevent the stirred and heated (60 °C) gold plating solution from removing the sputter-coated gold. The gold plating salts were prepared according to the manufacturer's instructions in 1 L of deionized water, and approximately 50 mL was used to electroplate several batches of columns or tips. The electroplating solution was used for this purpose over a 2-year period. To prevent blockage the capillary was continuously rinsed with deionized water (6 μL/min) during the plating process. A gold counter-electrode was used, and the plating current was maintained at 0.75 mA for 30 min. Typically, two columns or tips were electroplated at a time; this number was dictated by the capacity of the syringe pump used to maintain the water flow through the capillaries. Electron microscopy revealed that the thickness of the gold coating was approximately 2-3 μm. The tips could be used for several days, stored for over a month, and reused.

2.4 Capillary Coatings

Bare fused silica capillary was covalently modified with BCQ or MAPTAC in 5 m lengths and cut to a shorter length as required. The APS coating was bonded to tapered capillaries prior to gold coating. Dynamic coatings (polybrene solution) were applied to the complete assembly consisting of the tip butted to the CZE column.

2.4.1 MAPTAC and BCQ Coating

The method used for preparing the BCQ or MAPTAC coating was described previously [32]. The capillary was rinsed sequentially with 1 M NaOH, deionized water and methanol, each for 1 h at 20 psi. A solution of 7-oct-1-enyltrimethoxysilane (20 μL) and glacial acetic acid (20 μL) in methanol (4 mL) was passed through the column overnight (8-12 h) at 20 psi. The capillary was subsequently rinsed with methanol and deionized water (1 h each, 20 psi). TEMED (8 μL) and aqueous ammonium persulfate (15% (w/v), 56 μL) were added to a solution of BCQ in deionized water (2% (v/v), 4 mL), and this solution was immediately rinsed through the column for 8 h (or overnight) at 20 psi. The capillary was flushed with deionized water for 1 h and then stored. Prior to use, the column was flushed with CZE electrolyte solution for 5-10 min.

2.4.2 APS Coating

Columns derivatized with APS were prepared as described by Moseley *et al.* [94]. Acid treatment of the capillary was carried out with 6 M HCl for approximately 4 h, followed by He purging for 12 h at 300 °C in a GC oven. Toluene was pumped through the column for 10 min, followed by a 2-h rinse with a 5% (v/v) solution of (3-aminopropyl)trimethoxysilane in toluene. The column was flushed with toluene for 30 min, and dried by purging with N_2 at room temperature. Prior to use, the column was

flushed with CZE electrolyte for approximately 30 min. For these columns, the gold-coating of the tip was carried out after modification of the internal capillary surface.

2.4.3 Polybrene Coating

The polybrene coating procedure was based on a method described previously [92,95]. One-piece columns or columns with a butted tip in place were rinsed initially with 1 M NaOH, deionized water, Polybrene (5% w/v in 2% v/v ethylene glycol), and CZE electrolyte for 20 min each at 2000 mbar using the CE instrument. Between CZE analyses, the column was reconstituted by rinsing with NaOH and deionized water (1 min each), followed by polybrene solution and CZE electrolyte (4 min each).

2.5 CZE-UV

CZE-UV experiments were carried out using a P/ACE system (Beckman, Palo Alto, CA) at a detection wavelength of 200 nm. Separation was achieved by applying 20 kV to the outlet end of an 87 cm x 50 μm i.d. capillary previously coated with APS or BCQ. The background electrolyte was formic acid (0.1 M or 1.0 M). The sample was introduced by pressure (35 mbar, 15 s), resulting in typical injection volumes of ~15 nL.

2.6 CZE-ESMS

CZE-ESMS experiments were carried out using a Thermo CE system (Thermo Capillary Electrophoresis, Franklin, MA). Typically, electrolytes used for CZE-ESMS experiments were 0.1 to 2 M formic acid and in some instances contained up to 25% acetonitrile. A detailed description of the co-axial CZE-ESMS interface has been reported previously [58]. The nanoelectrospray interface used in this work is described in detail in the results section. The nanosprayer tip was coupled to the separation capillary using various connectors as described below. Optimization of the interface was achieved by

electro-infusion of a peptide standard (Leu-enkephalin, 10 μg/mL) dissolved in the electrolyte used for separations.

All mass spectrometric experiments were conducted using a Perkin Elmer/SCIEX API III$^+$ triple quadrupole mass spectrometer (Concord, ONT). A separate power supply (Glassman EH Series, Glassman, Whitehouse Station, NJ) was used to provide the electrospray voltage. Typical mass spectral acquisition parameters used a dwell time of 3.5 msec per 1 Da step in full mass scan mode. MS-MS experiments were conducted using collision energies between 20-35 eV in the laboratory frame of reference, at a collision gas (argon) thickness of 3.5 x 10^{15} atoms/cm^2. Tandem mass spectra were acquired using dwell times of 2 ms per step of 0.5 Daltons in full-scan mode. A Macintosh Quadra 950 computer was used for instrument control, data acquisition, and data processing.

2.7 PC-CZE Capillary Construction

The preconcentrator (Figure 2.1) was constructed by drawing packing material suspended in methanol into a 2 cm piece of Teflon® tubing (300 μm i.d.). The tubing was briefly dipped into the slurry while drawing on a syringe attached by fused silica capillary to the free end of the tubing. A bed of 1 mm, verified using a light microscope, was typically used. Frits were not necessary to prevent loss of packing material when the 40 μm irregular particles were used. However, the 5 μm material required the construction of frits, which was achieved by inserting a piece of 0.22 μm filter from a Millipore Ultrafree MC centrifuge filter unit into the Teflon® tubing before and after addition of the packing material. Similar preconcentration devices have been described [96-98].

The preconcentrator was attached to 15- and 80-cm pieces of BCQ-coated capillary that served as the inlet and the outlet end, respectively. The outer diameter of the capillary (360 μm) was appropriate for a push-fit attachment to the Teflon® tubing and did not require epoxy or other sealant to prevent leakage. The preconcentrator did not restrict the

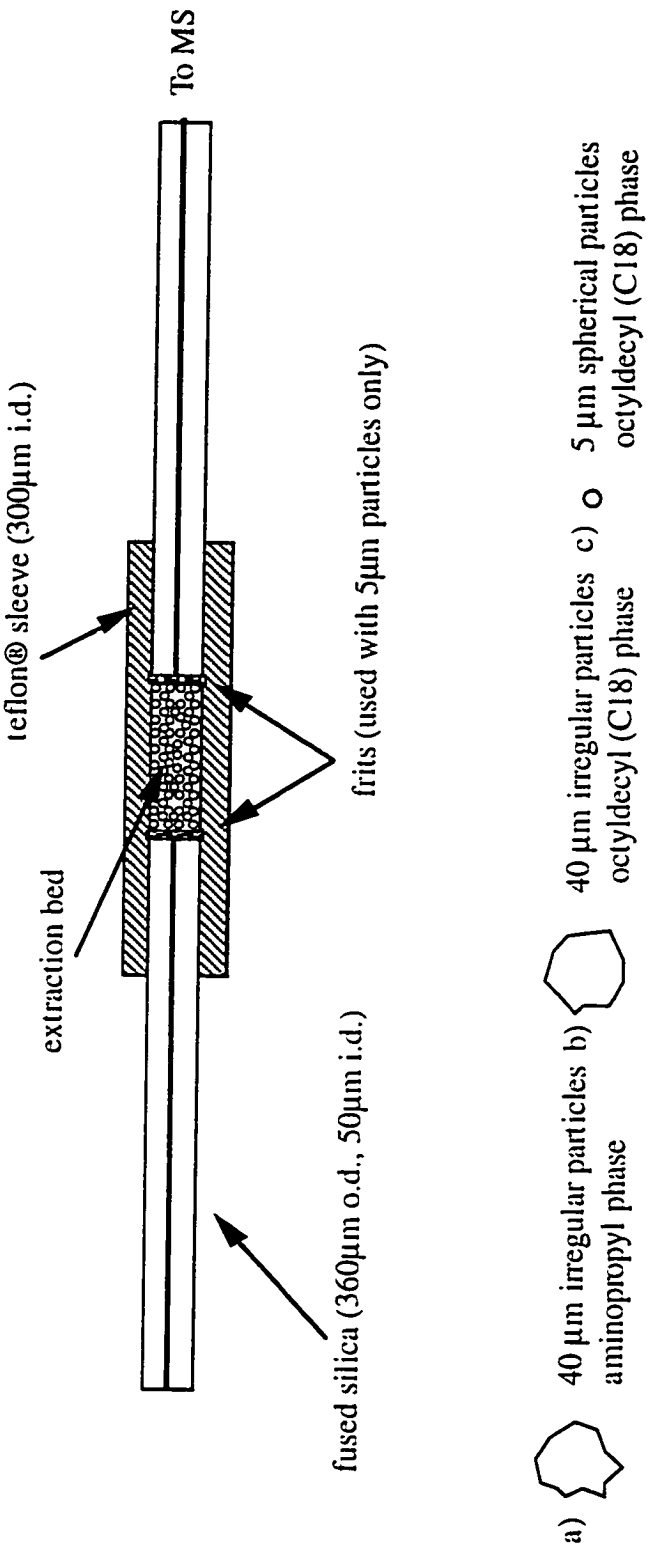

Figure 2.1 Schematic of the preconcentration device used with CZE-MS.

flow of solvent and could be replaced without changing the capillary. A further benefit of this system is that the mass spectrometer can be optimized without the preconcentrator in place. This is especially important when using the nanospray interface.

2.8 PC-CZE Separation

Reproducible conditions were maintained for the preconcentrator by adopting the following sequence. The capillary was rinsed with two column volumes of elution solvent (90/10 acetonitrile/1% HCl) followed by five column volumes of separation electrolyte. These rinses were carried out after each experiment (except where noted) in order to prevent memory effects as discussed below. In each experiment the sample was injected at 1000 mbar for 4-8 min, resulting in an injection volume of 4-8 μL. Larger volumes could be injected with a concomitant increase in sample loading time. Following injection, the capillary was rinsed with four column volumes of separation electrolyte. The sample was eluted from the stationary phase using a small plug (150 nL) of elution solvent, followed by a brief rinse (0.2 min at 2000 mbar) with separation electrolyte to push the elution solvent through the stationary phase and prevent re-adsorption of the analyte. Voltage was applied and the acquisition started after the sample was eluted from the preconcentrator.

Chapter 3

3.0 Nanoelectrospray Interface

A necessary first step in this research was the construction and optimization of a nanoelectrospray interface for CZE-ESMS. This interface would provide enhanced sensitivity for the analysis of digests of glycosylated and non-glycosylated proteins using the high resolution provided by CZE. In order to construct a practical interface that provides ease of use and reliability, several parameters were investigated including the use of disposable nanosprayers, tip geometry and capillary surface modification. The results of these experiments are presented below.

3.1 Interface Arrangements

Previous efforts at interfacing CZE to a nanoelectrospray source have typically used capillaries with inner diameters of 10-50 μm, which are mechanically and/or chemically tapered to a fine tip and subsequently metallized [34,35,62-64]. The disadvantage of the small inner diameters of the column used for the nanospray interface is the reduced amount

of sample that can be injected while maintaining the separation efficiency. For instance, a typical injection volume of 40 nL on a 1 m x 50 μm capillary becomes 1.6 nL for a 1 m x 10 μm capillary. The construction of these tapered and metallized columns is a time consuming process and does not lend itself to mass production methods.

Various approaches were investigated for the construction of a nanoelectrospray interface. One-piece columns were used successfully, but as mentioned previously, construction of these columns proved time consuming. Therefore, small tips that could be connected to a separate CZE column were studied as a potential nanoelectrospray source. The use of tips butted to the CZE column is an attractive approach to nanoelectrospray CZE-ESMS as it allows for disposal of the tip without loss of the CZE column. Also fabrication of multiple tips is less costly in time and resources than the construction of one-piece nanoelectrospray columns.

Initially, the use of stainless steel tubing (20 μm i.d.) coupled to the CZE capillary with fused silica and epoxy resin was evaluated for use as a nanoelectrospray tip. This arrangement produced satisfactory signal intensity using pressure to infuse the sample through the capillary. Unfortunately, when the CZE voltage was applied and the pressure removed, a stable spray could not be maintained and the CZE current dropped to zero, indicating disruption of the CZE circuit. The drop in current is indicative of bubble formation in the capillary due to electrolysis of water.

$$2H_2O \rightarrow 2H^+ + O_2(g) + 2e^-$$

When this electrolysis is sufficiently intense, oxygen bubbles form disupting the electrophoretic circuit. Electrolysis is most likely occurring inside the stainless steel tip precluding its use as a nanoelectrospray interface.

To eliminate the possiblity of electrolytic action in the tip, fused silica was used to construct nanoelectrospray tips as discussed in Section 2.3. Several methods for connecting the tip to the capillary were used (Figure 3.1) and separations were carried out to evaluate the different methods. The Teflon® connector, while the easiest to use, gave a

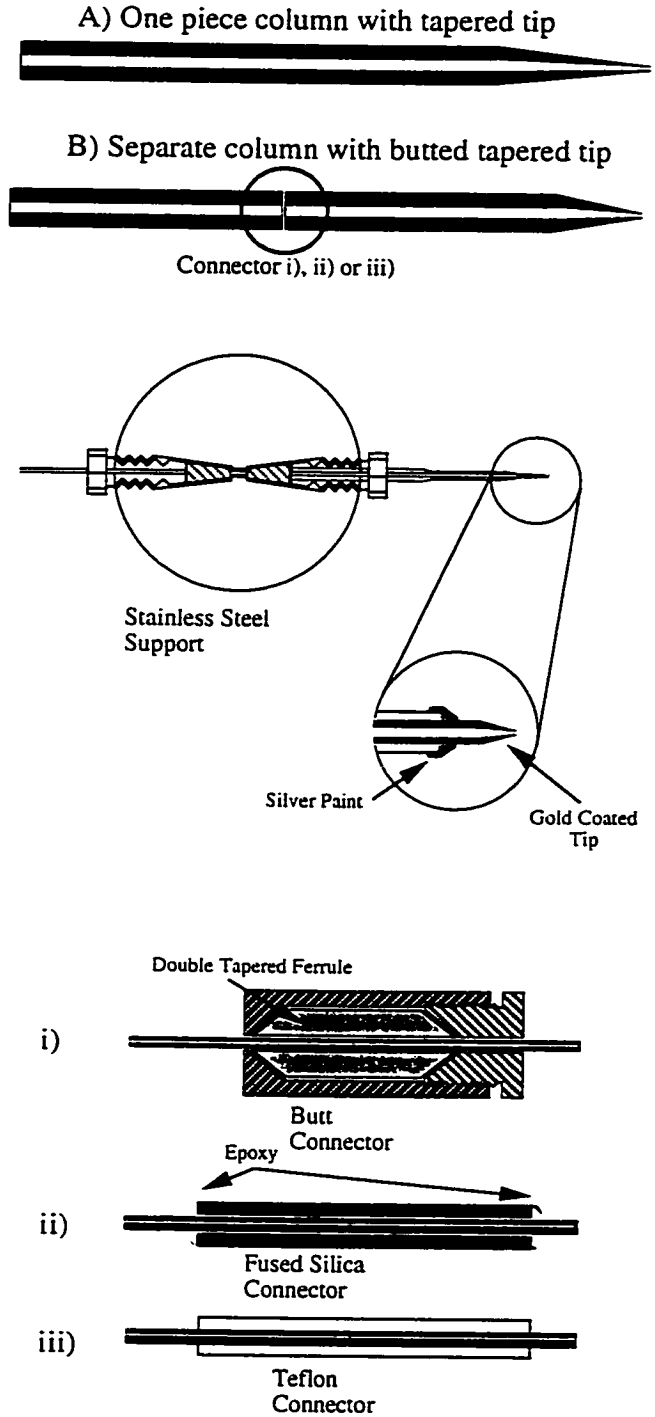

Figure 3.1 CZE-ESMS nanoelectrospray interface arrangements. For the butted-tips, connection is made before the stainless steel tee using connector i), ii) or iii).

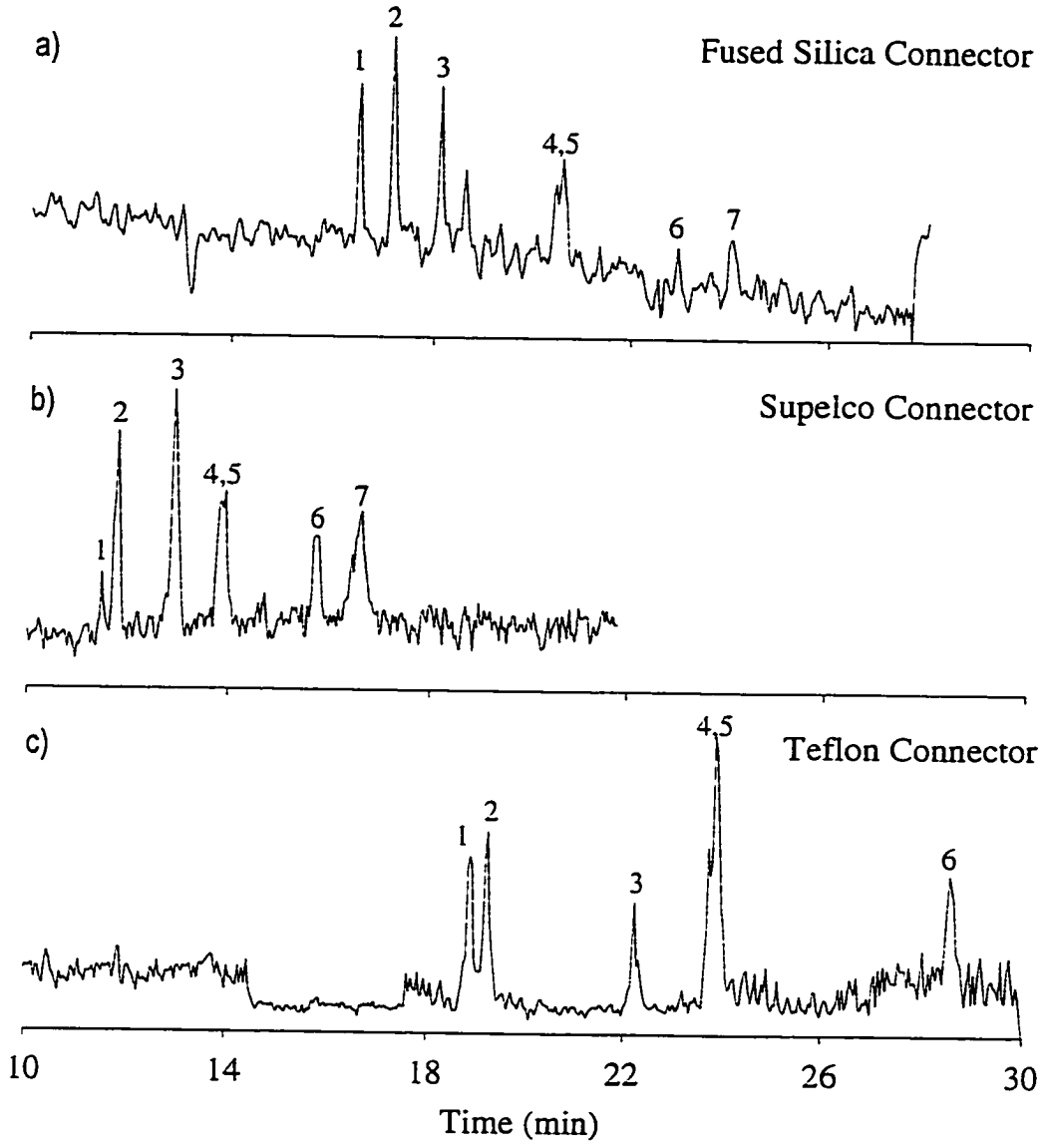

Figure 3.2 CZE separation of peptides using the nanoelectrospray interface with different connectors for the nanoelectrospray tips, a) fused silica connector, b) Supelco connector, and c) Teflon® connector. CZE conditions: 1 m columns, 20 μm i.d. tips, Polybrene coating, -28 kV, 0.1 M formic acid, 20 picograms of each peptide injected. 1) Leu-enkephalin, 2) Kassinin, 3) Substance P 2-11, 4) Cholecystokinin 10-20, 5) Somatostatin, 6) Bradykinin, 7) Angiotensin III.

high background signal and an increased analysis time relative to the other two connectors (Figure 3.2c). The fused silica connector also gave an extended analysis time (Figure 3.2a) relative to that observed using a one-piece column with UV detection. Only the Supelco connector gave a CZE-ESMS separation comparable to that obtained with the one-piece column (Figure 3.2b). The longer analysis times for the fused silica and Teflon® connectors is most likely due to misalignment at the connection point of the column and the tip. With the Supelco connector, insignificant (if any) dead volume and proper alignment of the tip with the column are ensured by a double ended ferrule that is drilled to the exact diameter required. To ensure a good connection between the tip and the column it was important to have a flat surface at each of the connecting ends. The Supelco connector was used in all subsequent experiments performed with the butted tips.

3.2 Tip Dimensions and Flowrate Optimization

When constructing a nanoelectrospray interface for CZE-ESMS, optimization of the flowrate is one of the most important considerations for interface design. In CZE-ESMS experiments the flowrate is dictated by the electroosmotic flow and the flow resistance associated with the inner diameter of the nanosprayer tip. If the inner diameter at the tip is too small, the flow will be restricted and the analysis time will be extended. On the other hand, sensitivity can be compromised when the tip dimension is too large since the Taylor cone cannot then be stabilized.

In LC/MS or flow injection electrospray ionization, the "chromatographic" peak area of the ion signal from the mass spectrometer varies with flowrate while the peak height is insensitive to flow rate. This behavior resembles that expected for a concentration-dependent detector [99]. However, at the very low flow rates used with nanoelectrospray interfaces, mass spectrometric detection becomes mass-flux sensitive, and the ion intensity (peak height) varies with flowrate as indicated in Figure 3.3. The interface was initially optimized for a flowrate of 200 nL/min using a 20 μm i.d. microsprayer, and the effect of

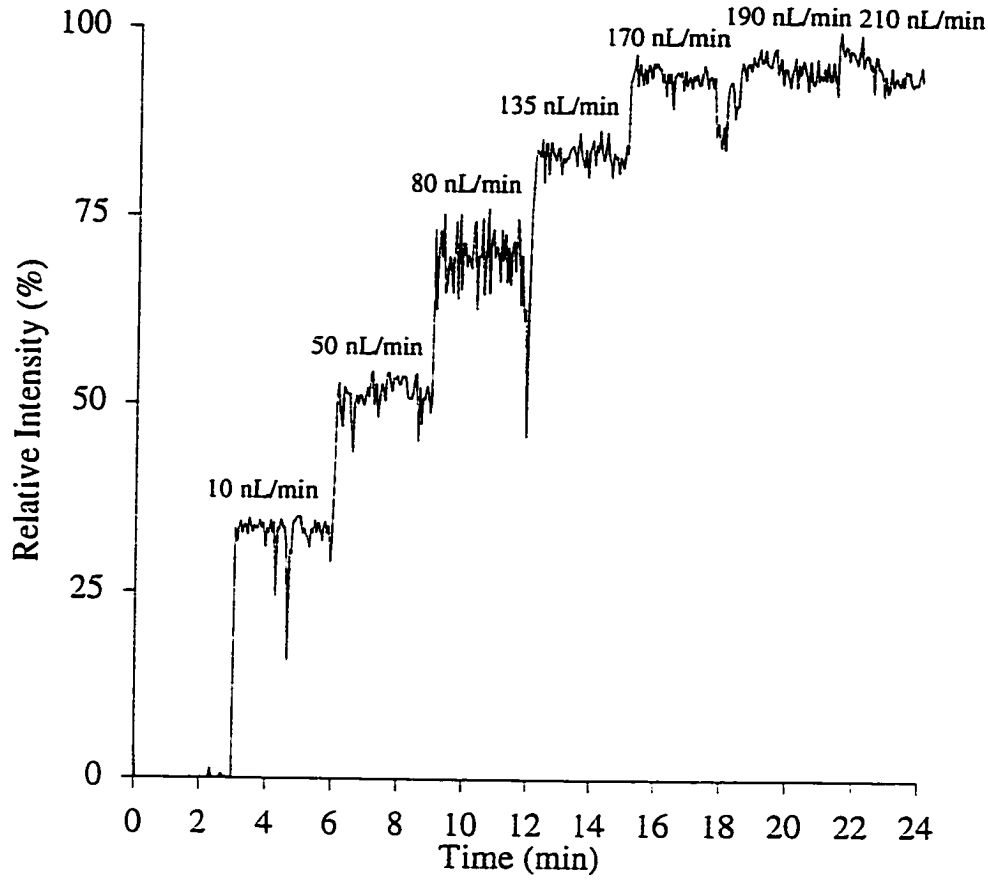

Figure 3.3 Influence of flowrate on sensitivity ("peak height") of nanoelectrospray interface at a fixed position. Butted-tip arrangement using a 20 μm i.d. tip; infusion of Leu-enkephalin (10 μg/mL) in 0.1 M formic acid.

flowrate was examined from 0 to 220 nL/min. The ion intensity increased regularly with flowrate, up to 180 nL/min consistent with a mass-flux sensitive detector. However, this increase in ion signal was not linearly proportional to the flowrate, suggesting a behavior intermediate between a mass-flux and a concentration dependant detector. At flowrates greater than 180 nL/min the ion intensity reached a plateau, and the response resembled that of a concentration sensitive detector for the continuous infusion of sample (i.e., peak height is independent of flowrate). The question of mass spectrometer response as a function of flowrate in terms of both peak height and peak area is an important consideration for the construction of a nanoelectrospray interface for CZE-ESMS. Ideally, a flowrate that gives maximum peak detectability without compromising separation efficiency is preferred.

In CZE-ESMS experiments using nanoelectrospray ionization the flowrate is determined by both the i.d. of the nanosprayer tip and the electroosmotic flow. If the tip i.d. is too small, the flow is restricted and the flowrate is decreased to such an extent that the time for analysis is impractically long. The low flowrates generated by tip apertures of 1-2 μm allow for long analysis times in infusion experiments, and this is the basis of the nanoelectrospray interface developed by Mann and coworkers [55-57]. For larger i.d. tips, stabilizing the Taylor cone becomes more difficult because larger droplets are formed during the electrospray process, resulting in a loss of sensitivity.

For CZE-ESMS, the electroosmotic flow (eof) generated by each coating was determined by filling the CZE column with a peptide standard (Leu-enkephalin, 10 μg/mL) dissolved in the electrolyte used for separation (0.1 M formic acid), and measuring the length of time required to electro-infuse the solution through the capillary. The rates of eof, measured in this way, were all within the 150-250 nL/min range for a 20 μm i.d. tip. With the smaller i.d. tips (10 μm), the flow restriction led to lower flowrates, longer analysis times, and frequent blockages. With larger i.d. tips (25 μm), a stable spray was more difficult to maintain at the flowrate now controlled by the eof. The 20 μm i.d. tips were

found to be a suitable compromise between sensitivity and separation efficiency, and were used for the investigations described below.

3.3 Capillary Coating and Separation Efficiency

The use of acidic buffers with bare fused silica capillaries results in reduced flowrate (eof) and adsorption of cationic analytes by surface silanol groups [100,101]. The flowrate can be manipulated by chemically modifying the inner surface of the capillary with dynamic coating agents or covalent modifications [12]. In order to reduce analyte/wall interactions, the preferred CZE-ESMS method for the separation of analytes of interest in the positive ion mode uses volatile buffers at acidic pH values together with cationic coating of the capillary. Thus, construction of a practical nanospray source for CZE-ESMS involves both optimization of the nanosprayer tip inner diameter and modification of the capillary surface, to give a flowrate compatible with both stable electrospray and a fast, efficient separation. For these reasons a series of coatings was investigated for use with the nanoelectrospray CZE-ESMS interface (Figure 3.4).

The most widely reported cationic coating used for CZE-ESMS is (3-aminopropyl)trimethoxysilane (APS) [94,102,103]. With the one-piece column and nanoelectrospray interface the coating provided a relatively fast eof, compatible with the nanosprayer, but the separation efficiency for a mixture of 10 peptides was poor (Figure 3.5a).

The use of dynamic capillary derivatization with Polybrene for use with CZE-ESMS has been reported [14,92,95], and is especially well suited to the butted-tip version of the nanoelectrospray interface, since the column and the tip can be coated relatively quickly and at the same time. The shortcomings of this method are the requirement for recoating between analyses, and the higher incidence of tip blockage from the multiple rinsing steps.

a) Aminopropyltrimethoxysilane (APS)

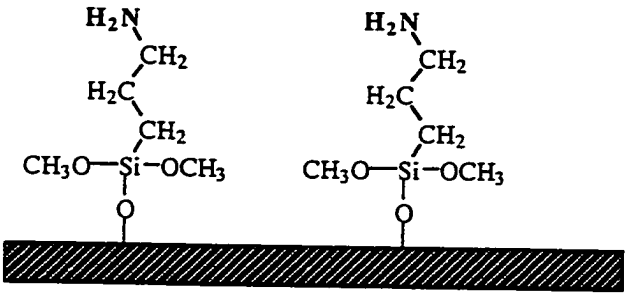

b) Polybrene (hexadimethrine bromide)

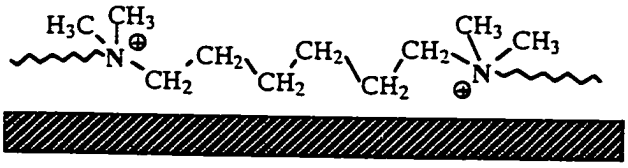

c)

BCQ

[(Acryloylamino)propyl]-trimethylammonium chloride

MAPTAC

[3-(Methyacryloylamino)propyl]-trimethylammonium chloride

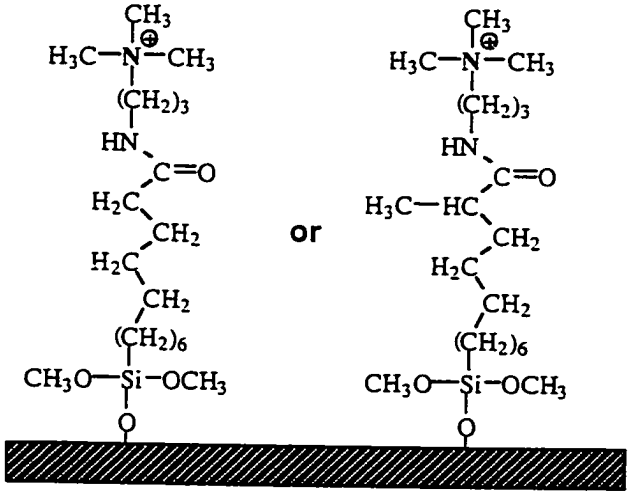

Figure 3.4 Schematic of the different capillary surface modification agents used.

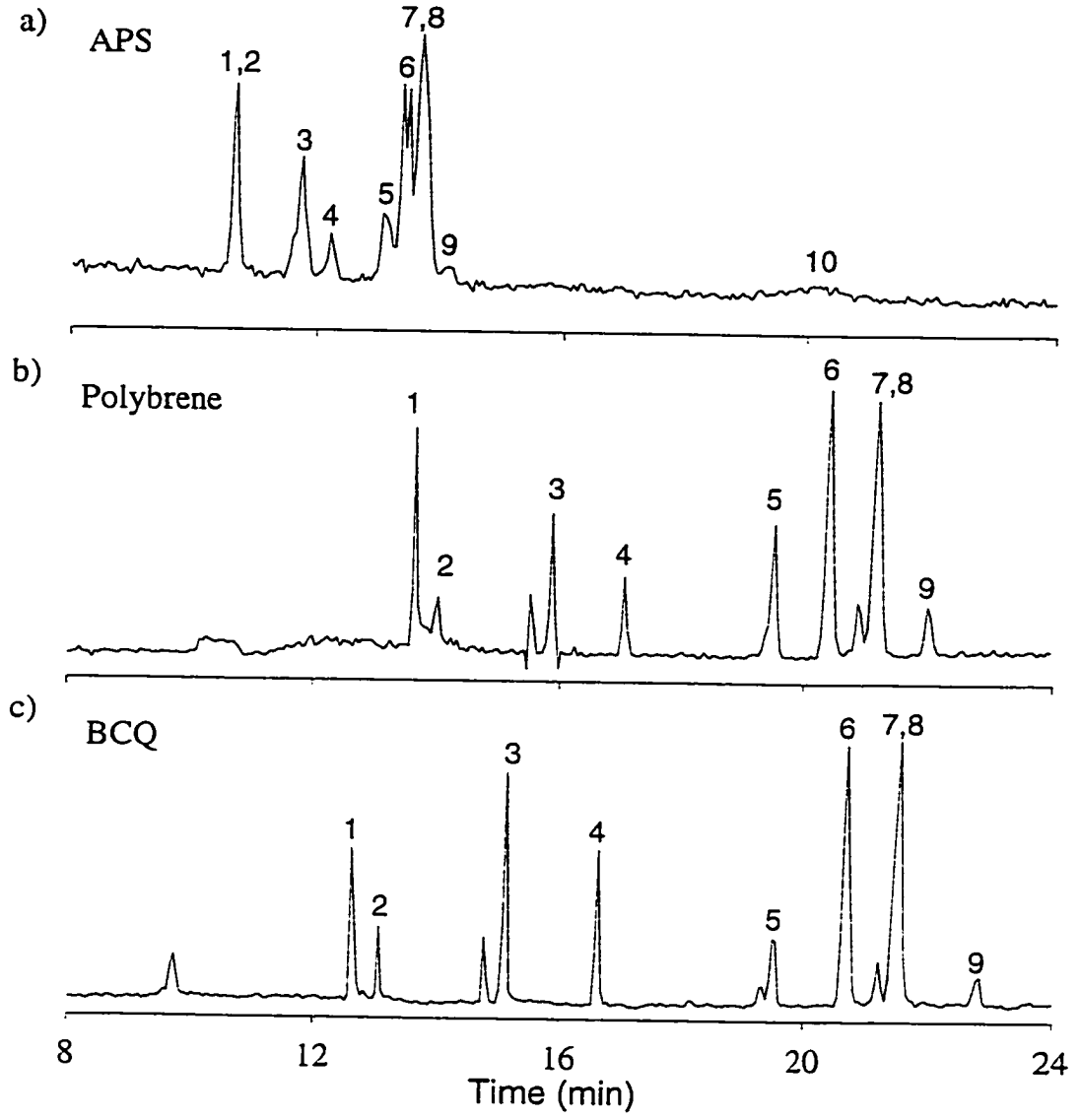

Figure 3.5 Effect of capillary coating and interface arrangement on separation efficiency for nanoelectrospray CZE-ESMS analysis of a peptide mixture. CZE conditions: 1 m columns, 20 μm i.d. tips, -28 kV, 0.1 M formic acid, 20 picograms of each peptide injected. a) One-piece column with aminopropylsilane coating, b) butted-tip with Polybrene coating, and c) one-piece column with BCQ coating (the MAPTAC coating gave same result). 1) Leu-enkephalin, 2) Glu-Fibrinogen, 3) Substance P 3-11, 4) Cholecystokinin 10-20, 5) Substance P 1-9, 6) Angiotensin I, 7) Val4, Ile7 Angiotensin III, 8) ACTH 4-10, 9) pGlu4-Myelin Basic Protein (MBP) 4-14, and 10) ACTH 11-24.

The separation efficiency of this coating with a butted tip arrangement (Figure 3.5b) is greatly enhanced relative to that obtained using the APS coated capillary (Figure 3.5a).

The inner surface of CZE columns was also covalently modified with MAPTAC and BCQ, coatings not previously used for CZE-ESMS. The molecular structures of the two reagents differ only by a single methyl group, and their performance in the present context was similar for the separation of the 10-peptide mixture using a one-piece nanoelectrospray column (Figure 3.5c). Good resolution and peak shape were obtained, and the separation is comparable to that obtained using the Polybrene coating. Moreover, the use of a covalent coating is advantageous, requiring only a buffer rinse between analyses. In addition, a comparison of the separations in Figures 3.5b and 3.5c demonstrates that the butted tip arrangement does not degrade the performance relative to that of the one-piece nanoelectrospray column. The comparison of separation efficiencies obtained for the different coatings and construction arrangements investigated is presented in Table 3.1. As observed, both Polybrene- and BCQ-coated capillaries yielded theoretical plates significantly higher than those obtained using the APS-coated column, and separation efficiencies typically exceeded 150,000 plates for most of the peptides analyzed. An additional advantage of the eof observed with both polybrene and BCQ-coated columns is the inherent improvement in peak resolution and lower chemical background contribution (Figure 3.5).

3.4 Performance of the Butted tip Nanoelectrospray Interface

As mentioned above, the butted tip interface using the Supelco connector gave the same separation efficiency as the one-piece nanoelectrospray columns for the separation of a mixture of peptides. Previously, detection limits in the attomole range have been demonstrated for one-piece nanoelectrospray CZE-ESMS, using selected ion monitoring [33], and the butted tip arrangement was examined to test whether this reponse was

maintained. The sensitivity of the interface in full scan acquisition mode was also of interest for analyzing unknown samples or complex mixtures such as protein digests.

Table 3.1 Comparison of separation efficiencies for different capillary coatings[a].

Peptides	m/z	Theoretical Plates		
		APS	Polybrene	BCQ
Leu-Enkephalin	556	62 000	185 000	352 000
Glu-Fibrinogen	786	38 000	185 000	380 000
Substance P_{3-11}	548	76 000	249 000	505 000
Cholecystokinin$_{10-20}$	418	49 000	273 000	312 000
Substance P_{1-9}	553	29 000	355 000	355 000
Angiotensin I	433	31 000	230 000	237 000
Val_4Ile_7 Angiotensin III	442	26 000	152 000	152 000
$ACTH_{4-10}$[b]	482	60 000	111 000	256 000
$pGlu_4$-MBP_{4-14}[c]	459	18 000	268 000	288 000

[a] One-piece column for APS and BCQ coatings and butted-tip arrangement for Polybrene.
[b] Adrenocorticotropic Hormone
[c] Myelin Basic Protein

Figure 3.6a shows the full-scan reconstructed ion electropherogram (RIE) for the full-scan CZE-ESMS analysis of a mixture of 10 peptides (10 pg each, injection of 6.25 to 18 fmoles). A S/N ratio of 10:1 in the RIE for angiotensin I , MW 1296 (peak 6 in Figure 3.6a), indicates that a detection limit approaching the 2 femtomole range can be obtained in the full-scan mode. The corresponding detection limits for the other peptides in the mixture ranged from 2 to 10 fmole. The extracted mass spectra for two of the peptides (Figures 3.6b and 3.6c) clearly indicate the excellent S/N ratios obtained for the full scan analysis of low fmole amounts of peptides using the butted tip nanoelectrospray CZE-ESMS interface.

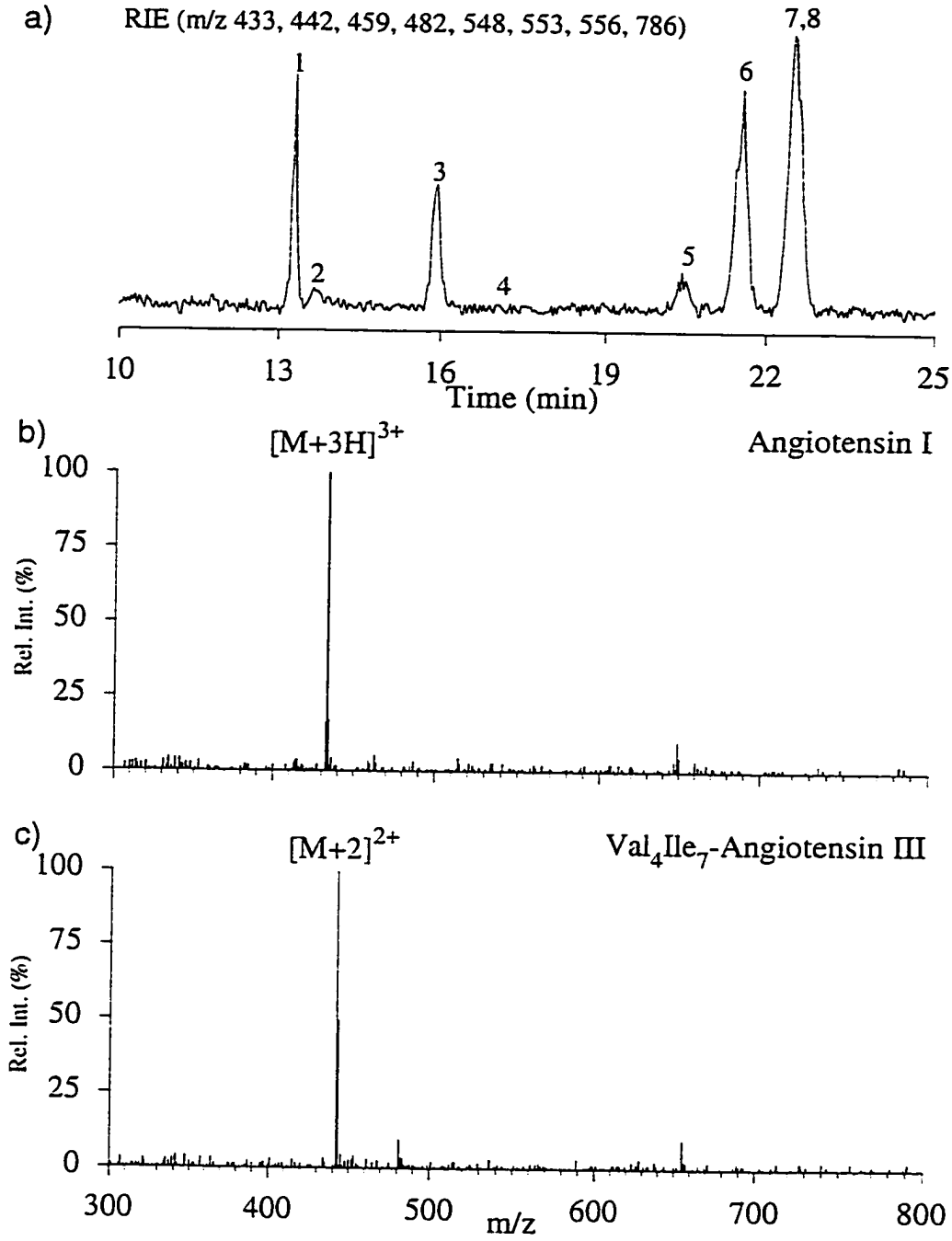

Figure 3.6 CZE-ESMS full scan acquisition analysis of a peptide mixture using the butted-tip nanoelectrospray interface and a BCQ coated column. a) Reconstructed ion electropherograms (Σ 8 ions), extracted mass spectra of b) peptide 6 and c) peptide 7. Separation conditions: Inj. of 1 pg of each peptide, 1 m length column, 20 µm i.d. tips, -28 kV, 0.1 M formic acid, Supelco butt-connector. Peaks labeled as in Figure 3.5.

The peptide mixture used for full-scan analysis was also examined by selected ion monitoring (SIM) to determine the limit of detection under this mode of acquisition. The data obtained are summarized in Table 3.2. For all the peptides analyzed, limits of detection were obtained in the low femtomole range except for Leu-enkephalin for which a detection limit of 160 attomoles was obtained. These limits of detection are comparable with those obtained previously using a single capillary arrangement [32,33].

Table 3.2 Limit of detection for peptides analyzed by CZE-ESMS using a butted capillary arrangement and a BCQ coated capillary.

Peptides	m/z	Amount injected[a]	S/N
Leu-Enkephalin	556	88 fg (160 amol)	2/1
Glu-Fibrinogen	786	1.7 pg (1.1 fmol)	3/1
Val_4Ile_7 Angiotensin III	442	0.9 pg (1.1 fmol)	7/1
$Cholecystokinin_{10-20}$	418	0.9 pg (700 amol)	5/1
Substance P_{1-9}	553	0.9 pg (770 amol)	5/1
Angiotensin I	433	1.7 pg (1.3 fmol)	2/1
Substance P_{3-11}	547	1.7 pg (1.6 fmol)	2/1

[a] Injection of 22 nL of a peptide solution.

The use of the CZE-ESMS interface with disposable nanoelectrospray emitters was particularly well suited to unattended operation, and yielded reproducibility comparable to that obtained using single capillary configurations. The reproducibility of the data produced by the present sheathless CZE-ESMS interface was investigated via an unsupervised overnight run. Replicate injections of a 1 μg/mL solution of the same peptide mixture described above were analyzed over an 8-hour period. The relative standard deviations (RSD) obtained for migration times and peak areas of each peptide are presented in Table 3.3. Excellent reproducibility of migration times was obtained, with RSD values less than 0.9 % for all peptides. Over the eight hours of operation, the reproducibility of peak areas

(n=10) for the peptides ranged from 3-9% RSD with a mean value of 5.8%. It is noteworthy that replicate injections conducted using CZE-UV, with an untapered BCQ-coated column of the same dimensions, gave RSD values of 2-7% for peak areas. The peak area reproducibility of the sheathless CZE-ESMS interface is thus comparable to those obtained using CZE-UV, although some variability is expected between individual columns prepared in a similar fashion. Microsprayers produced in this fashion were found to last for at least 3-4 days of uninterupted operation. An inherent advantage of such an interface design is the possibility of changing the microsprayer independently from the CZE column if tip blocking occurrs.

Table 3.3 Reproducibility of migration times and peak areas for CZE-ESMS separations conducted using a BCQ coated capillary and a butted tip.

Peptides	m/z	Retention Time RSD	Peak Area RSD
Leu-Enkephalin	556	0.99	3.56
Glu-Fibrinogen	786	0.91	5.64
Cholecystokinin$_{10-20}$	418	0.75	3.81
Substance P$_{1-9}$	553	0.41	5.44
Angiotensin I	433	0.38	8.81
Val$_4$Ile$_7$ Angiotensin III	442	0.42	7.12
ACTH$_{4-10}$[a]	482	0.30	7.48
pGlu$_4$-MBP$_{4-14}$[b]	459	0.63	5.18

[a] Adrenocorticotropic Hormone
[b] Myelin Basic Protein

3.5 Conclusions

The method described here for coupling nano-electrospray technology with CZE provides attomole sensitivity in the separation and detection of peptides. It is essential to optimize flowrates by adjusting both the i.d. of the nanosprayer tip and the electroosmotic

flow. Optimization of tip geometry and capillary coating indicated that 20 μm i.d. tips with BCQ or Polybrene capillary coatings gave the best analytical performance under the acidic conditions compatible with positive ion detection. Butted nanoelectrospray tips gave the same performance as one-piece nanoelectrospray columns, but with less time-consuming construction. The tips used in this work provided degrees of ruggedness at least equaling, and in most cases surpassing, previously described methods for interface fabrication.

Chapter 4

4.0 Preconcentration CZE-ESMS

As mentioned in the introduction, a major limitation of CZE is its poor concentration detection limits resulting from the small injection volumes needed to maintain separation efficiency. The use of a preconcentrator (a small bed of C_{18} material) allows for the injection of volumes much larger than the total volume of the capillary. This chapter discusses results obtained using a chromatographic preconcentration step online with the CZE separation and nanoelectrospray MS detection (PC-CZE-nESMS). Parameters such as choice of stationary phase, elution volume and sample carry over (memory effects) were studied. When coupled with the nanoelectrospray interface, full-scan analysis at the fmole/μL level was readily obtained for the separation of peptides.

4.1 Co-axial CZE-ESMS and PC-CZE-ESMS

Initially a co-axial interface was used to develop the conditions necessary for the reliable use of a preconcentator on-line with CZE-ESMS. The BCQ-coated capillaries, previously shown to be compatible with the separation of peptide mixtures and protein

digests, were used in all experiments [32]. Selected ion monitoring (SIM) was used with a mixture of standard peptides in order to compare detection limits as well as to assess the effect of the preconcentrator on CZE performance. A typical CZE-ESMS analysis of a mixture of seven peptides (1 μg/mL each) is shown in Figure 4.1. The concentration used was close to the detection limits for some of these peptides; the limits of detection are summarized in Table 4.1.

Table 4.1 Limits of detection for peptides analyzed by co-axial CZE-ESMS and PC-CZE-ESMS.

			Limits of Detection			
			CZE		PC-CZE	
Peptide	**m/z**	**M_r**	**nM**	**fmol**	**nM**	**fmol**
Cholecystokinin 10-20	418	1251	800	22	6	6
Angiotensin I	433	1296.5	800	20	4	4
Val^4, Ile^7 Angiotensin III	442	883	300	10	4	3.4
Substance P 3-11	548	1094	700	18	2	2.3
Substance P 1-9	553	1104	400	11	1	1
Leu-Enkephalin	556	555	140	4	1	1
Cholecystokinin 10-20	626	1251	800	22	8	8
Glu-Fibrinogen	786	1570.6	250	8	1	1.3

The separation of the same mixture of peptides (0.01 μg/mL each) using a preconcentrator constructed from the 40 μm irregular C_{18} material (as described in section 2.7) is shown in Figure 4.2. The peak at 9 min is due to organic solvent migrating with the eof. Despite the two orders of magnitude decrease in concentration, the signal to noise ratio (S/N) for this analysis is at least equal and in most cases better than the analysis without the preconcentrator (Table 4.2). Detection limits based on a 4 μL injection volume are summarized in Table 4.1. Absolute detection limits in the low femtomole range were obtained for the two analyses, with the PC-CZE analysis being 2.75 to 11 times more

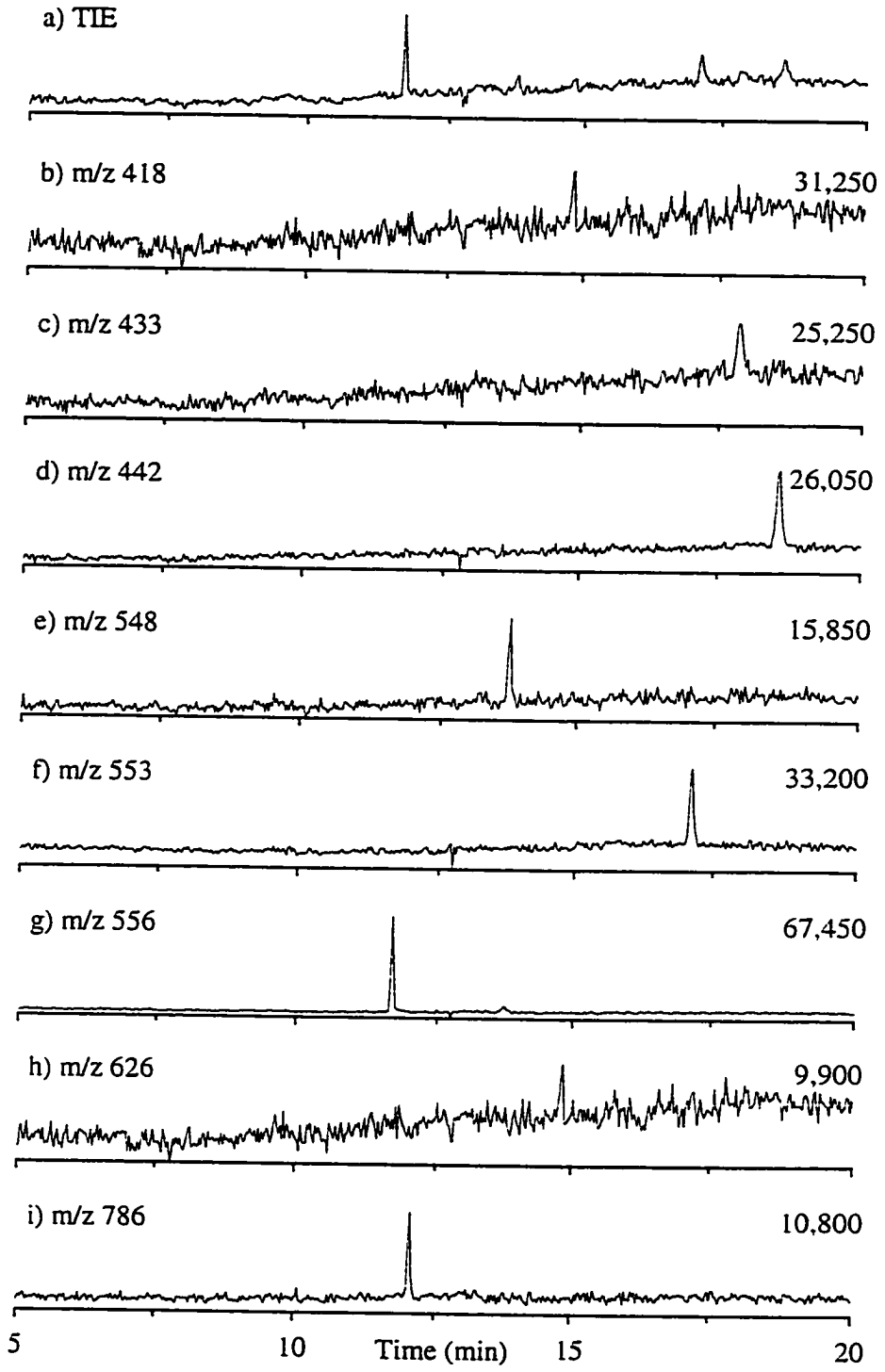

Figure 4.1 Co-axial CZE-ESMS analysis of a mixture of seven peptides at the 1 µg/mL level using selected ion monitoring. Separation conditions: BCQ coated capillary (50 µm), 0.1 M formic acid, -30 kV effective, 6 s injection at 100 mbar. (a) Total ion electropherogram, (b) Cholecystokinin 10-20, (c) Angiotensin I, (d) Val^4, Ile^7-Angiotensin III, (e) Substance P 3-11, (f) Substance P 1-9, (g) Leu-Enkephalin, (h) Cholecystokinin 10-20, (i) Glu-Fibrinogen.

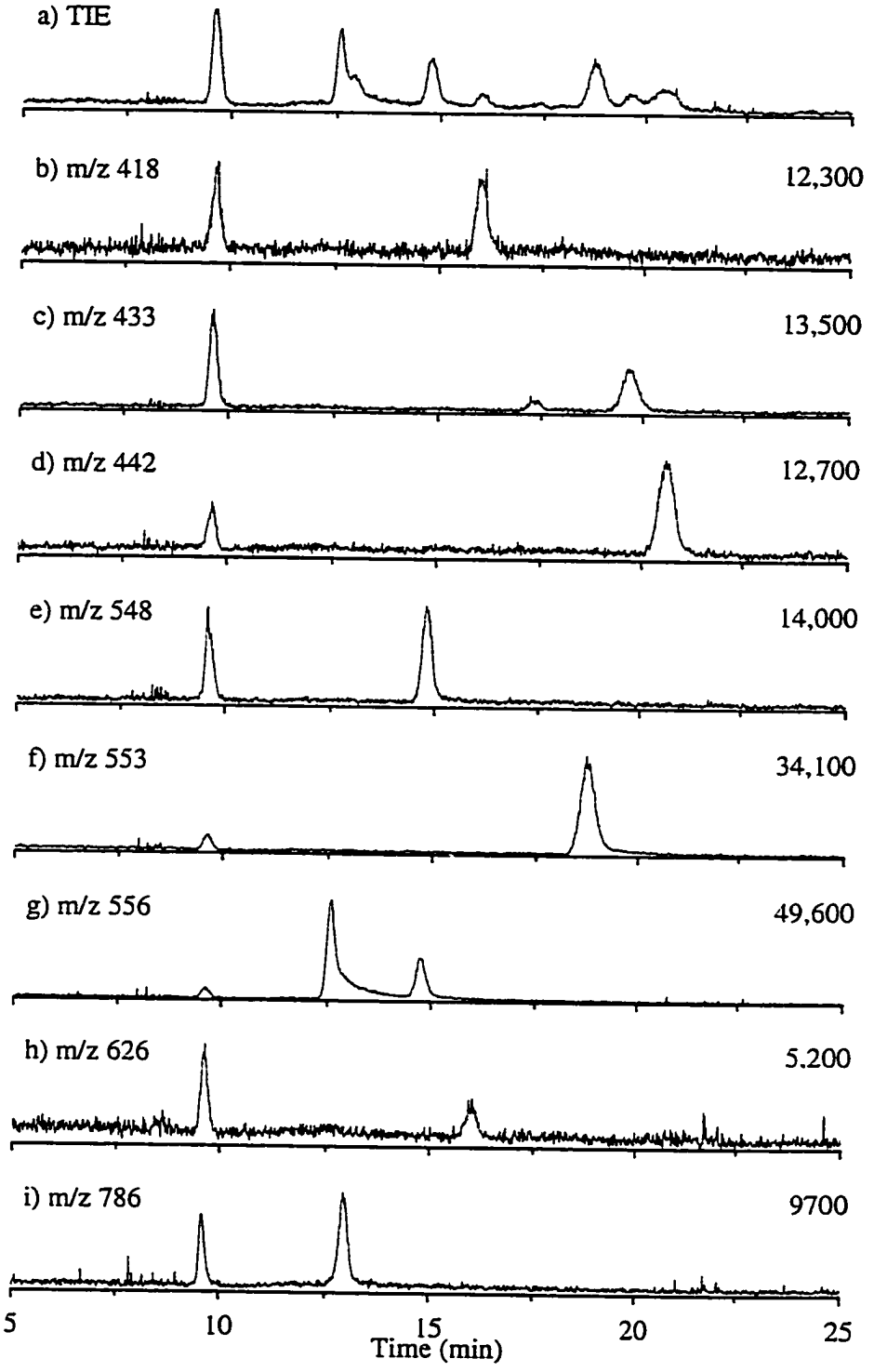

Figure 4.2 Co-axial PC-CZE-ESMS analysis of seven peptides at the 10 ng/mL level using selected ion monitoring. Conditions as for Figure 2 and as noted in the experimental section. Sample injection was 4 min at 1000 mbar.

sensitive. Moreover, the concentration detection limits are 75 to 400 times lower for the preconcentration method. This is due to the much larger injection volume (4000 nL vs. 30 nL). The variation in detection limits observed for different analytes indicates that selective enrichment is occurring, i.e., some peptides are retained more strongly than others. This phenomenon is discussed in more detail below.

The separation efficiency of the preconcentration method is only 1/10th to 1/20th of that obtained under the standard CZE separation conditions (Table 4.2). Development of conditions that eliminate the loss in efficiency would produce even lower detection limits through an increase in S/N. Improved PC-CZE performance in conjunction with nanoelectrospray CZE-ESMS would also provide improved sensitivity, which is necessary for full-scan acquisition at low analyte concentrations.

Table 4.2 Theoretical plate values and signal to noise ratios for the analysis of peptides by co-axial CZE-ESMS and PC-CZE-ESMS.

		Theoretical Plates (N)		S/N	
Peptide	**m/z**	**CZE**	**PC-CZE**	**CZE**	**PC-CZE**
Cholecystokinin 10-20	418	216 000	13 600	1.5/1	4/1
Angiotensin I	433	122 000	10 300	2/1	6/1
Val^4, Ile^7 Angiotensin III	442	234 000	9 900	9/1	9/1
Substance P 3-11	548	288 000	18 900	4/1	12/1
Substance P 1-9	553	197 000	11 850	7/1	30/1
Leu-Enkephalin	556	207 000	15 600	40/1	46/1
Cholecystokinin 10-20	626	147 000	13 600	1/1	2/1
Glu-Fibrinopeptide B	786	221 000	16 570	7/1	16/1

4.2 Nanoelectrospray CZE-ESMS and PC-CZE-ESMS

The use of a nanoelectrospray mass spectrometry (nESMS) with CZE provides detection limits in the low femtomole range for the full-scan analysis of peptides [32]. An example of a CZE-nESMS analysis of a mixture of 9 peptides (10 µg/mL each, Table 4.3)

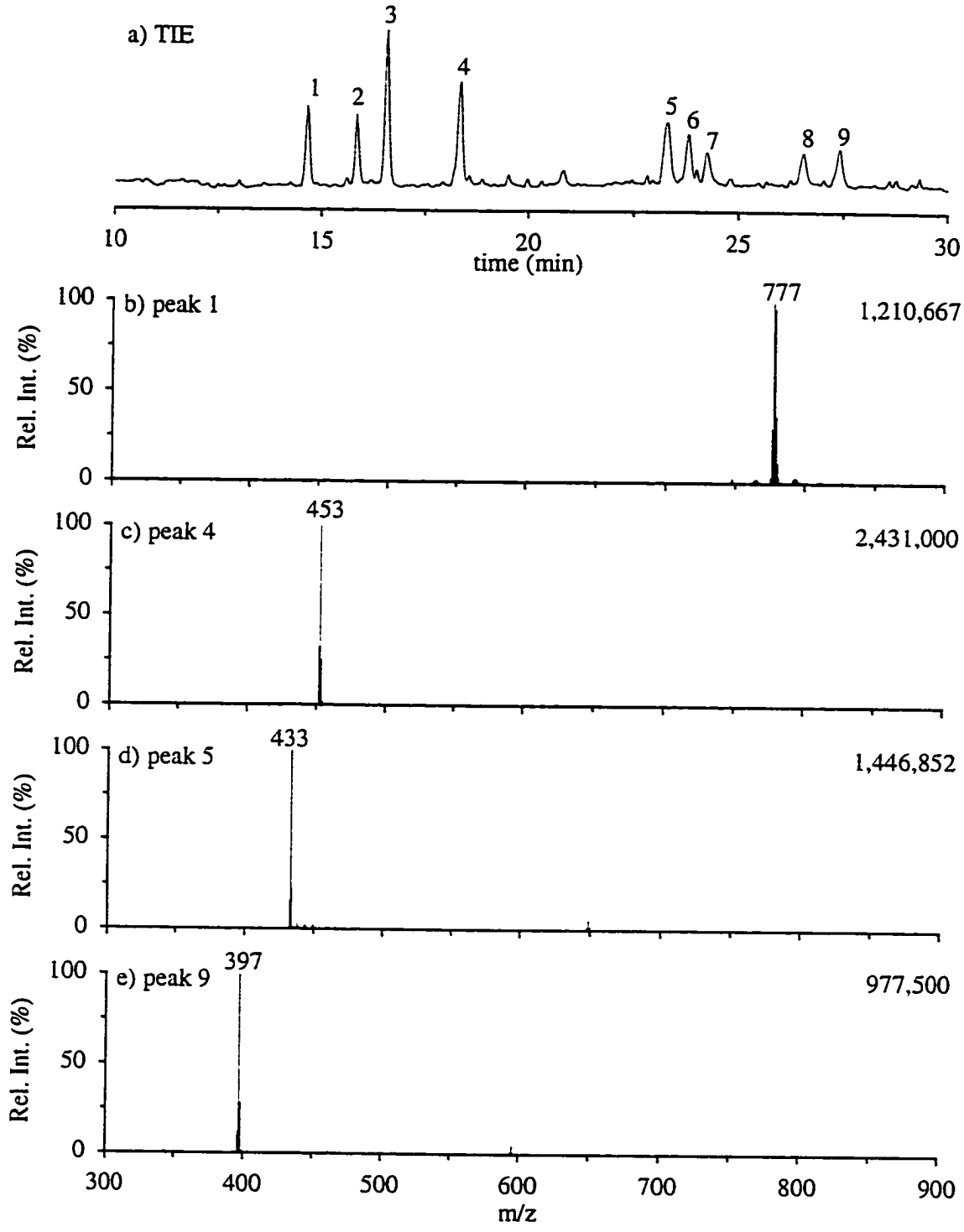

Figure 4.3 CZE-nESMS analysis of a mixture of nine peptides at the 10 µg/mL level using full-scan acquisition. Separation conditions: BCQ coated capillary (50 µm), 0.1 M formic acid, -22 kV effective, 6 s injection at 100 mbar. (a) Total ion electropherogram, (b) Neurotensin 1-6, (c) des-Arg-Bradykinin, (d) Angiotensin I, (e) Lys-Bradykinin.

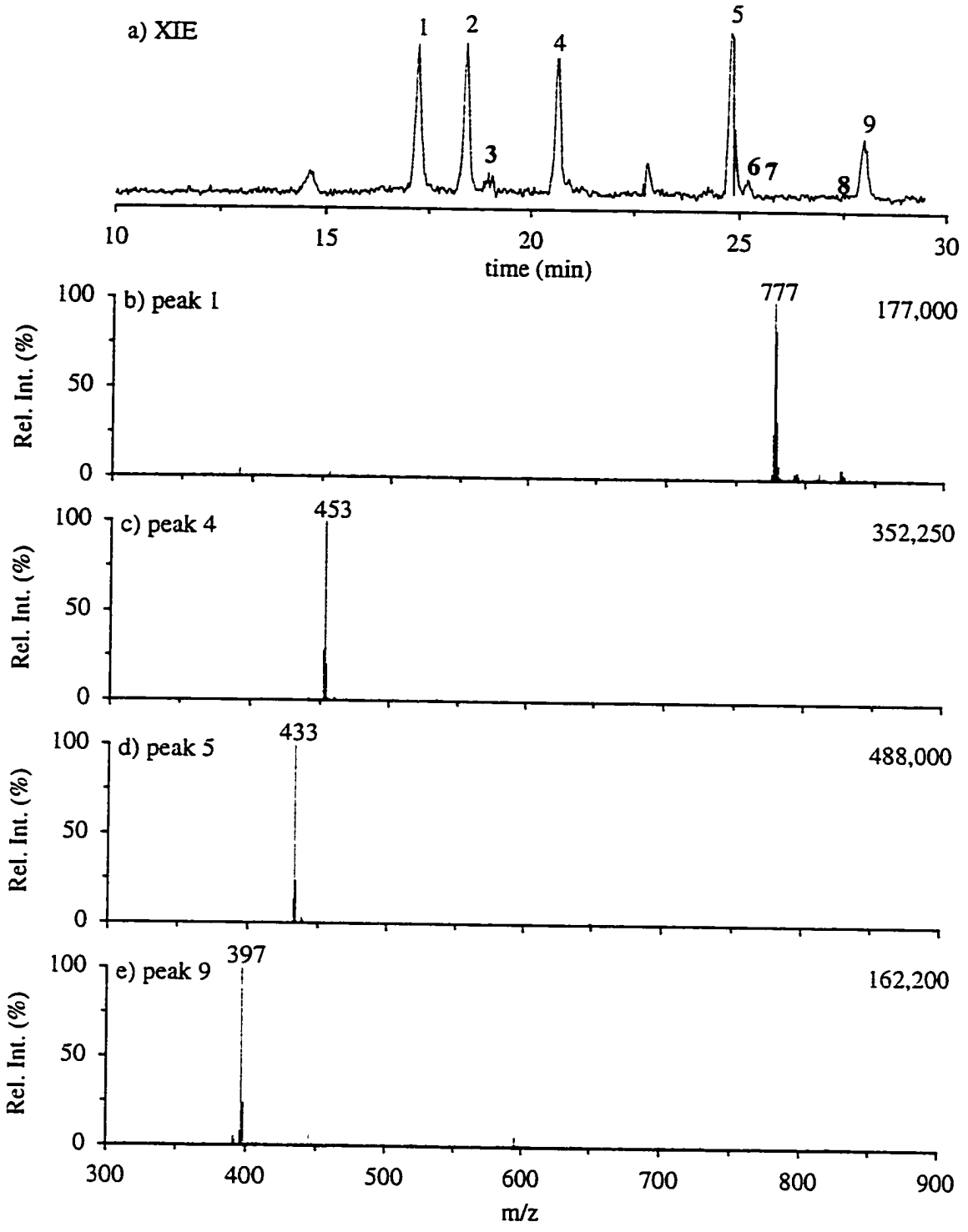

Figure 4.4 PC-CZE-nESMS analysis of a mixture of nine peptides at the 100 ng/mL level using full-scan acquisition. Conditions as for Figure 4.3 and as noted in the experimental section. Sample injection was 4 min at 1000 mbar.

is shown in Figure 4.3. Representative full-scan mass spectra extracted from the crests of peaks are shown in Figure 4.3b-e. The corresponding CZE analysis using a preconcentrator on-line with the nanoelectrospray interface (PC-CZE-nESMS) is shown in Figure 4.4. In this analysis the concentration of each peptide is only 0.1 μg/mL. The representative extracted full-scan mass spectra are shown in Figure 4.4b-e.

Table 4.3 The sequence, average molecular mass, pI value and ion monitored for the peptides used to optimize the PC-CZE-nESMS method.

Peak	Peptide	Sequence	M_r	pI[a]	m/z
1	Neurotensin 1-6	pGlu-LYENK	776	7.1	777
2	Glu-Fibrinopeptide B	EGVNDNEEFFSAR	1570.6	4.2	786
3	Lys^3-Bombesin	pGlu-EKLGNQWAVGHLM-NH_2	1592	8.2	797
4	des-Arg-Bradykinin	PPGFSPFR	904	11.3	453
5	Angiotensin I	DRVYIHPFHL	1296.5	7.0	433
6	des-pGlu-LH-RH[a]	HWSTYGLRPG-NH_2	1071	10.5	536
7	Melittin	GIGAVLKVLTTGLPALISWIKR KRQQ-NH_2	2847	12.6	570
8	Thymopoietin 32-36	RKDVY	680	10.3	341
9	Lys-Bradykinin	KRPPGFSPFR	1188	12.6	397

[a] Calculated using MacBioSpec version 1.0.1 (PE-SCIEX).

There are several features of note in the PC-CZE-nESMS analysis (Figure 4.4a), the most prominent being the change in the separation profile. Four of the peaks in the CZE-nESMS analysis are not present or have reduced intensity in the PC-CZE-nESMS analysis. Also, the relative intensities of some peaks have changed. The loss of peaks for some of the peptides can be attributed to several factors including non-retention of analyte during sample loading, wash-off of analyte during separation electrolyte rinsing or non-elution of analyte from the stationary phase. An understanding of these effects is important in developing a reliable technique. Consideration of these factors led to experiments aimed at optimizing the choice of stationary phase and elution volume to reduce sample loss and maximize separation efficiency.

4.3 Stationary Phase Comparison

Three different stationary phases were evaluated for use in the preconcentrator: 40 μm aminopropyl particles, 40 μm C_{18} particles and 5 μm C_{18} particles. Each phase was evaluated for its ability to retain analyte during sample loading and electrolyte rinsing, and release sample during elution (eg. minimum memory effects). Each preconcentrator was initially conditioned using the protocol described in the Section 2.7. The peptide mixture used in Figure 4.3 (100 ng/mL) was injected (6 min, 1000 mbar), followed by rinsing with separation electrolyte (6 min, 2000 mbar) and triplicate elutions with the elution solvent (0.5 min, 100 mbar). These rinses were monitored using selected ion monitoring and the total ion currents (TIC) for these analyses are shown in Figure 4.5.

The aminopropyl phase (Figure 4.5a) had the least retentive properties of the three test phases as evidenced by the large peak at 4 to 8 min. The split in the middle of this peak (and of those for the other phases) is due to the switch from sample to separation electrolyte. The poor retention of analyte on this phase is not suprising considering its polar nature and short hydrophobic chain. This phase was tested because of its compatibility with the cationic coating on the capillary and its charged nature assisted in maintaining the electroosmotic flow. Early experiments used a mixed C_{18}/aminopropyl phase to prevent loss of current due to low eof generated in the uncharged C_{18} phase. This problem was overcome when a smaller bed of material (1 mm) was used in subsequent experiments.

The 40 μm C_{18} phase had the least sample breakthrough and wash-off as revealed by the low intensity peak generated between 4 and 8 min in Figure 4.5b. The elution of sample appeared to be efficient. However, memory effects were apparent with multiple elutions. The 5 μm C_{18} material (Figure 4.5c) had retention properties less favourable than the 40 μm C_{18} particles. This phase appeared to have better elution properties as the

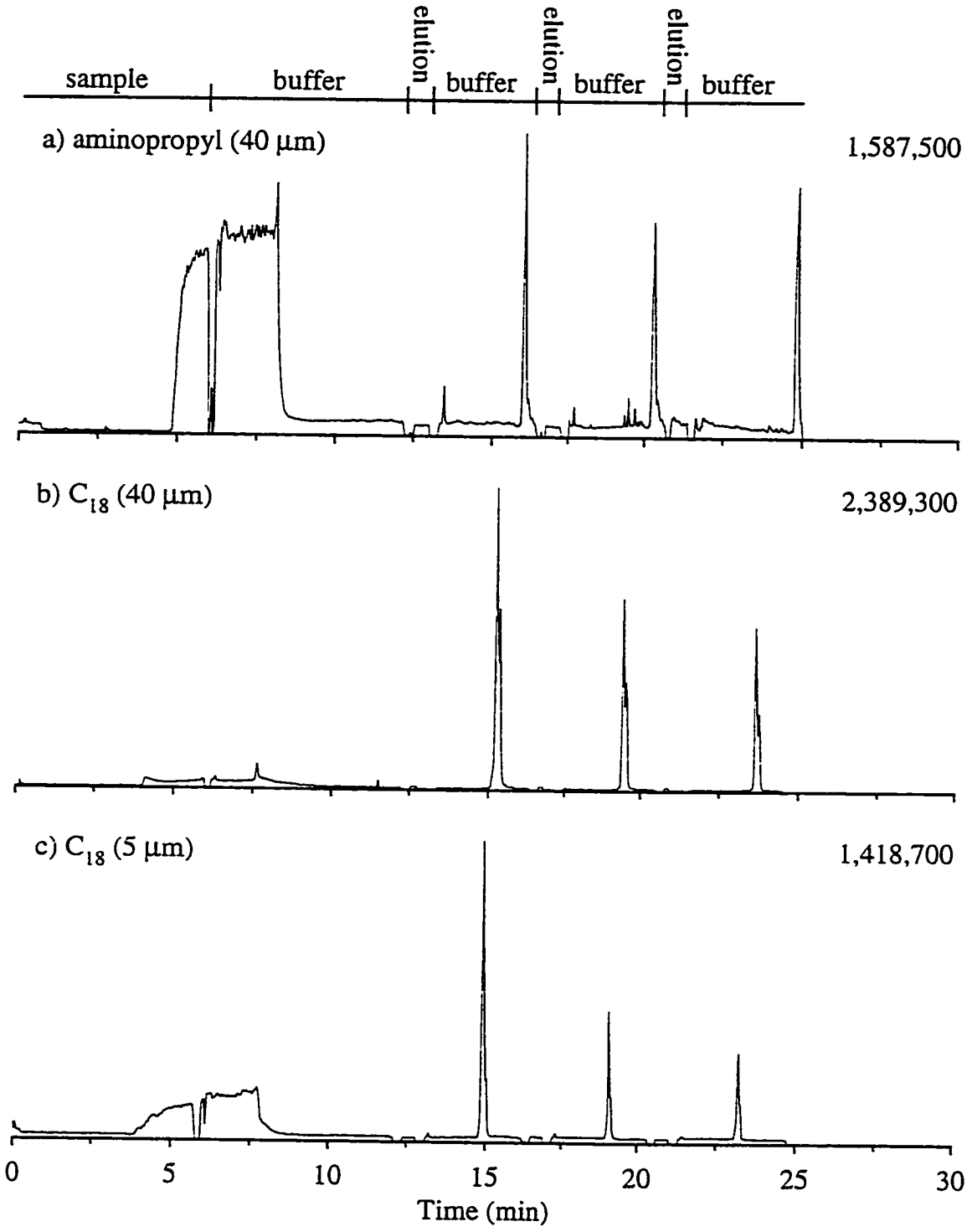

Figure 4.5 Comparison of stationary phases using flow injection nESMS. (a) 40 µm Aminopropyl particles, (b) 40 µm C18 particles, (c) 5 µm C18 particles. Buffer was 0.1 M formic acid and elution solvent was 90:10 acetonitrile/1% HCl.

intensity of the eluted peak decreased more rapidly than with the other phases. However, the requirement for frits made the construction more time consuming and less attractive. Therefore the 40 μm C_{18} phase was used in all subsequent experiments.

It should be noted that the intensity of the peptide elution peaks is also a result of background ions generated by the elution buffer. The intensity of these ions varies depending on the optimization of the interface and is different for each set of experiments. The memory effects shown by the phases are due to background ions as well as to peptides not extracted in the first elution.

4.4 Multiple Elutions and Memory Effects

The evaluation of the different phases revealed that individual peptides were retained to different extents; some peptides were lost during the sample loading and rinsing stages and others remained bound to the preconcentrator even after multiple elutions. Loss of peptides during sample injection and elution was minimized by using the optimal bed material as discussed above. Losses due to rinsing prior to separation are dependent on the electrolyte used. The use of 0.1 M formic acid was a compromise between sample loss and separation efficiency. Higher acid concentration provides better separation efficiency but at the expense of sample loss due to the higher organic content.

The selectivity or discrimination for some peptides was investigated using a single injection of sample followed by five separate elutions and CZE separations (Figure 4.6). A large elution volume was used to maximize sample recovery at the expense of separation efficiency. This allowed for a higher recovery of peak 3 in this instance relative to Figure 4.4. Peak areas calculated for each electropherogram (Table 4.4) indicate that smaller amounts of peptide are detected with each successive elution. However there is anomalous behaviour for some of the peptides. For instance, thymopoietin$_{32\text{-}36}$ (peak 8) appears in only the first analysis with a low intensity, indicating that most of this compound is not

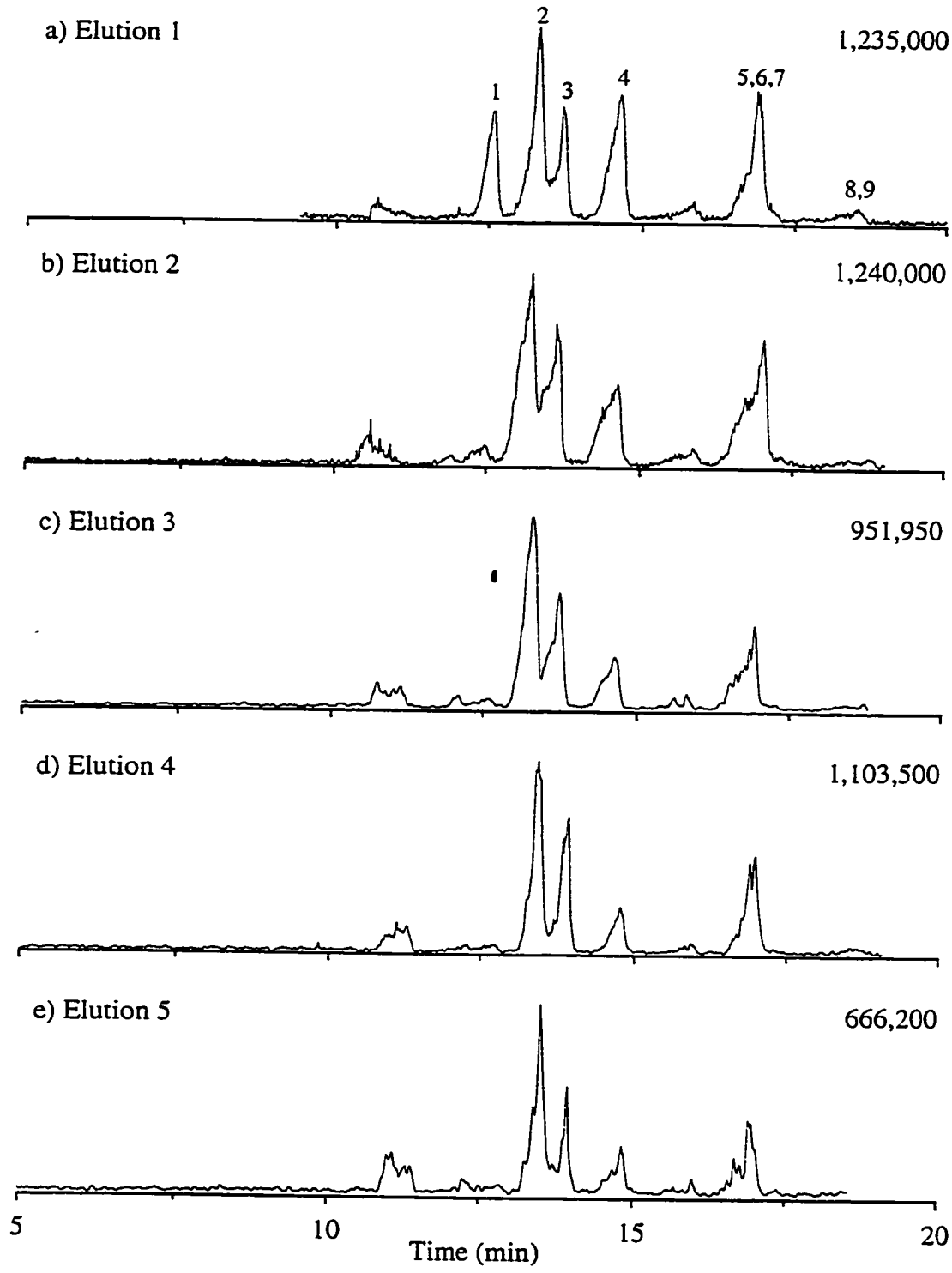

Figure 4.6 Effect of multiple elutions on nanoelectrospray PC-CZE-nESMS analysis of a mixture of nine peptides at the 100 ng/mL level. Conditions as for Figure 4.3. (a) Analysis after sample injection, (b)-(e) subsequent elutions without further sample injection.

retained and the remainder is eluted in the first analysis. This peptide has five amino acids and a pI of 10.3 and therefore will be highly ionized in 0.1 M formic acid (pH 2.3). Small, charged molecules undergo limited hydrophobic interaction with C_{18} phases, and this may explain their poor chromatographic behaviour.

Table 4.4 Peak areas for the multiple elution PC-CZE-nESMS analyis of a single injection of a peptide mixture.

		Peak Areas (x10^6) Elution Number				
Peak	Peptide	1	2	3	4	5
1	Neurotensin 1-6	2.8	0.39	0.10	0.11	0.097
2	Glu-Fibrinopeptide B	7.3	9.4	6.8	6.0	3.4
3	Lys^3-Bombesin	5.7	9.1	4.9	4.8	1.6
4	des-Arg-Bradykinin	9.9	8.1	3.4	2.8	1.6
5	Angiotensin I	9.5	11.7	4.9	5.8	1.9
6	des-pGlu-LH-RH[a]	0.93	0.56	0.10	0.24	0.056
7	Melittin	-	0.39	0.0087	-	-
8	Thymopoietin 32-36	0.16	-	-	-	-
9	Lys-Bradykinin	1.3	1.2	0.40	0.54	0.050

[a] Luteinizing Hormone Releasing Hormone

$Neurotensin_{1-6}$ (peak 1) behaves almost ideally; a large signal initially and a relatively small signal in subsequent runs. Recovery for this peptide in the first elution is greater than 75% based on peak areas, assuming no losses occur during loading and rinsing. Melittin (peak 7) is an example of a peptide that is strongly bound to the preconcentrator. The first elution did not show any of this peptide to be present in the analysis, however the next elution had a peak corresponding to this analyte. This can be rationalized by assuming that the peptide was eluted and readsorbed on the stationary phase after moving partially through the bed. The second and third elutions were able to remove the peptide so that it could migrate and be detected. This peptide had the highest molecular weight of the test compounds (26 amino acids, 2847 Da), which permits more hydrophobic interaction with the C_{18} phase and therefore stronger retention.

The peptide with the lowest pI (Glu-Fibrinopeptide B, peak 2) produced the most intense peak in all analyses. The low pI means the peptide will be relatively uncharged in 0.1 M formic acid (pH 2.3), the electrolyte used for CZE separation. Glu-Fibrinopeptide B contains 19 amino acids (1571 Da), and the combination of low pI and relatively high molecular weight makes hydrophobic interactions between the peptide and C_{18} phase favourable. The relatively weakly ionized state of this peptide permits elution with organic solvent, although the volume used in these experiments was not sufficient to completely elute the peptide.

The remaining peptides behaved similarly to Glu-Fibrinopeptide B, with signals that increased from the first elution to the second and then decreased over the last three elutions. The increase in peptide recovery from elution one to elution two indicates that chromatographic separation is occuring in the 1 mm bed of reversed phase material. Figure 4.7 summarizes what is occurring. The peptides are injected and the bed is washed with separation buffer, leaving the sample retained on the C_{18} material (Figure 4.7a). The first elution removes some of the sample from the bed (Figure 4.7b) However, the majority of the sample travels a short distance and is readsorbed on the C_{18} material. These peptides are eluted with the second elution (Figure 4.7c) and subsequently separated and detected. Further elutions (Figure 4.7d) remove the remaining peptides with decreasing signal strength as the amount of peptide on the bed is depleted.

Previous reports of on-line preconcentration methods state that post-analysis rinsing with elution buffer is important to limit sample carry over (memory effects) [104]. The injection of a larger plug of organic solvent to more efficiently extract the analytes prior to separation is not feasible as it leads to poor separation efficiency (see below). An interesting possibility that takes advantage of the incomplete elution of sample would be to carry out multiple analyses from a single injection as demonstrated in Figure 4.6. The goal of PC-CZE is to be able to analyze dilute samples that are usually in limited supply such as

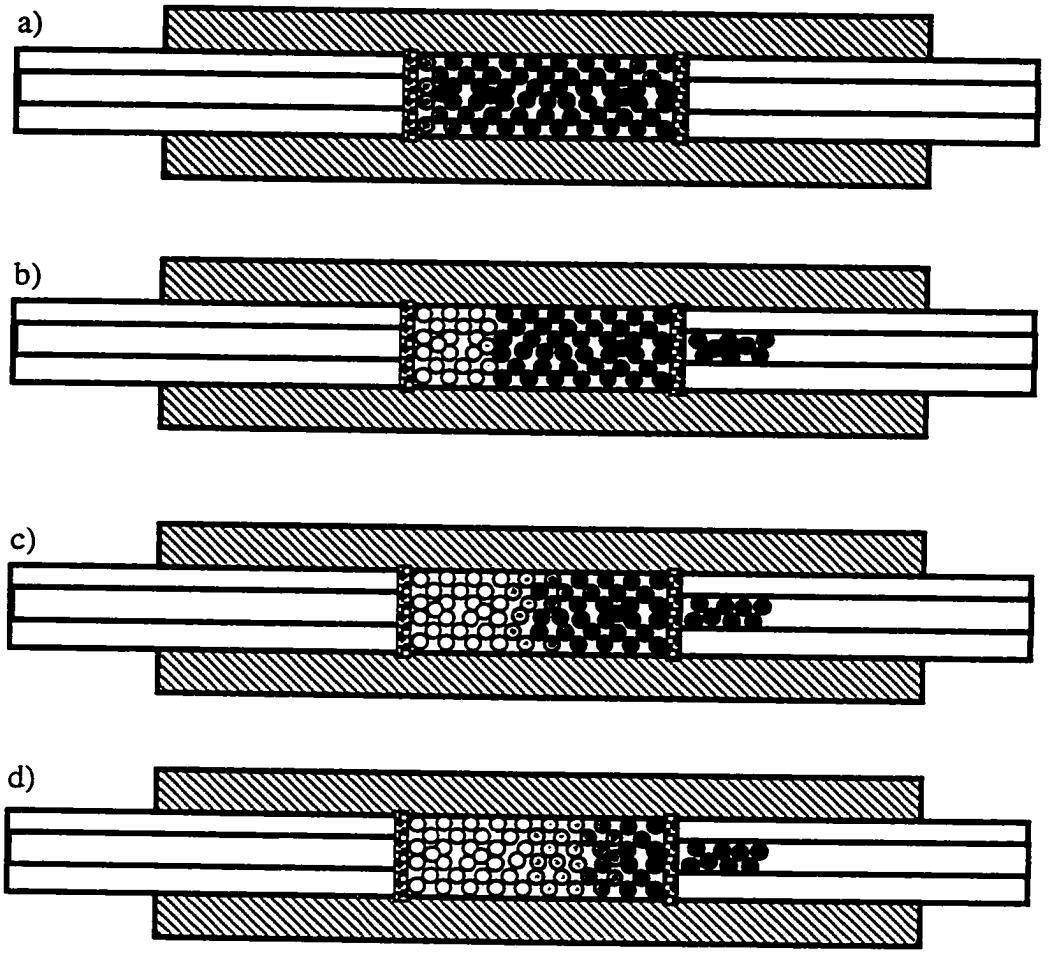

Figure 4.7 Schematic of multiple elutions of peptides from the preconcentrator. (a) The bed after sample loading and washing. (b) The first elution releases some peptides and moves the rest further down the bed. (c) The second elution removes the majority of the peptides. (d) The subsequent elutions remove the remaining peptides.

biological fluids. By using a "single-injection/multiple-elution" protocol, more data could be obtained with less sample wasted. Analytes that are not initially eluted and otherwise go undetected, would be detected using such a protocol. Multiple elutions would be especially useful when using tandem mass spectrometry (MS-MS) to obtain sequence data from peptides. This method would allow for acquisition of MS-MS data from closely eluting or co-eluting peaks in consecutive runs from a single injection of sample.

4.5 Optimization of Elution Buffer Volume

As mentioned above, the use of a larger volume of elution buffer leads to a degradation of separation efficiency. An example of this effect is demonstrated in Figure 4.8. The largest peak in each electropherogram is due to the elution solvent migrating with the eof. The conditions for each analysis of the peptide mixture were identical except for the volume of the elution solvent. The separation carried out using the optimal volume of elution buffer (150 nL) with respect to separation efficiency, gave theoretical plate counts similar to those obtained without the preconcentrator (Figure 4.8a and Table 4.5).

Table 4.5 Effect of increasing elution volume on separation efficiency of PC-CZE-nESMS compared to CZE-nESMS.

Peak	Peptide	Theoretical Plates (N)			
		CZE	PC-CZE (150 nL)	PC-CZE (225 nL)	PC-CZE (300 nL)
1	Neurotensin 1-6	202 000	155 400	37 800	7 700
2	Glu-Fibrinopeptide B	163 000	116 000	42 000	5 250
3	Lys^3-Bombesin	178 000	170 000	25 000	3 200
4	des-Arg-Bradykinin	123 000	140 000	50 000	4 100
5	Angiotensin I	190 500	193 000	51 000	6 400
6	des-pGlu-LHRH[a]	205 000	143 000	-	-
7	Melittin	214 000	-	-	5 000
8	Thymopoietin 32-36	114 000	-	-	-
9	Lys-Bradykinin	180 000	133 000	43 000	8 800

[a] Luteinizing Hormone Releasing Hormone

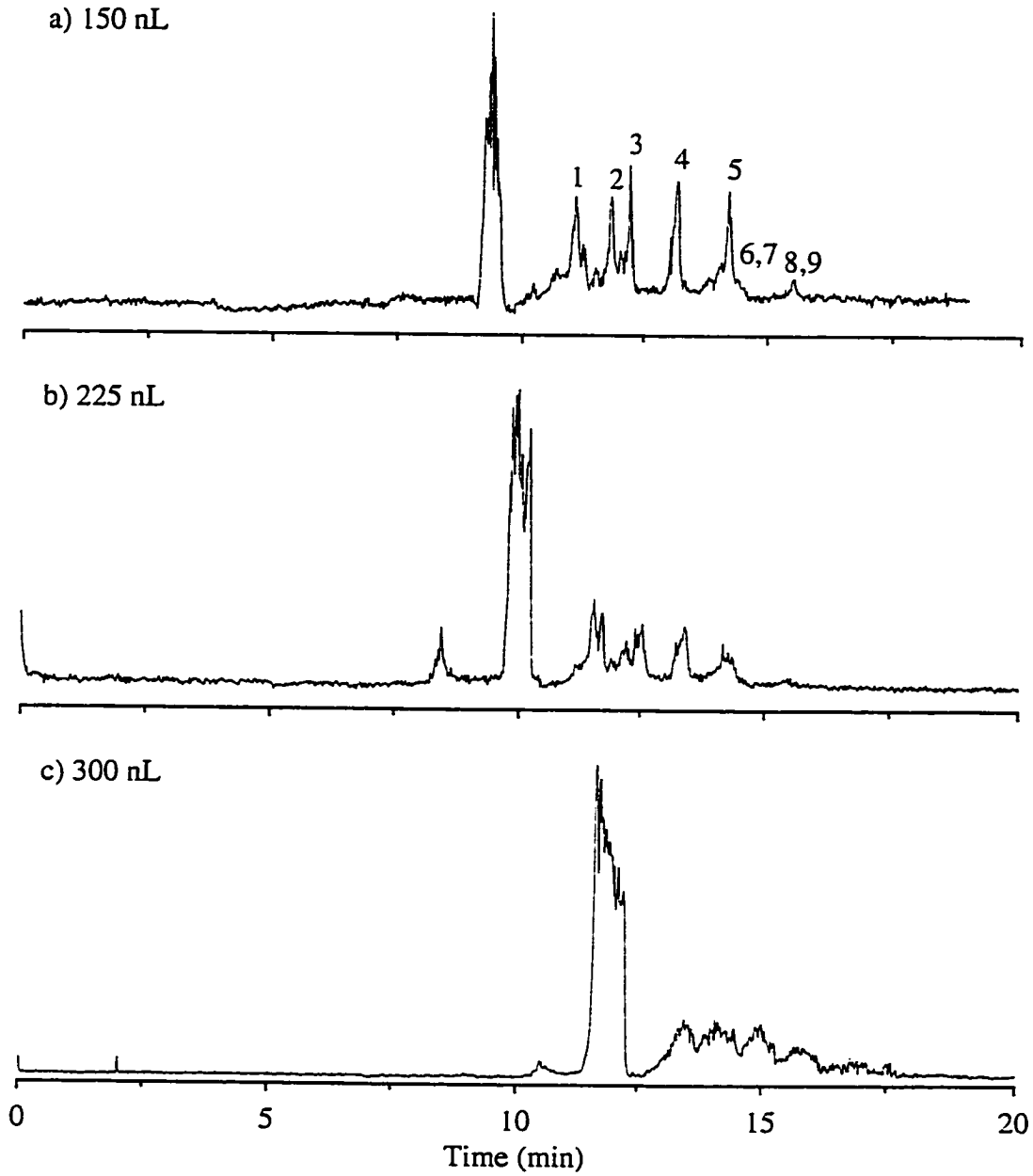

Figure 4.8 Effect of elution buffer volume on separation efficiency. PC-CZE-nESMS analysis of nine peptides at the 100 ng/mL level using full-scan acquisition. (a) 0.2 min elution at 100 mbar, (b) 0.3 min elution at 100 mbar, (c) 0.4 min elution at 100 mbar. Conditions as for Figure 4.3.

Extracted ion current plots for four of the peptides from the above full-scan PC-CZE-nESMS (Figure 4.8a) analysis are presented in Figure 4.9. Signal to noise ratios of 100 to 500 for these peptides indicates that concentration detection limits approaching the amol/μL range can be obtained in the full-scan mode for a 4 μL sample size. The extracted mass spectra for these peptides (Figures 4.9) clearly indicates the excellent S/N ratios obtained for the full-scan analysis of peptides at the 100 pg/μL concentration level using PC-CZE-nESMS. Analysis of more dilute samples could be achieved by the injection of a larger volume of sample.

With increased volumes of elution buffer (225 nL, Figure 4.8b and 300 nL, Figure 4.8c) the efficiency decreases rapidly, with the peaks becoming less resolved and much broader. As the volume of organic solvent is increased, the time for analysis is also lengthened. When the volume of elution buffer is increased further (>300 nL) unresolved peptides are detected only if pressure is applied to the capillary.

Poor CZE performance has been attributed to the presence of large zones of organic solvent between aqueous buffer within the CZE capillary during electrophoresis [105,106]. The organic phase tends to lower the current in the CZE capillary, which results in reduced eof until its dispersion in the separation buffer has occurred. This ultimately leads to zone broadening and increased analyte peak widths and associated peak tailing (Figure 4.8c).

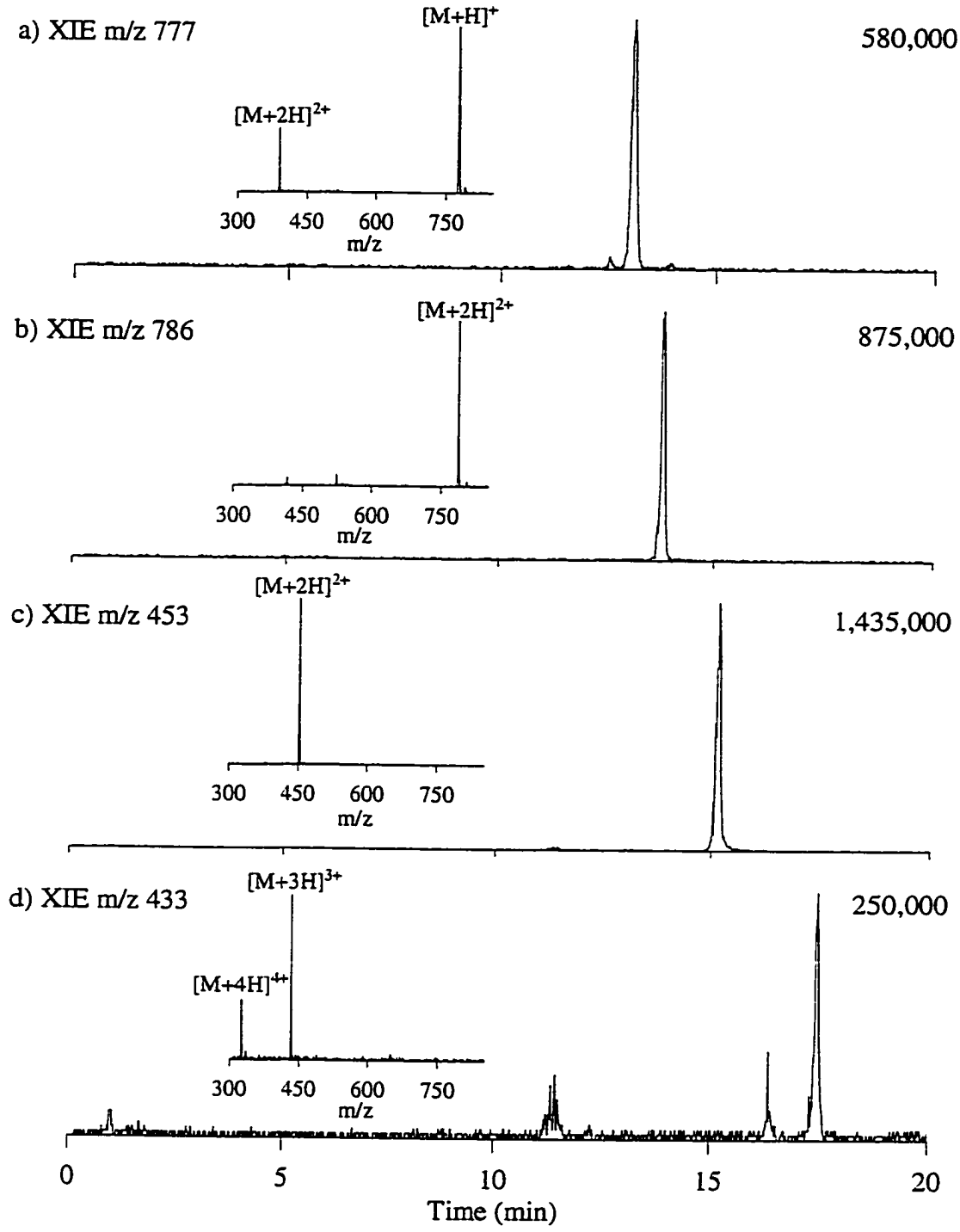

Figure 4.9 Extracted ion electrophergrams and their corresponding mass spectra of four peptides from the PC-CZE-nESMS analysis of nine peptides at the 100 ng/mL level. (a) m/z 777, (b) m/z 786, (c) m/z 453, (d) m/z 433.

4.6 Conclusions

The use of a C_{18}-based solid phase extraction device online with CZE-nESMS allows for the detection of peptides well below the detection limits of conventional CZE-UV and CZE-ESMS methods. Careful consideration of the type of stationary phase used is important in maximizing the effectiveness of this technique for reliable analysis of dilute samples. Awareness of the inherent memory effects of PC-CZE allows this characteristic to be used to the advantage of the operator by permitting multiple analyses from a single injection of sample. Optimized conditions permit the analysis of peptides at the low attomol/μL level.

Development of a simple and rugged preconcentration technique should permit the wider acceptance of CZE as a routine analytical tool. Such an advance would allow the analysis of samples routinely analyzed by HPLC. Tomlinson and coworkers have used polymer-based stationary phases, i.e., styrenedivinylbenzene membranes, with PC-CZE-ESMS and these membranes were shown to have good chromatographic behaviour [40,43]. Alternatively, affinity-based stationary phases, such as immobilized lectins and immobilized metal affinity columns, may permit the highly specific extraction and analysis of compounds from complex matrices. The matching of buffer requirements for affinity phases with the requirements for sensitive mass spectrometric detection will be a challenge.

Chapter 5

5.0 Glycoprotein Analysis

This chapter describes the use of nanoelectrospray CZE-nESMS for the study of N- and O-linked glycoprotein digests. The nanoelectrospray interface provided the high sensitivity necessary for the analysis of these complex molecules. The high resolution obtained using CZE provided information on glycoform populations at individual sites of glycosylation. Stepped-orifice voltage scanning was used to generate carbohydrate-specific oxonium ions for identification of glycopeptides in the complex peptide maps. The composition of oligosaccharides in the studied glycoproteins was elucidated using CZE-MS-MS. More significantly, new CZE-MS-MS-MS methodologies developed as part of this work provided structural information about the glycopeptide sequence from injection of sub-picomole quantities of original protein. Further sensitivity for the analysis of protein digests is demonstrated using the PC-CZE-nESMS method described in the previous chapter.

5.1 Optimization of Separation Conditions

As discussed in Section 3.3, the analysis of proteins and peptides by CZE using bare fused-silica capillaries is hampered by adsorption on the silanol surface [100,101]. This is especially true when using acidic solutions compatible with positive ion electrospray, and can be overcome to some extent by using cationic coating agents. A common method for surface modification of capillaries for CZE-ESMS makes use of (3-aminopropyl)trimethoxysilane (APS) [24,27,28]. Recently an alternative cationic coating, BCQ, was reported for CZE analysis using acidic buffers [32].

A T E T S F I I/D/A F N K T N L I L Q G/ D/A T V S S N G N L 30
Q L S Y N S Y/D/S M S R A F Y S A P I Q I R/D/S T T G N V A 60
S F/D/T N F T M N I R T H R Q A N (77)

Figure 5.1 The amino acid sequence of the α-chain of α-amylase inhibitor 1. The slashes indicate cleavage sites for mild acid hydrolysis.

A comparison of the APS and BCQ coatings was carried out using CZE-UV analysis of peptides arising from the mild acid hydrolysis of the α-chain of α-amylase inhibitor 1, a small N-linked glycoprotein. The sequence of this glycoprotein is given in Figure 5.1. Figure 5.2 shows electropherograms using the APS and BCQ coatings each at two different concentrations of formic acid. Using 0.1 M formic acid, the separation performed using the BCQ coating (Figure 5.2b) generally yielded improved resolution over that obtained using the APS coating (Figure 5.2a). Electroosmotic flow (eof) calculations at this electrolyte concentration gave values of 7.1×10^{-8} m^2 V^{-1} s^{-1} and 5.5×10^{-8} m^2 V^{-1} s^{-1} for the APS and BCQ coatings, respectively. Theoretical plate numbers N (peak width at half height definition), calculated for the latest migrating component in Figures 5.2a and 5.2b, gave N values of 185,000 and 322,000 for the APS and BCQ coatings, respectively. The improvement in performance is attributed to the decrease in electroosmotic flow. The analyte migrates in the direction opposite to that of

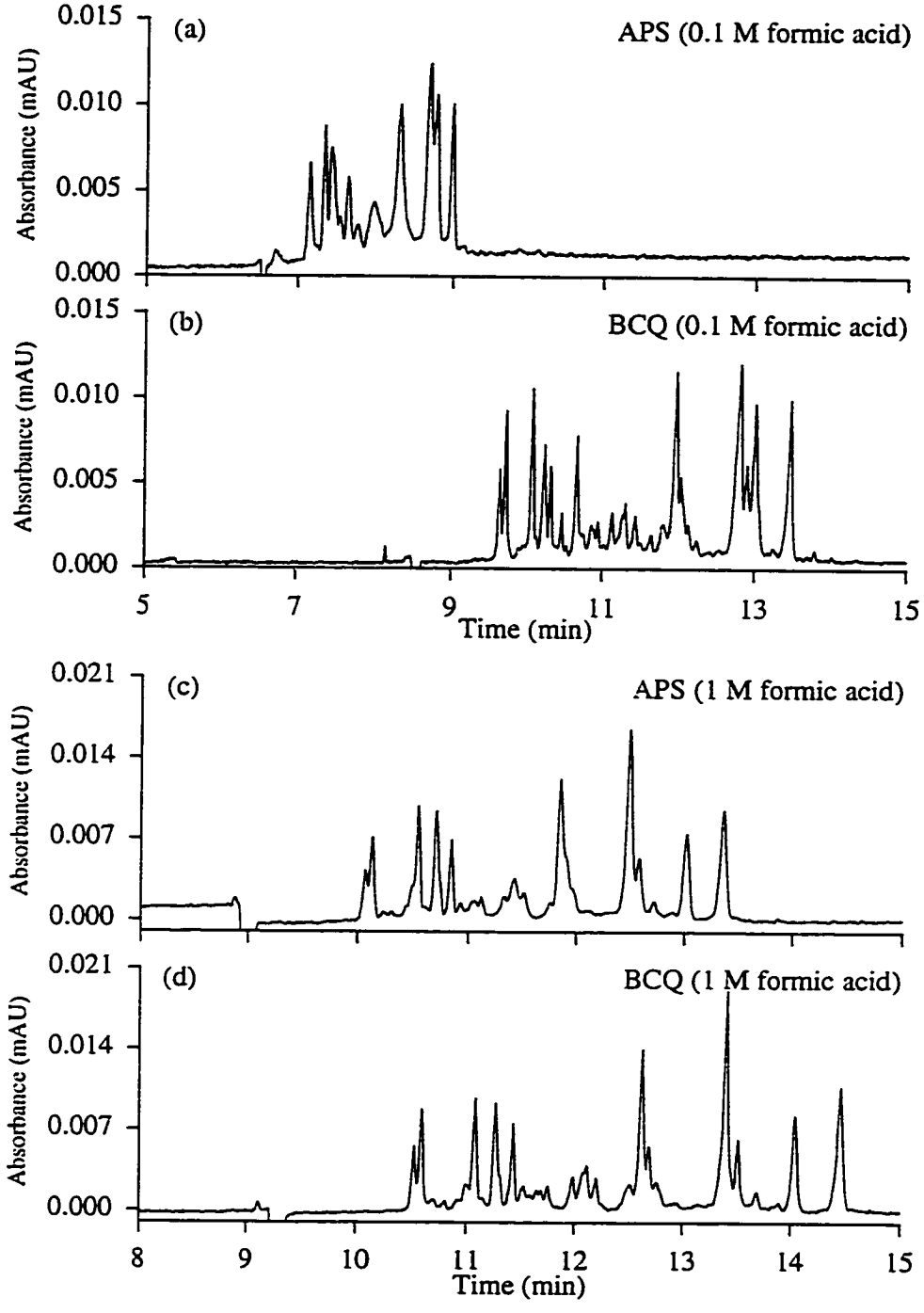

Figure 5.2 Effects of capillary coatings and electrolyte buffers on the CZE-UV analysis of a mild acid hydrolysate of the α-chain from α-amylase inhibitor 1. Separation conducted using the following coatings and buffers (a) APS, 0.1 M HCOOH, (b) BCQ, 0.1 M HCOOH, (c) APS, 1 M HCOOH, (d) BCQ, 1 M HCOOH. Conditions: Injection of 15 nL on an 87 cm (total length) x 50 μm i.d. coated capillary using reversed polarity (-20 kV).

the anodal electroosmotic flow, and the improvement in resolution comes as a result of the reduced zone velocity.

Electropherograms obtained using 1 M formic acid are shown in Figures 5.2c and 5.2d for the APS- and BCQ-coated capillaries, respectively. In this instance the eof measurements calculated for both coatings were similar (5.0×10^{-8} m^2 V^{-1} s^{-1}). The increased acid concentration results in decreased eof and improved peak resolution for both APS- and BCQ-coated capillaries. However, theoretical plate numbers calculated for the late-migrating peak of each electropherogram were significantly different for the APS (220,000) and BCQ (505,000) coatings. Interestingly, closely migrating peaks such as those observed at approximately 12.6 min in Figure 5.2d are more clearly resolved for the BCQ capillary than for the APS coating (Figure 5.2c), achieved under similar separation conditions. In a separate experiment using CZE-nESMS (see following discussion), this set of peaks was identified as a series of high mannose glycopeptides, and the heterogeneity observed here corresponds to the natural glycoform population at this particular site of attachment.

The differences in separation performance of the BCQ- and APS-coated capillaries are mainly attributed to differences in chemical structure and surface coverage. The structure of BCQ contains a quaternary ammonium ion that acts as a permanent positive charge at the end of a 15-carbon alkyl chain, whereas a primary amine terminates the propyl chain of the APS coating (Figure 3.4). The overall charge imparted on the inner surface of the capillary will also depend on the ability to mask free silanol groups (pKa 2.5). As the acid strength is increased the eof is progressively reduced possibly through protonation of unreacted silanol groups. The short alkyl chain of the APS may not efficiently mask free silanol groups which are inevitably present, whereas the longer alkyl chain of the BCQ coating could provide a better surface coverage.

5.2 Identification of Glycopeptides Using CZE-nESMS

The optimization of the CZE-UV separation facilitated the selection of electrophoretic conditions conducive to the analysis of glycoprotein digests using CZE-nESMS. Accordingly, separations of glycoprotein digests were usually conducted using the BCQ-coated capillary. To aid the identification of glycopeptides, a mixed-scan function was used to promote the in-source formation of selected oxonium ions under high orifice voltage conditions (120 V), while enabling detection of multiply protonated ions using low orifice voltage (50 V). The analysis of the peptides arising from mild acid cleavage of the α-chain from α-amylase inhibitor 1 is presented in Figure 5.3. The total ion electropherogram (TIE) corresponds to the injection of approximately 2 picomoles of the original protein (Figure 5.3a). The difference in resolution noted between Figure 5.3a and the corresponding CZE-UV analysis (Figure 5.2b) is attributed to several factors, including the use of a longer capillary (1 m), lower field strength (228 V cm^{-1}), and the relatively slow MS scan speed (3 s) used in the CZE-nESMS experiment.

Identification of glycopeptides in the TIE was achieved by extracting the m/z 204 ion electropherogram (Figure 5.3b), corresponding to the GlcNAc oxonium ion generated by collision induced dissociation in the orifice/skimmer region of the mass spectrometer. Resolution of closely related components is evident in the extracted ion electropherogram (Figure 5.3b), including partial resolution of a series of four high mannose glycopeptides centered at 19.0 min.

The microheterogeneity at a single site of glycosylation is more evident in the contour profile (Figure 5.3c), where families of diagonal lines of negative slopes reflecting the concurrent changes in molecular mass and electrophoretic mobilities, are easily visualized. The first family of glycopeptides indicated by 1 in Figure 5.3c, is spaced by m/z 54 consistent with triply-protonated ions and corresponds to the peptide $A_{1\text{-}20}$ to which is bonded a variable oligosaccharide composed of $GlcNAc_2Man_x$ (where x ranges from 3 to

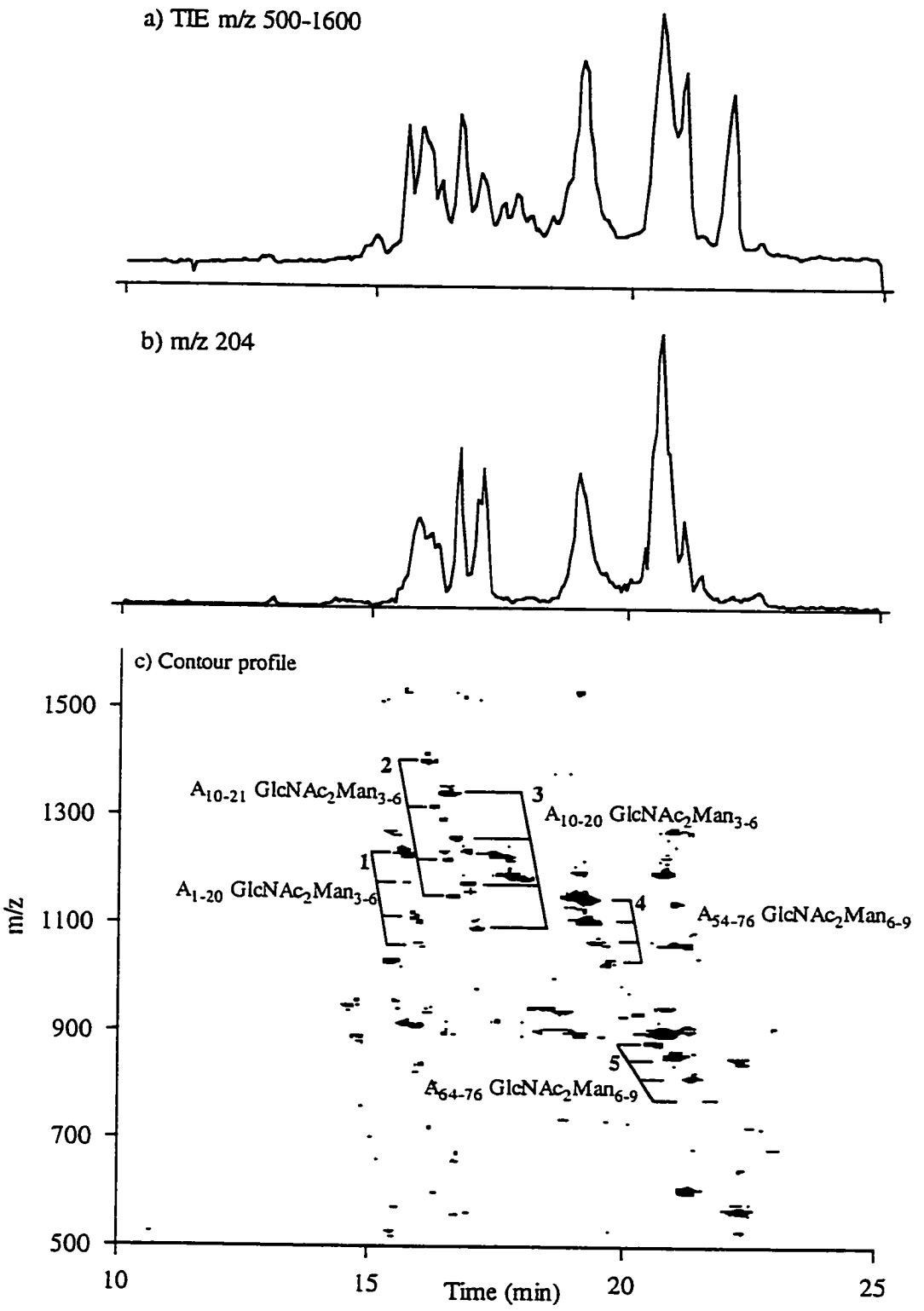

Figure 5.3 Nanoelectrospray CZE-ESMS analysis of a mild acid hydrolysate of the α-chain from α-amylase inhibitor 1. (a) Total ion electropherogram (m/z 500-1600), (b) Extracted ion for m/z 204, (c) Contour profile of m/z *vs.* time. Conditions: Injection of 27 nL (2 picomoles of original digest) on a 1 m (total length) x 50 μm i.d. BCQ-coated capillary using reversed polarity (-20 kV), and 0.1 M HCOOH.

6 mannose residues). Based on the relative peak intensities the predominant glycoform for this glycopeptide is $GlcNAc_2Man_6$. The peptide sequence (ATETSFIIDAFNKTNLILQG) contains two asparagine residues, but only the first one (identified in bold) has the tripeptide sequon characteristic of an N-linked glycopeptide. It is interesting to note that the second and third series of doubly-charged glycopeptide peaks, at 16-17 min, comprise the shorter chain peptides $A_{10\text{-}20}$ and $A_{10\text{-}21}$, which display the same carbohydrate distribution.

The last two series of glycopeptide peaks centered at 19.0 and 21.0 min (labeled as 4 and 5 in Figure 5.3c) correspond to the peptide fragments $A_{54\text{-}76}$ and $A_{64\text{-}76}$, respectively. Both series of glycopeptides possess a variable oligosaccharide $GlcNAc_2Man_{6\text{-}9}$ where the predominant form is the Man_9 member. In this case the $A_{54\text{-}76}$ peptide (STTGNVASFDTNFTMNIRTHRQA) contains a total of three asparagine residues, and only one encodes for a potential site of glycosylation.

5.3 Identification and Characterization of N-linked Glycopeptides Using CZE-ESMS and CZE-MS-MS

The techniques of high resolution CZE separation combined with nanoelectrospray MS detection described above were applied to the study of lectins from *P. vulgaris* (kidney bean) and *L. tetragonolobus* (asparagus pea) also referred to as *Tetragonolobus purpureas*. Lectins are carbohydrate binding proteins and have been used extensively to study animal cell glycoconjugates [107,108]. Many plant lectins are glycoproteins, but little information is available on either the structure of the oligosaccharide units or the factors that determine the glycosylation pattern of glycoprotein lectins [109]. The development of analytical techniques for the analysis of these molecules is a necessary requirement to aid in the understanding of their function.

5.3.1 Analysis of *P. vulgaris* Lectin

The heterogeniety of the erythroagglutinating phytohemagglutinin (PHA-E), a lectin isolated from *P. vulgaris* has been noted previously; at least 6 components with molecular masses ranging from 28,808 Da to 29,537 Da, and three consensus sequons for N-glycosylation have been identified [110,111]. The sequence of the protein (Figure 5.4) [111] and the structure of the oligosaccharide portion of this glycoprotein has also been reported previously [112]. These factors make this lectin a suitable standard for testing the methods developed as part of this research. The analysis of the tryptic digest using the mixed-scan function is shown in Figure 5.5. This analysis was achieved by acquiring the m/z 204 fragment ion using selected ion monitoring at a high orifice voltage (200 ms duration) together with the full mass scan (m/z 500-1600) at a lower orifice voltage (3.5 s duration). The glycopeptides are identified as two distinct peaks at 9.3 and 10.5 min in the m/z 204 ion electropherogram (Figure 5.5a). The first peak corresponds to the large tryptic glycopeptide $T_{70\text{-}121}$ while the second peak was tentatively identified as the tryptic glycopeptide $T_{32\text{-}41}$. The selectivity of this analysis is clearly visualized in Figure 5.5a compared to the full-scan acquisition (Figure 5.5b) where a complex series of peaks is observed.

MASSNLLSLA LFLVLLTHAN SASQTSFSFQ	30
R/F<u>NET</u>NLILQ R/DATVSSK/GQ LR/LTNVNDNG	60
EPTLSSLGR/A FYSAPIQIWD <u>NTT</u>GAVAASP	90
TSFTFNIDVP <u>NNS</u>GPADGLA FVLLPVGSQP	120
K/DK/GGLLGLF NNYK/YDSNAH TVAVEFDTLY	150
NVHWDPKPR/H IGIDVNSIK/S IK/TTTWDFVK/	180
GENAEVLITY DSSTK/LLVAS LVYPSLK/TSF	210
IVSDTVDLK/S VLPEWVIVGF TATTGITK/GN	240
VETNDILSWS FASK/LSDGTT SEALNLANFA	270
LNQIL (275)	

Figure 5.4 Amino acid sequence of erythroagglutinating phytohemagglutinin from *P. vulgaris*. Slashes indicate sites of cleavage by trypsin.

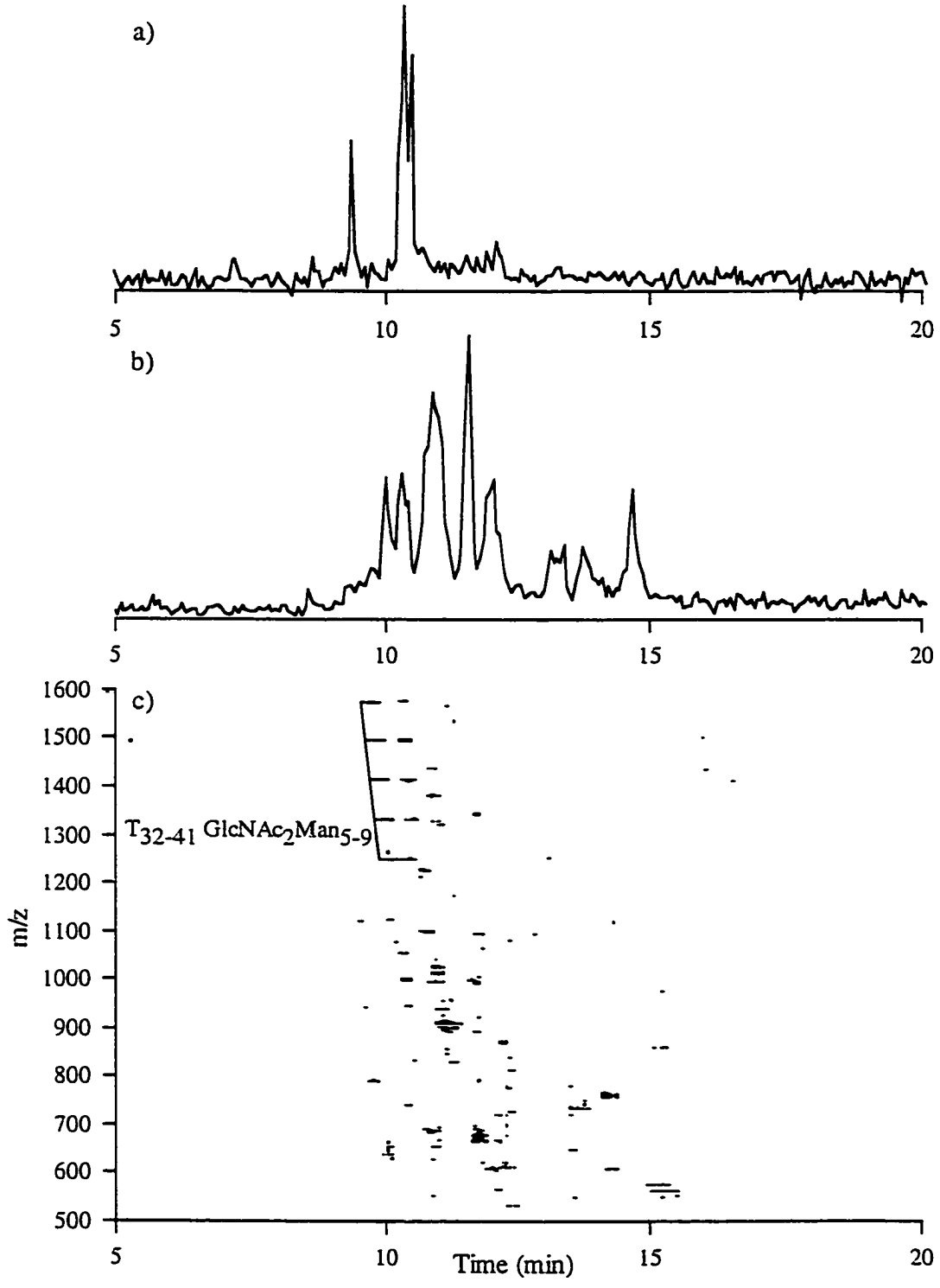

Figure 5.5 Nanoelectrospray CZE-ESMS analysis of tryptic digest of *P. vulgaris* lectin. Conditions: 1 m BCQ coated column coupled a microsprayer via a butt-connector, 800 femtomol injected, -23 kV, 1 M formic acid. a) Monitoring of oxonium fragment ions of Man (m/z 163) and GlcNAc (m/z 204) using an orifice voltage of 100 V. b) Full scan analysis using an orifice voltage of 50 V. c) Contour profile from full-scan analysis showing the separated glycopeptides (diagonal line).

It is noteworthy that the glycopeptide T_{32-41} exhibits significant heterogeneity in the number of mannose residues appended to the pentasaccharide core structure as evidenced by a series of peaks spaced by m/z 81 in the contour profile of the same analysis (Figure 5.5c). As mentioned above, the glycoform patterns arising from a single glycosylation site were easily identified using contour intensity profiles of m/z vs. time by observation of a diagonal line corresponding to a concurrent change of electrophoretic mobilities and molecular masses. CZE-nESMS analyses of the tryptic peptides from PHA-E enabled identification of a high-mannose series extending from five to nine residues on T_{32-41}. The heterogeneity noted here is consistent with earlier investigations on the intact lectin where a high mannose series of glycoforms was observed [110].

Structural characterization of the carbohydrate moiety of the glycopeptides was carried out by nanoelectrospray CZE-MS-MS using an injection of only 1.5 pmol of digested protein. The product ion spectrum of m/z 1314 is presented in Figure 5.6a. The precursor ion was tentatively assigned as the doubly protonated glycopeptide T_{32-41} $GlcNAc_2Man_6$. This glycoform assignment was supported by the observation of a series of protonated carbohydrate fragments, $GlcNAc_1Man_{1-6}$ (Figure 5.6a). This low energy MS/MS spectrum is dominated by cleavages of glycosidic bonds from the oligosaccharide side chain, with no fragmentation of the peptide amide bonds. Unambiguous location of the glycopeptide position within the protein would be difficult to achieve without prior information from the gene sequence [111].

In order to facilitate the sequence assignment of this glycopeptide, more specific tandem mass spectral analyses were necessary. Peptide backbone cleavages could be obtained by selecting the precursor ion at m/z 726 (Figure 5.6a) corresponding to the doubly charged fragment ion $[T_{32-41}\ GlcNAc]^{2+}$. This ion could be formed as a first-generation fragment ion by raising the orifice/skimmer voltage to 100 V. The MS/MS spectrum of m/z 726 obtained in this fashion is shown in Figure 5.6b. The second-

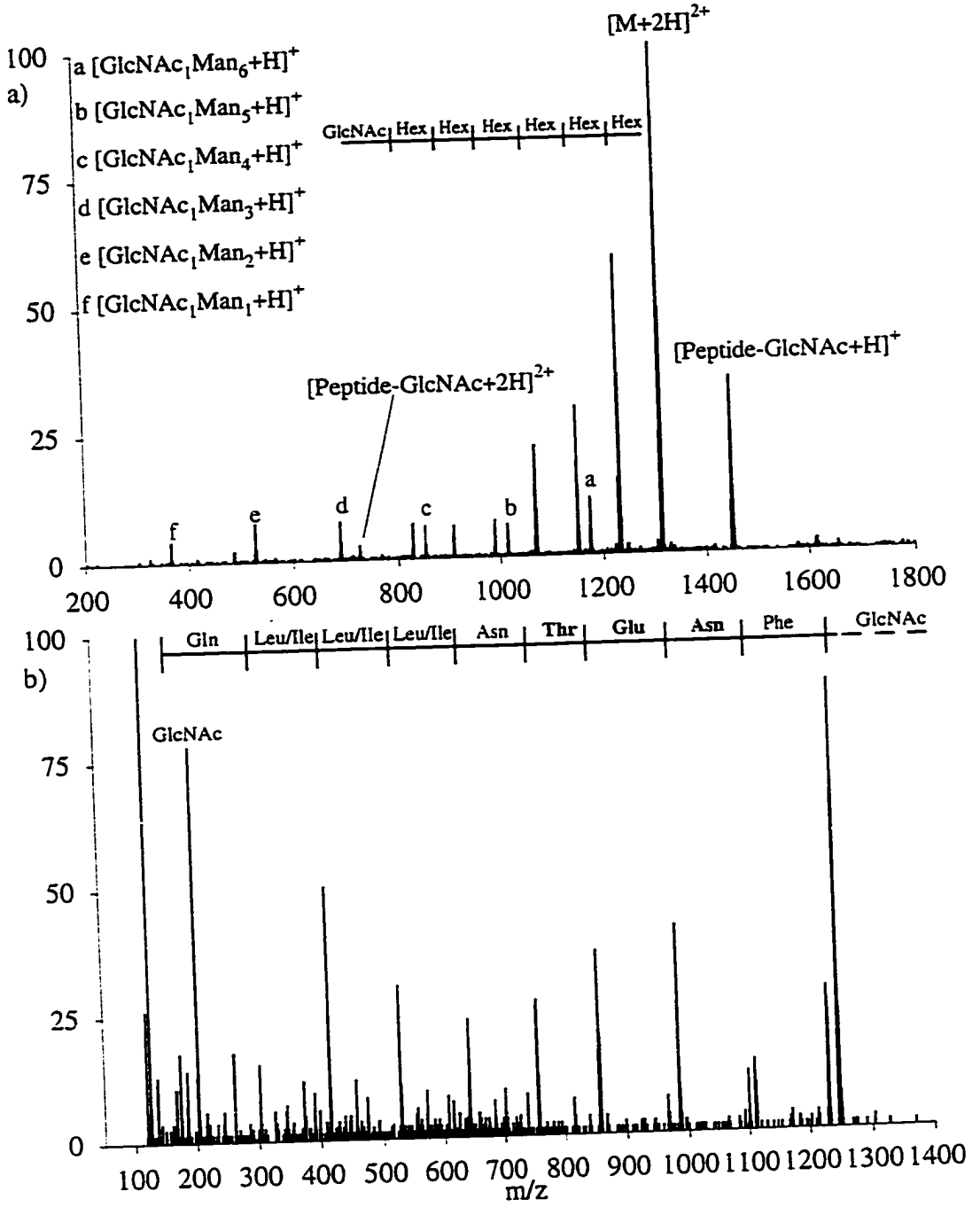

Figure 5.6 Nanoelectrospray CZE-MS-MS analysis of glycopeptide from *P. vulgaris* lectin. Product ion spectrum of (a) m/z 1314 and (b) m/z 726. Separation conditions as for Figure 5.3 except separation voltage decreased to -13 kV at 9 min, argon target gas, collision gas thickness of 3.5 x 10^{-15} atoms.cm^{-2}, orifice voltage of 50 V for (a) and 100 V for (b).

generation fragment ions thus obtained are typical of tryptic peptides, in that the spectrum is dominated by cleavage of the amide bonds, yielding abundant y-type fragment ions, from which the peptide sequence can be deduced. The tandem mass spectrometric data obtained for this glycopeptide support the structural assignment made earlier, and confirm the site of carbohydrate attachement as Asn_{33}.

5.3.2 Analysis of *L. tetragonolobus* Lectin

Similar analyses as described above for the lectin from *P. vulgaris* were applied to the study of the seed lectin *L. tetragonolobus* . This lectin has been described as a 4:2:4 combination of three different subunits with molecular weights of 120, 58, and 117 kDa, respectively [113,114]. More recently, a sequence (Figure 5.7) was reported for a single isolectin having a sub-unit molecular mass of approximately 26,000 Da by SDS-PAGE and 26,298 Da on the basis of the sequence determined by Edman degradation [115]. However, no information on the composition or structure of the oligosaccharide has been reported for this lectin.

VSF<u>NYT</u>EFK/D DGSLILQGDA K/IWTDGR/LAM	30
PTDPLVNNPK/TTR/SAGR/ALY ATPVPIWDSA	60
TGNVASFVTS FNFLFVIR/EL K/YTPTDGLVF	90
FLAPVGTEIP SGSTGGFLGI FDGSNGFNQF	120
VAVEFDSYHN IWDPK/SLR/SS HVGIDVNSIM	150
SLK/AVNWNR/V SGSLEK/ATII YDSQTNILSV	180
VMTSQNGQIT TIYGTIDLK/T VLPEK/VSVGF	210
SATTGNPER/E K/HDIYSWSFT STLK/EPEEQA	240

Figure 5.7 Amino acid sequence of the lectin from *L. tetragonolobus*. Slashes indicate tryptic cleavage sites.

The mass spectrum and the molecular mass profile calculated from the multiply-charged ions generated by infusion of approximately 15 picomoles of the intact lectin using the nanoelectrospray interface is shown in Figure 5.8. The predominant peak has a

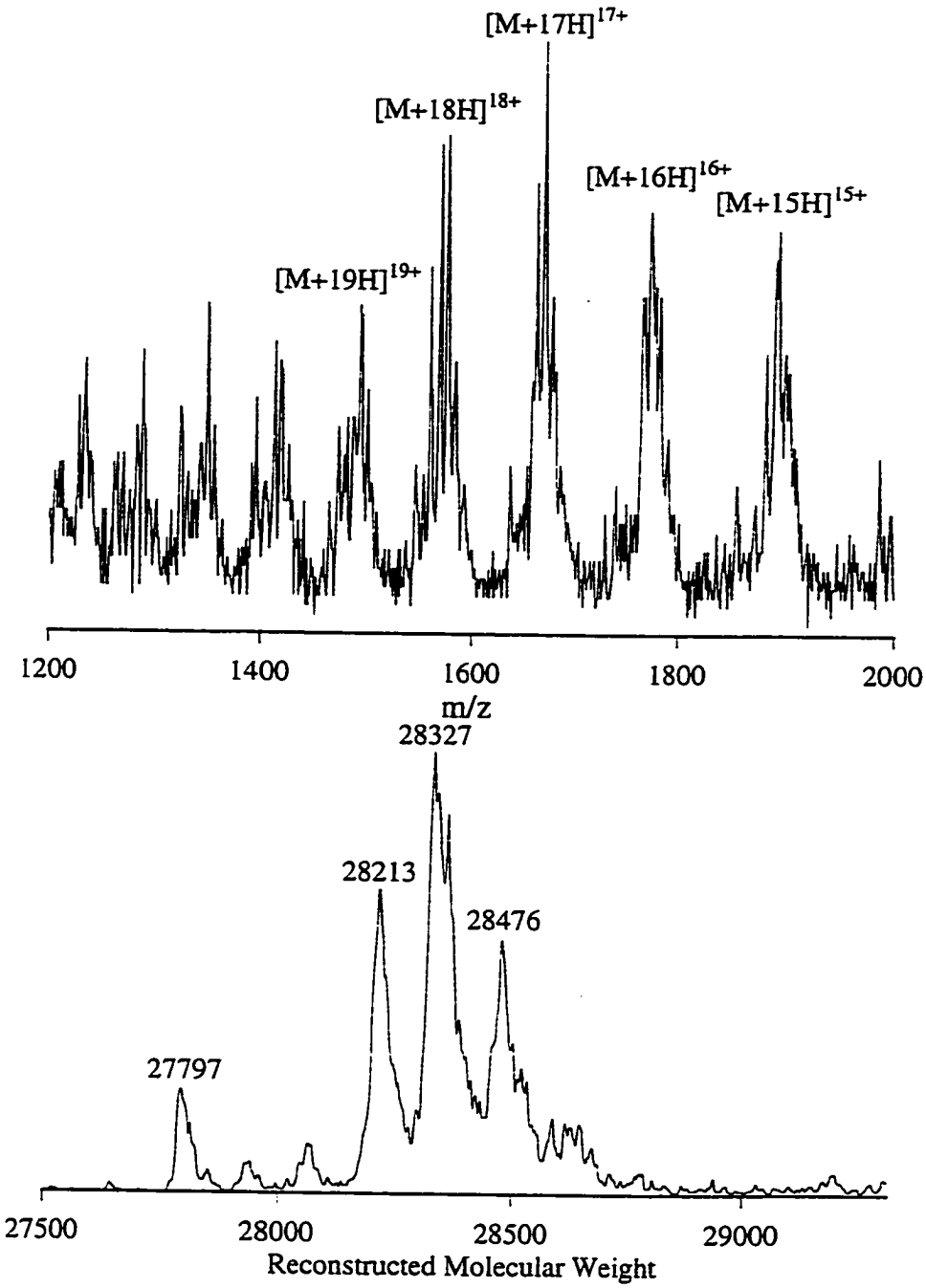

Figure 5.8 Mass spectrum of *L. tetragonolobus* lectin obtained using nanoelectrospray. The reconstructed molecular mass is shown as an inset. Infusion of a total of 15 picomoles of lectin in 0.1 M HCOOH).

molecular mass of 28,327 Da which is approximately 2 kDa higher than that calculated from the published protein sequence [115]. The mass difference observed here was first presumed to arise from the presence of up to two possible glycosylation sites. Further microheterogeneity could also be present in terms of addition or removal of carbohydrate residues. For example, a satellite peak at 28,476 Da would be consistent with the addition of a deoxyhexose (fucose) residue on the main glycoprotein shown in Figure 5.8a. However, other molecular species with mass differences of 114 Da were more difficult to explain, and further investigations were carried out to establish the glycoform distribution.

In order to identify the nature of the oligosaccharide(s) linked to this lectin, the glycoprotein was digested using trypsin and analyzed by nanoelectrospray CZE-MS. The TIE for the injection of approximately 1.5 picomoles of the original glycoprotein is shown in Figure 5.9a. Selective identification of glycopeptides using the m/z 204 oxonium ion revealed two possible glycopeptides at approximately 16.9 and 17.5 min (Figure 5.9c). It is noteworthy that earlier investigations by Carr and others have indicated that false positives for glycopeptides may occur using this HexNAc oxonium ion due to the large number of amino acid combinations coinciding with this m/z value [90,116]. More selective identification of glycopeptides can be accomplished using two or more oxonium ions. In this instance, extracted ions for m/z 163 (Hexose, Fig. 5.9b) and m/z 366 (Hexosamine-Hexose, Fig. 5.9d) were used along with m/z 204 to confirm the presence of one glycopeptide (17.5 min) while rejecting a possible false positive (16.9 min).

The extracted mass spectrum from the peak identified as a glycopeptide at 17.5 min in Figure 5.9 is presented in Figure 5.10a. This spectrum was acquired using a normal orifice voltage of 50 V. The potential drop between the orifice and the front rods (Q0 or ion guide) does not provide sufficient energy to induce fragmentation by collision-induced dissociation in this relatively high pressure region of the vacuum chamber. The spectrum contains $[M+2H]^{2+}$, $[M+3H]^{3+}$, and $[M+4H]^{4+}$ ions and corresponds to a calculated

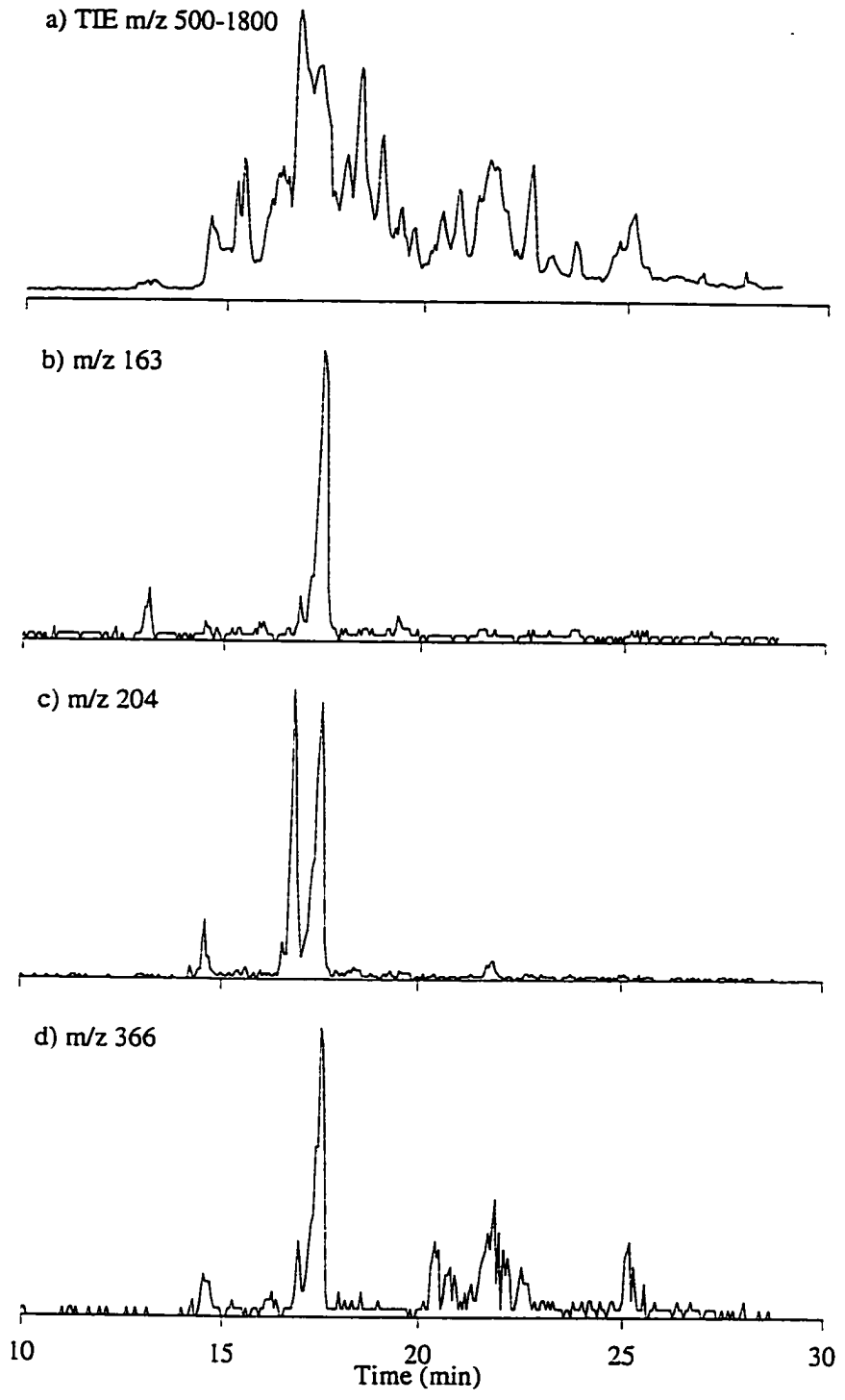

Figure 5.9 Nanoelectrospray CZE-MS analysis of a tryptic digest of *L. tetragonolobus* lectin. (a) Total ion electropherogram (m/z 500-1800), (b) Extracted ion profile for m/z 163, (c) m/z 204, and (d) m/z 366. Conditions: 1.5 picomole injection of original digest on a 1 m (total length) x 50 μm i.d. BCQ-coated capillary using reversed polarity (-20 kV), and 0.1 M HCOOH.

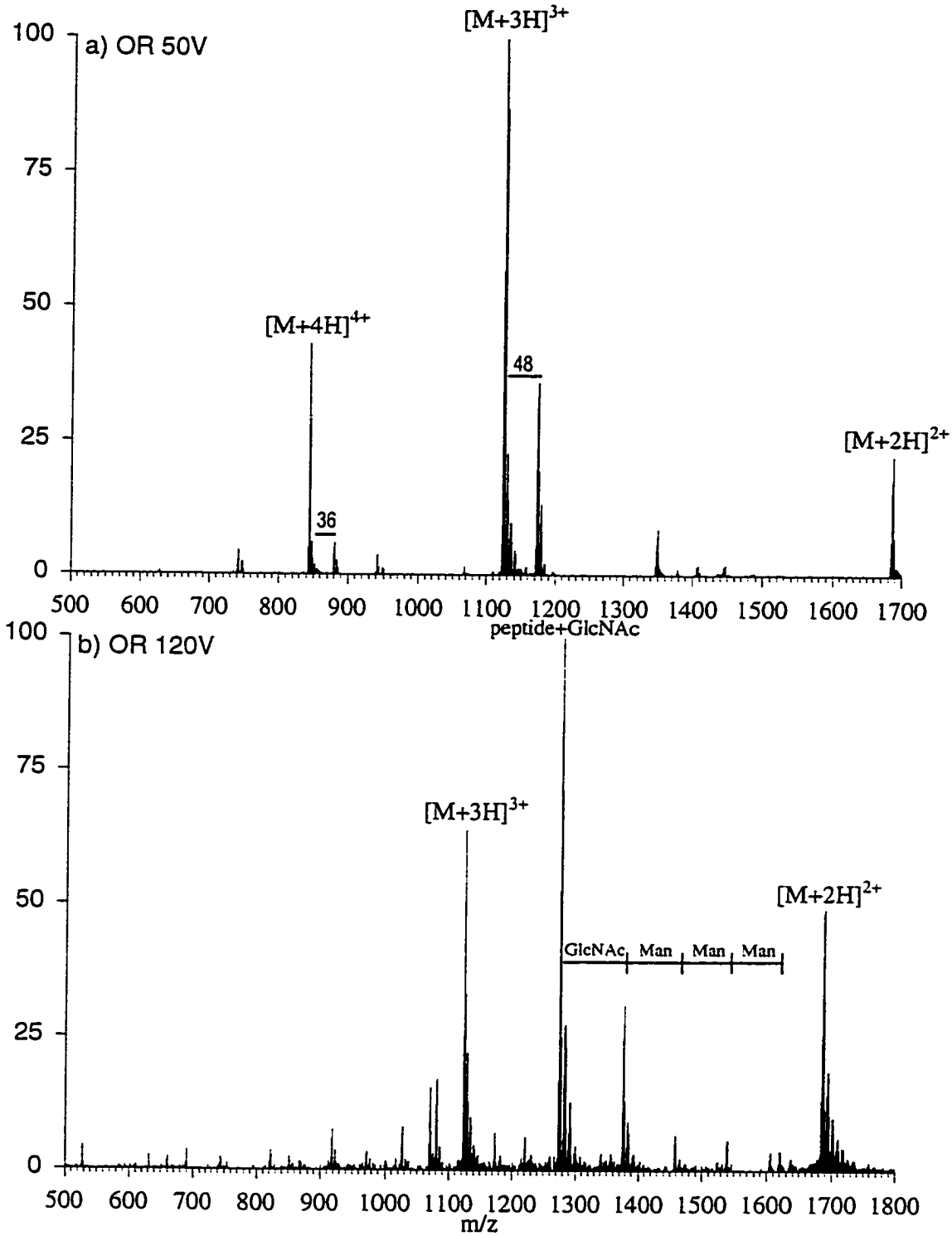

Figure 5.10 Extracted mass spectra from the nanoelectrospray CZE-MS analysis of the tryptic digest of *L. tetragonolobus* lectin using an orifice voltage of (a) 50V (peak migrating at 17 min in Figure 5 a) and (b) 120V (obtained from a separate CZE-ESMS analysis). Conditions as for Figure 5.7.

molecular mass of 3372 Da. Interestingly, closely migrating peaks spaced by m/z 48 and 36 from the predominant $[M+3H]^{3+}$, $[M+4H]^{4+}$ species may correspond to an additional glycopeptide containing an extra deoxyhexose residue. The larger glycopeptide migrating slightly before the predominant peak is consistent with the pattern of glycosylation described above.

Analysis of the same digest, using identical separation conditions except for the use of higher orifice voltage (120 V), produced abundant fragmentation of the glycopeptide prior to mass analysis (Figure 5.10b). The corresponding mass spectrum is obviously more complicated than that shown in Figure 5.10a, but provided valuable information concerning the nature of the oligosaccharide appended to the peptide backbone. For example, the most abundant ion in Figure 5.10b is observed at m/z 1276, and was tentatively assigned to a doubly-charged peptide fragment plus a GlcNAc residue. Previous investigations using low energy tandem mass spectrometry have indicated that cleavage at the glycosidic bond between two GlcNAc residues is commonly observed for N-linked glycopeptides [117]. The molecular mass of the corresponding deglycosylated peptide would be 2347 Da. The sequence of this peptide must contain the consensus sequon Asn_4-Tyr-Thr_6 and the calculated mass of the tryptic peptide containing this sequence is 1134 Da. The mass of the peptide $T_{1\text{-}21}$ when cleaved at the next available site is 2347 Da (VSFNYTEFKDDGSLILQGDAK), in close agreement with that observed in Figure 5.10b. The occurrence of this tryptic peptide presumably arose from an unfavorable cleavage at K_9 due to the close proximity of the adjacent aspartic acid residue.

Analysis of the spectrum produced using a high orifice voltage (Figure 5.10b) allows tentative assignment of the carbohydrate composition. A series of doubly-charged fragment ions is present in the spectrum, corresponding to additional GlcNAc and hexose residues from the $[peptide\text{-}GlcNAc]^{2+}$ fragment ion. Based on the spectra shown in Figure 5.10a and 5.10b, the mass of the oligosaccharide attached to $T_{1\text{-}21}$ was calculated to be

1025 Da (3372-2347 Da). The conserved pentasaccharide ($GlcNAc_2Man_3$) of N-linked glycopeptide has a residue mass of 892 Da which is 133 Da shorter than the expected mass for the oligosaccharide, a difference which could be accounted for by a pentose residue (xylose).

Additional confirmation of the structural identity of this tryptic glycopeptide was obtained using on-line CZE-MS-MS. Structural features of the glycopeptide were probed using low energy collision activation of the multiply-protonated precursor ions. The CZE-MS-MS spectrum of the $(M+3H)^{3+}$ ion of the tryptic peptide at m/z 1125 (Figure 5.10a) is shown in Figure 5.11a, and was produced from the injection of 1.5 picomoles of original protein. The appearance of the spectrum is similar to that of the high orifice full-scan spectrum (Figure 5.10b), in that the most abundant ions are the $[M+3H]^{3+}$ ion of the intact glycopeptide and the $[M+2H]^{2+}$ ion of the peptide+GlcNAc. However, the 2+ and 3+ fragment ions arising from the cleavage of carbohydrate residues from the precursor ion are significantly more abundant than in the high voltage orifice experiment (Figure 5.10b). From this spectrum the structure of the oligosaccharide is assigned as $GlcNAc_2Man_3$ with a pentose sugar attached to the central mannose residue. The location of the pentose residue is based on the ion pairs associated with loss of either mannose or pentose and from the oligosaccharide fragment ions observed below m/z 900 (Figure 5.11a). A full assignment of the glycopeptide peaks is provided in Table 5.1.

The low mass ions produced by low energy CID of the glycopeptide correspond to singly charged oligosaccharides. The oxonium ions at m/z 163, 204 and 366 used for selective detection of the glycopeptide in the CZE-nESMS analysis of the tryptic digest of the lectin are clearly observed in Figure 5.11a. These ions, along with those at m/z 295, 325, 498, 528, 660, 690 and 822, were consistent with the structure of the oligosaccharide described above (Table 5.2).

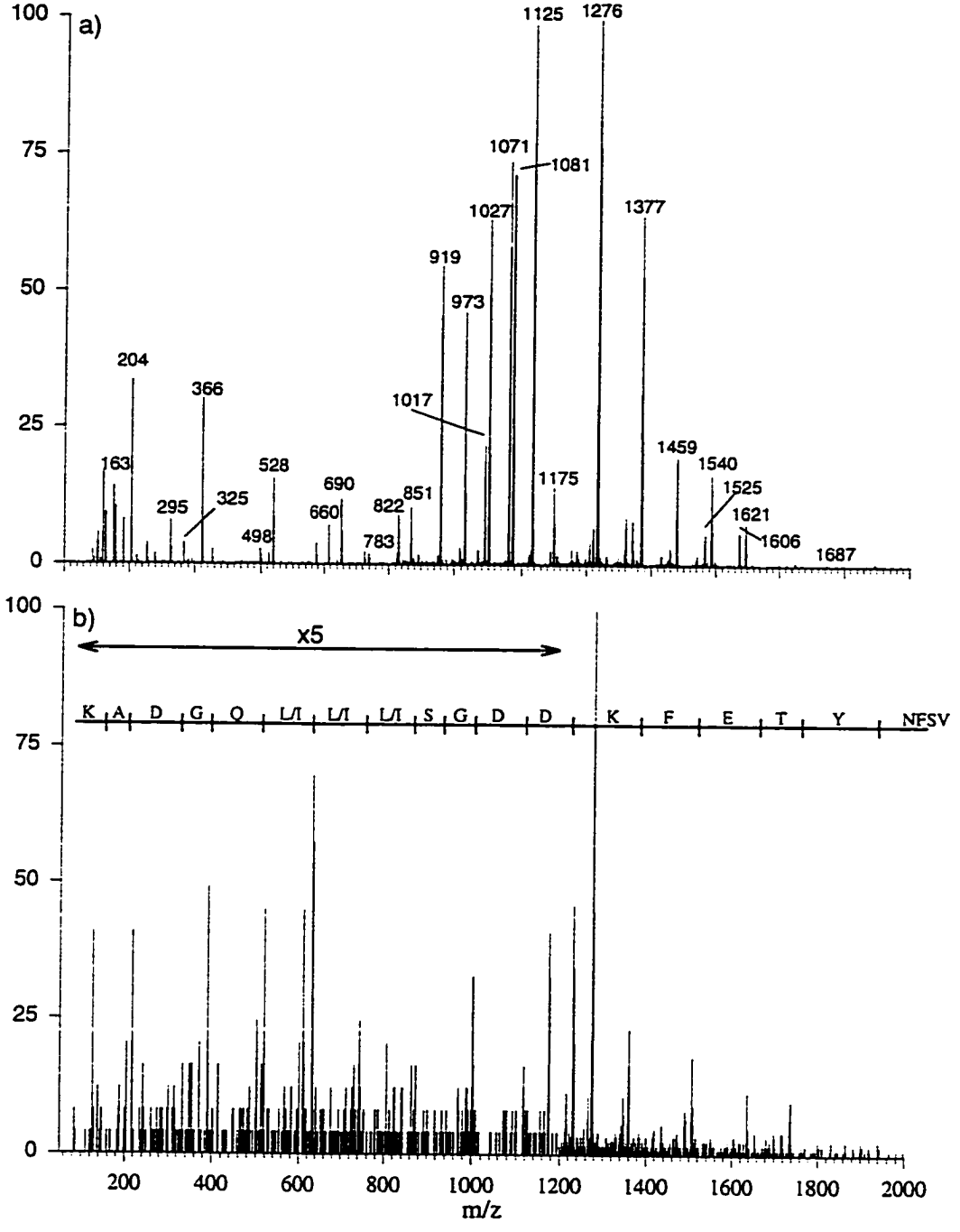

Figure 5.11 Nanoelectrospray CZE-MS-MS analysis of a glycopeptide from the tryptic digest of *L. tetragonolobus* lectin. (a) Product ion scan of m/z 1125 corresponding to $[M+3H]^{3+}$ glycopeptide ion shown in Figure 6a. (b) Product ion scan of m/z 1276 corresponding to $[peptide+GlcNAc]^{2+}$ fragment ion shown in Figure 6b obtained at an orifice voltage 120V. Conditions as for Figure 5 except that the separation voltage was decreased to -5 kV at 16 min, argon target gas, collision gas thickness of 3.5×10^{-15} atoms.cm^{-2}, collision energy (laboratory frame of reference) of 75 eV for (a) and 60 eV for (b).

Table 5.1 Proposed fragment ion assignment for CZE-MS-MS analysis of *L. tetragonolobus* glycopeptide.

Structure	$[M+3H]^{3+}$	$[M+2H]^{2+}$	M_r (Det.)
peptide+$GlcNAc_2Man_3Xyl$	1125	1687	3372
peptide+$GlcNAc_2Man_3$	1081	1621	3240
peptide+$GlcNAc_2Man_2Xyl$	1071	1606	3210
peptide+$GlcNAc_2Man_2$	1027	1540	3078
peptide+$GlcNAc_2Man_1Xyl$	1017	1525	3048
peptide+$GlcNAc_2Man_1$	973	1459	2916
peptide+$GlcNAc_2$	919	1377	2754
peptide+GlcNAc	851	1276	2550
peptide	783	1175	2347

peptide sequence: VSFNYTEFKDDGSLILQGDAK (M_{calc} 2347.5)

Table 5.2 Proposed structures for the oxonium ions of the oligosaccharide from *L.tetragonolobus* glycopeptide.

Structure	$[M+H]^+$
Man	163
GlcNAc	204
Man-Xyl*	295
Man-Man*	325
GlcNAc-Man*	366
GlcNAc-Man-Xyl*	498
GlcNAc-Man-Man*	528
GlcNAc-Man-Man-Xyl	660
GlcNAc-Man-Man-Man	690
GlcNAc-Man-Man-Man-Xyl	822

*indicates 2 or more bond cleavages

One of the limitations of the low energy spectra generated by triple quadrupole instruments is the lack of information about the peptide backbone of the glycopeptide. The collision energy is dissipated through cleavage of the most labile bonds, which in the case

of glycopeptides are the glycosidic linkages. Observation of highly abundant fragment ions corresponding to the peptide backbone plus GlcNAc in the high orifice full-scan data of glycopeptides prompted the investigation of these ions as possible precursors for MS-MS studies of peptide sequences. In the case of the *L. tetragonolobus* lectin, the fragment ion at m/z 1276 $[peptide+GlcNAc]^{2+}$ served as the precursor. This ion was produced as a first-generation fragment ion by CID in the orifice/skimmer region of the mass spectrometer and was subjected to further CID in the collision cell. The spectrum generated by this technique is shown in Figure 5.11b. The assignment of the y series ions was in excellent agreement with the sequence published previously [115]. Liu *et al.* reported an approach similar to this using microcolumn LC-MS-MS, but considered the peptide plus GlcNAc ion to be an artifact of the ionization process and did not attempt to purposely exploit these ions [118].

It is noteworthy that the work described above confirmed the existence of only one site of glycosylation, with minor heterogeneity involving the incorporation of an additional fucose residue. The corresponding oligosaccharide would increase the protein molecular mass by 1044 Da to 27,342 Da. The significant mass difference noted between the published sequence and the results of the present work is possibly accounted for by variation in the gene sequence or by the nature of the seeds extracted from different samples of *L. tetragonolobus*. Indeed a single potential site of glycosylation was expected from the reported sequence [115] and no additional glycopeptide was observed in experiments described above. Since the tryptic peptide expected from the N-terminus of this glycoprotein was confirmed in this study, one possible explanation for the present findings could be the occurrence of truncations at the C-terminus. Previous investigations on recombinant and natural plant lectins have highlighted that C-terminal proteolytic processing often results in heterogeneity and can be a major contributor to the appearance of isolectin forms [110].

5.4 Analysis of O-linked Glycoproteins

The established method of Edman degradation for the study of O-glycosylation is only useful for those sites that are extensively modified (80-100%). This is due to the poor recovery of glycosylated anilinothiazolinone-amino acids in the solvents typically used in automated sequencers. The use of solid-phase Edman degradation has overcome these limitations to some extent [119]. In the present study, the use of CZE nanoelectrospray-MS was investigated for the study of O-glycosylation sites especially in instances where only partial glycosylation occurs.

The TIE for the CZE-nESMS analysis of 5 picomoles of a Glu-C digest of the rennin fragment of κ-casein, an O-glycosylated milk protein (Figure 5.12), is shown in Figure 5.13a. This glycoprotein is known to have N-acetylneuramic acid (Neu5Ac) residues as part of the oligosaccharide structure, and selective identification of the glycopeptides is shown in Figure 5.13b. Using a mixed scan function to generate oxonium ions for the Neu5Ac (m/z 292), or in this instance Neu5Ac minus water (m/z 274), provides a higher degree of selectivity. Although the Neu5Ac residues are known to be acid labile, the analysis using 0.1 M formic acid did not give rise to noticeable degradation. The contour profile for the analysis of the digest is shown in Figure 5.13c and reveals the complexity of the sample.

M A I P P K K N Q D K T E/I P T I N T I A S G E/P T S T P T 30
T E/A V E/S T V A T L E/D S P E/V I E/S P P E/I N T V Q V T 60
S T A V (64)

Figure 5.12 Amino acid sequence of the renin fragment of κ-casein [120]. Slashes indicate sites of endoproteinase Glu-C cleavage.

An alternative approach to the selective identification of the glycopeptides is to use precursor ion scanning. In this method, a normal orifice voltage is used and the peptides are fragmented in the r.f.-only quadrupole collision cell of the mass spectrometer. The

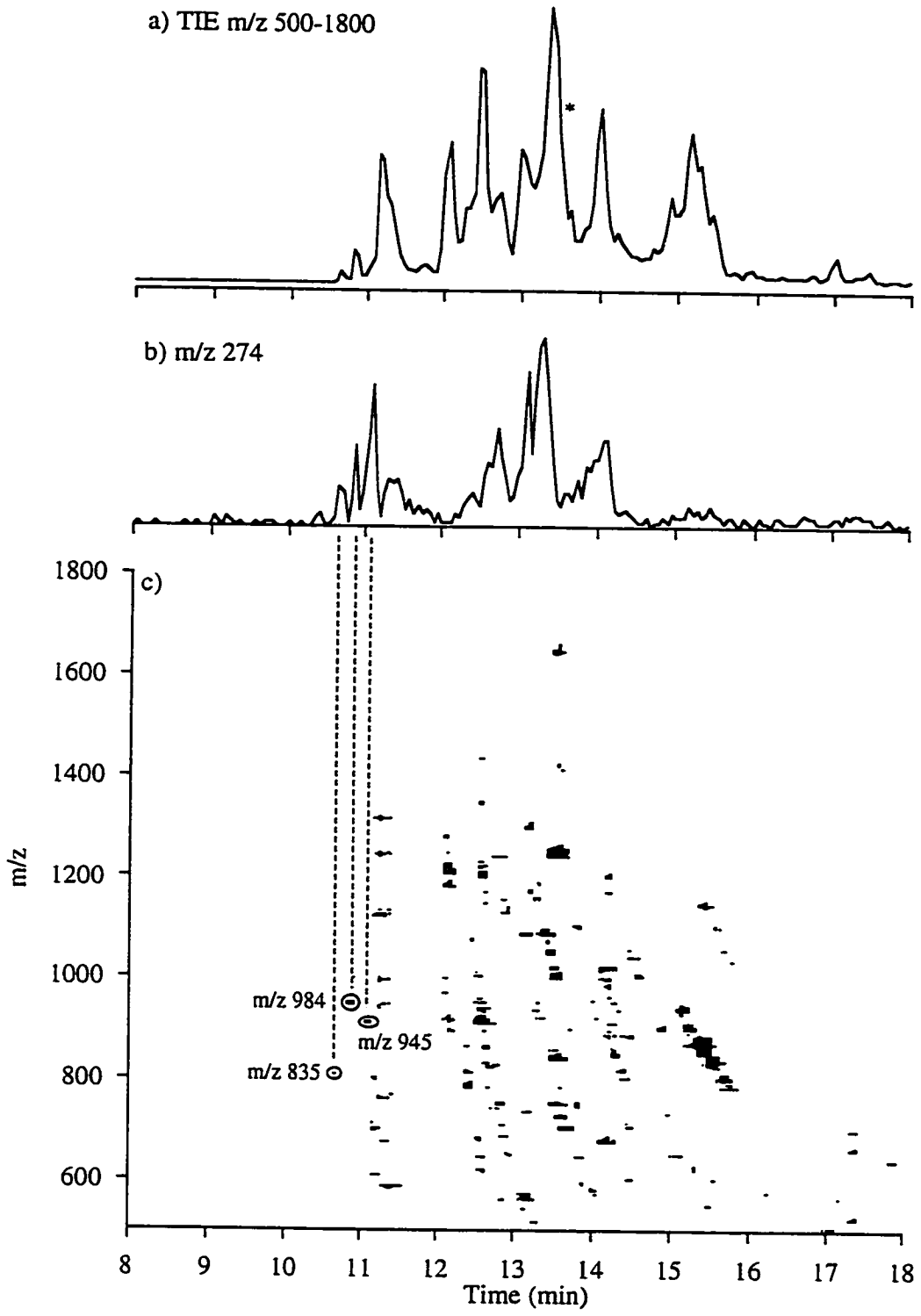

Figure 5.13 Analysis of Glu-C digest of κ-casein using nanoelectrospray CZE-MS. (a) Total ion electropherogram (m/z 500-1800), (b) Extracted ion electropherogram for m/z 274 obtained at orifice voltage of 120 V, (c) Contour profile of m/z *vs.* time. Conditions: 5 picomoles injection of original digest on a 1 m (total length) x 50 μm i.d. BCQ-coated capillary using reversed polarity (-20 kV), and 0.1 M HCOOH. The asterisk indicates the non-glycosylated peptide $S_{36}TVATLE_{42}$.

third quadrupole is set to transmit only m/z 274, a fragment ion specific to Neu5Ac as discussed above. The first quadrupole is scanned over the mass range of interest (m/z 500-1500), and the corresponding spectra display only precusor ions for the selected transition. The TIE for the analysis of the κ-casein Glu-C digest using the precursor ion scanning for m/z 274 is shown in Figure 5.14a and the resulting electropherogram is similar to the stepped-orifice scanning profile shown in Figure 5.13b. However, the peaks in the precursor-ion scan contain information on the molecular masses of the glycopeptides without interference from other nonglycosylated peptides of this digest. Examples of the mass spectra extracted from the first three peaks are shown in Figures 5.14b-d. The later peaks are due to higher molecular weight components resulting from incomplete digestion of the glycoprotein.

The composition of the carbohydrate component of the glycopeptide can be obtained using CZE-MS-MS as discussed above. These experiments were carried out on the digested O-linked glycoprotein, using m/z 835 and 984 as precursors. The resulting fragment ion spectra are presented in Figure 5.15 and clearly show abundant fragment ions at m/z 274 and 292, corresponding to Neu5Ac. These spectra also show that initial cleavage of a Neu5Ac residue is followed by loss of either a hexose or another Neu5Ac. This observation is consistent with the presence of a branched oligosaccharide and reveals that one of the Neu5Ac residues is attached to the core HexNAc residue. If both Neu5Ac sugars were attached to the hexose the ions at m/z 1216 and m/z 1515 in Figure 5.15a and 11b, respectively, would not be expected. Also evident in these spectra are the fragment ions for the naked peptides at m/z 721 and 1020 in Figure 5.15a and 5.15b, respectively. Comparison of these values with the predicted molecular masses for the digest fragments of κ-casein reveals that the sequences of the peptides are $S_{36}TVATLE_{42}$ (M_r 719.8) and $A_{33}VESTVATLE_{42}$ (M_r 1019.1). The second peptide arose from a skipped cleavage at E_{35}. According to previously published sequence analysis of κ-casein, T_{37} is expected

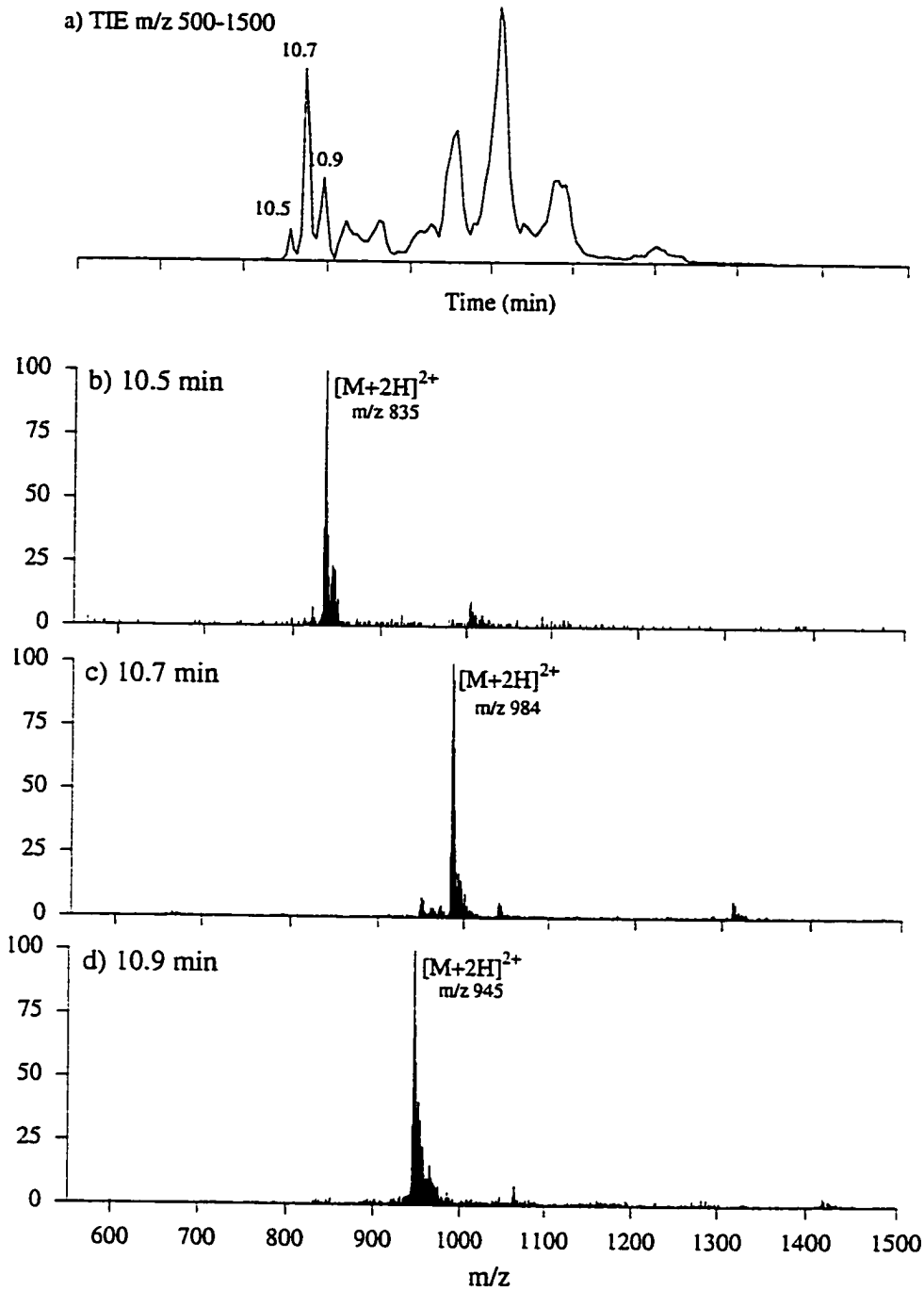

Figure 5.14 Analysis of sialylated glycopeptides from κ-casein using precursor ion scanning for m/z 274. (a) Total ion electropherogram of precursor ion (m/z 500-1500), extracted mass spectra at (b) 10.5, (c) 10.7 and (d) 10.9 min. Separation conditions as for Figure 5.11 except, argon target gas, collision gas thickness of 3.5×10^{-15} atoms cm^{-2}, collision energy of 60 eV (laboratory frame of reference).

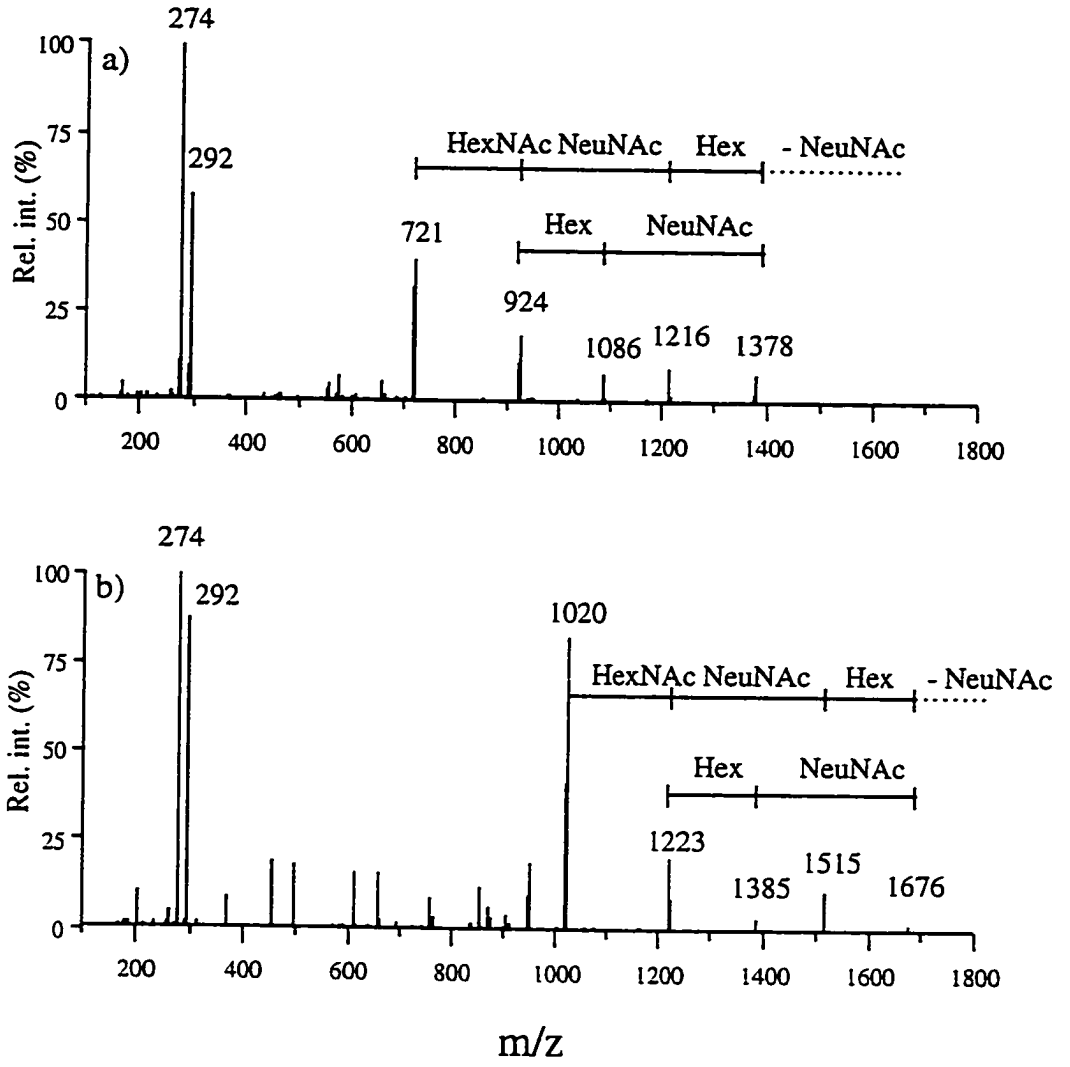

Figure 5.15 Nanoeletrospray CZE-MS-MS analysis of O-linked glycopeptides from Glu-C digest of κ-casein. (a) Product ion scan of m/z 835, (b) product ion scan of m/z 984. Conditions as for Figure 5.11 except that the separation voltage was decreased to -5 kV at 10 min.

to be glycosylated [120]. The non-glycosylated peptide, $S_{36}TVATLE_{42}$, is also present in the peptide map of this glycoprotein, and is marked with an asterisk in Figure 5.13a. No signal was detected for the non-glycosylated peptide corresponding to the skipped cleavage site, suggesting that the presence of the oligosaccharide may hamper the enzymatic cleavage at Glu_{35}. In the present case, the non-glycosylated peptide is significantly more abundant than the corresponding glycosylated peptide. Based on peak areas in the CZE-nESMS analysis this peptide is less than 5% glycosylated. However, the sensitivity of the present CZE-nESMS techniques enabled detection of both glycosylated and non-glycosylated peptides.

As emphasized above, the low energy CZE-MS-MS analysis of glycopeptides provided information only on the oligosaccharide structure and composition, but failed to generate peptide sequence fragments. The identification of sequence segments could only be made by matching the calculated molecular masses with those expected from the reported sequence when available. However, since there is no consensus sequence for predicting sites of O-glycosylation, knowing the sequence of the peptide from cDNA does not help in assigning the actual location of the oligosaccharide on the peptide. Further complications arose from the fact that both threonine and serine can be glycosylated and in the present example there are three possible sites for attachment of the oligosaccharide.

The formation of first-generation fragment ions to produce the peptide+HexNAc ion, which is subsequently analyzed by MS-MS, can be used to provide additional information on the peptide sequence. This is demonstrated in Figure 5.16 for the tandem mass spectrum of m/z 924 (Figure 5.15a), obtained from combined CZE-MS-MS. Fragmentation of the peptide occurs to produce the well defined series of y and b ions. Loss of water from the b series ions is also a common fragmentation pathway when an acidic residue (glutamic acid) is located at the C-terminus of the peptide ($S_{36}TVATLE_{42}$). Notably absent from the spectrum are the b_2 and y_6 ions at m/z 189 and 633, respectively.

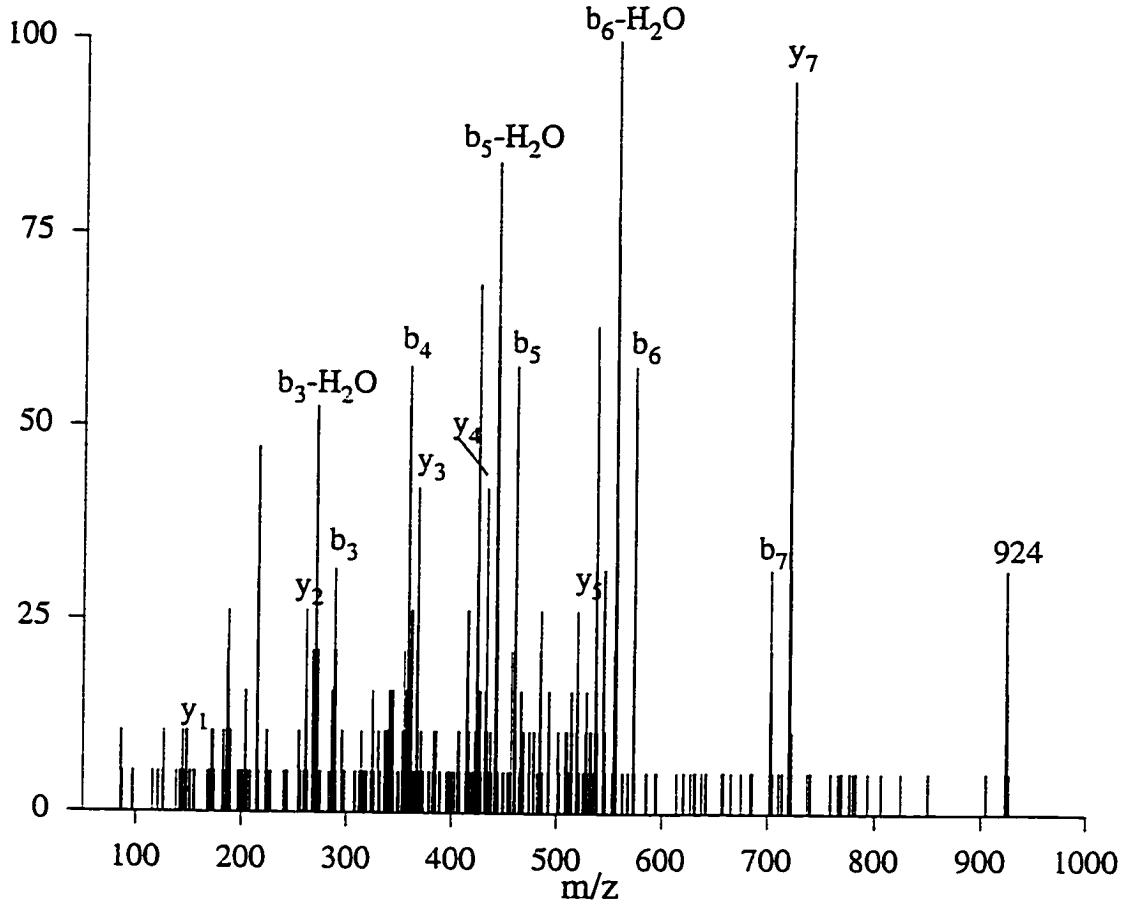

Figure 5.16 Product ion spectrum of precursor m/z 924 corresponding to [peptide+GalNAc]$^+$ ion identified in Figure 5.12a. Conditions as for Figure 5.11 except collision energy of 32 eV (laboratory frame of reference).

The absence of these fragment ions might be coincidental as the corresponding fragment ions containing the HexNAc residue were not observed in this MS-MS spectrum.

5.4 Protein Digest Analysis Using PC-CZE-nESMS

In practical terms, circulating and recombinant glycoproteins are usually not sample-limited, unlike many other natural glycoproteins of major importance such as cell-surface receptors [121]. Two-dimensional polyacrylamide gel electrophoresis (2D PAGE) has been used to simultaneously separate and visualize, by suitable staining, hundreds of proteins present in cell lysates [122]. However, this method does not provide structural information on the separated proteins. Silver staining is the most sensitive technique for the detection of proteins in gels and typically can visualize 1 to 5 ng of protein [56]. For a protein with a molecular weight of 30000 Da, this represents approximately 30 to 150 femtomoles. Methods used for the extraction and digestion of proteins excised from 2D gels commonly result in 50% recovery with final sample volumes of 10 to 20 μL, giving concentrations of 1 to 5 fmol/μL of protein digest [44]. The detection limit of CZE-nESMS using full-scan acquisition is in the 50-100 fmol/μL range (Section 3.4), and therefore would not be able to detect peptides at the concentrations typical for the 2D PAGE of proteins. The analysis of a protein tryptic digest was undertaken to assess the potential of PC-CZE-nESMS for studying proteins separated using two-dimensional gel electrophoresis.

The lectin from *Glycine max* (soybean) was analyzed using the stepped-orifice voltage-scanning method previously described. This analysis was carried out using a concentration of 2.2 μg/μL of original protein. Extracted ion electropherograms for carbohydrate specific oxonium ions (m/z 163, 204, 366) contained no peaks that were present in all three XIE's and indicated that this lectin is non-glycosylated (Figure 5.17).

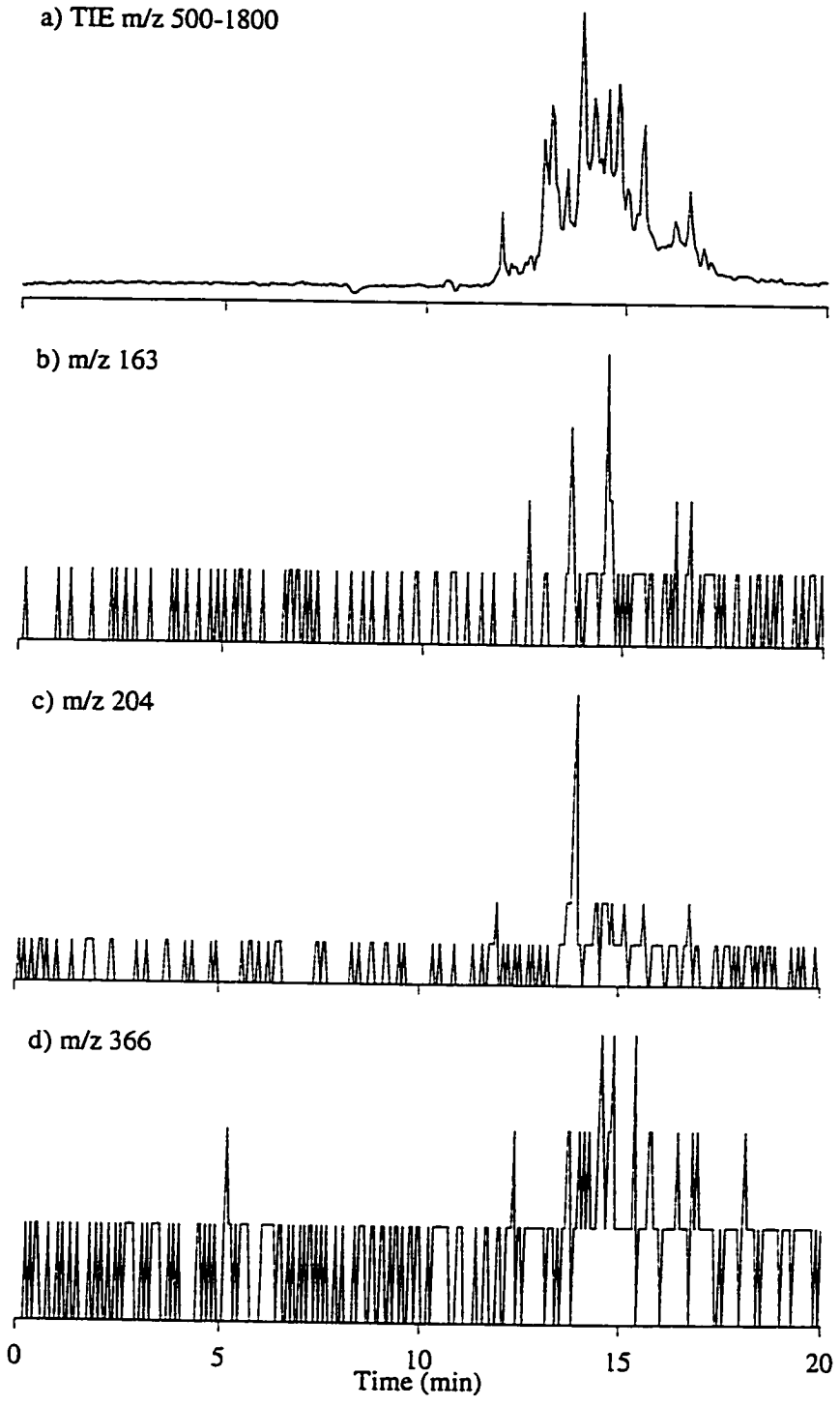

Figure 5.17 Nanoelectrospray CZE-ESMS analysis of a tryptic digest of *Glycine max* lectin. (a) Total ion electropherogram (m/z 500-1800), (b) Extracted ion profile for m/z 163, (c) m/z 204, and (d) m/z 366. Conditions: 1.8 picomole injection of original digest on a 1 m (total length) x 50 μm i.d. BCQ-coated capillary using reversed polarity (-20 kV), and 0.1 M HCOOH.

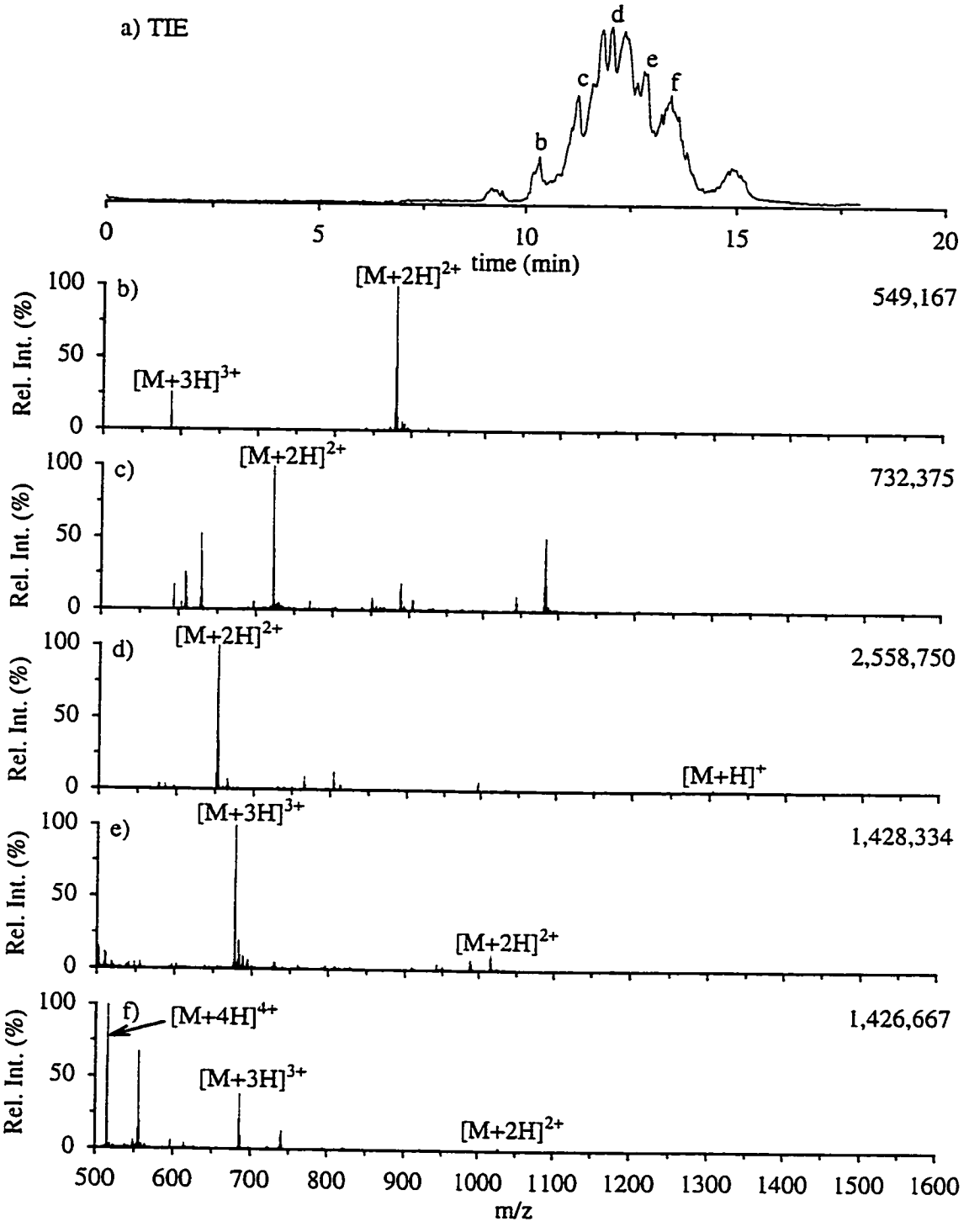

Figure 5.18 Analysis of the tryptic digest of the lectin *Glycine max* at the 22 ng/μL level using PC-CZE-nESMS. Condtions as for Figure 4.3. Sample injection at 1000 mbar for 7 min. Letters on the peaks in the TIE correspond to the extracted mass spectra shown in (b)-(f), respectively.

The optimized conditions for on-line preconcentration with nanoelectrospray MS detection were used for the analysis of the tryptic digest of the lectin from *Glycine max*. The total ion electropherogram (TIE) for the injection of 7 μL containing 22 ng/μL of original protein (Figure 5.18) is similar to the CZE-nESMS analysis with a partial loss of resolution. This represents the analysis of approximately 5 picomoles (0.15 ng) or 700 fmol/μL of protein. Mass spectra (Figure 5.18b-f) were extracted from several peaks in the TIE. These spectra show an excellent signal to noise ratio and indicate that the analysis could readily be carried out on a more dilute solution.

The average masses of the tryptic peptides were calculated from the mass spectra shown in Figure 5.19. These values were entered into a protein database searching program (PeptideMap™, PE-SCIEX) [66,74,75] as shown in Figure 5.19. The program was able to exclusively identify the protein from a database of ~32000 proteins based on the data obtained from the analysis of a solution containing approximately 700 fmol/μL of protein digest. This analysis was carried out well above the detection limit of the technique which can be further improved if necessary by increasing the injection volume. These data are of sufficient quality for reliable database searching. In cases where an unknown protein is encountered, tandem mass spectrometry could be used to obtain sequence data for more rigorous database searching [123].

The use of PC-CZE-nESMS for the analysis of glycoproteins is expected to be enhanced by the use of an affinity-based stationary phase. The use of immobilized lectins for the purification of glycoproteins is a well established technique [124-127], and extension of this method to PC-CZE should provide unparalleled specificity and sensitivity for the structural analysis of these molecules.

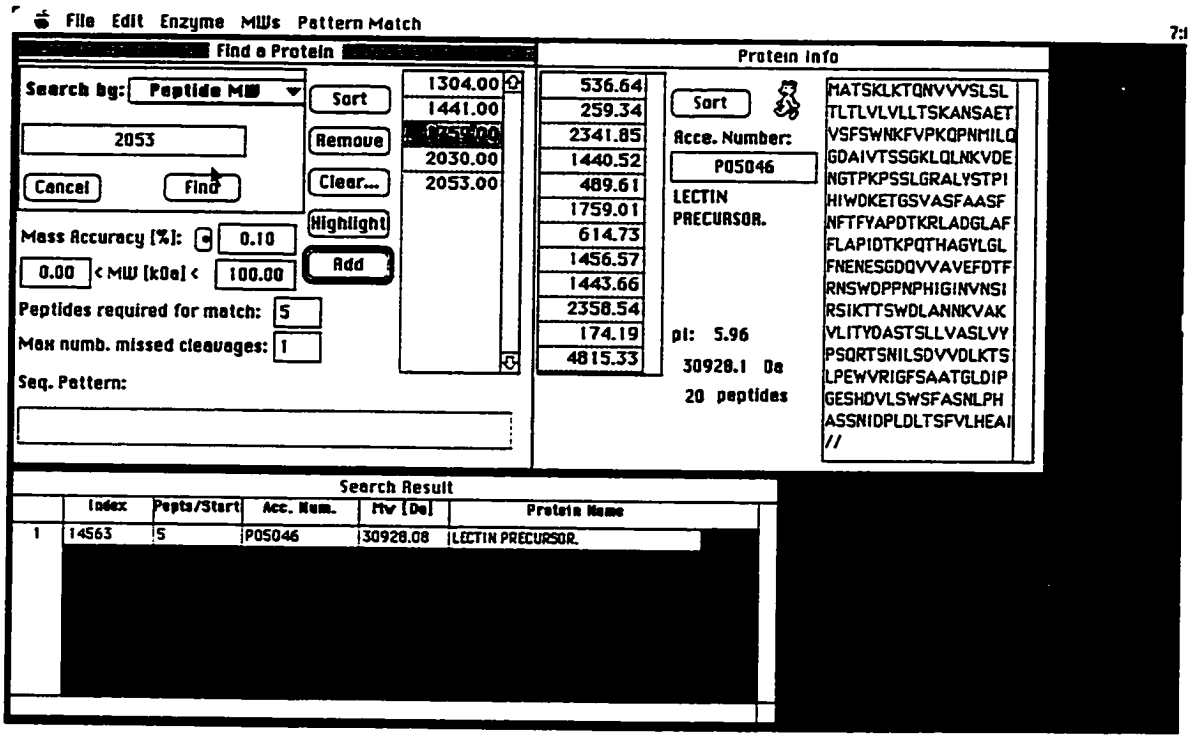

Figure 5.19 Protein database search results using peptide masses extracted from tryptic digest of the lectin *Glycine max*.

5.6 Conclusions

The application of CZE to the analysis of complex mixtures resulting from enzymatic and chemical digests of glycoproteins has been demonstrated. The use of BCQ-modified capillaries with dilute formic acid electrolyte provides high resolution of glycopeptides while maintaining compatibility with MS detection. The use of CZE combined with nanoelectrospray mass spectrometry enabled identification of glycopeptides using low picomole injections of original protein digests. Stepped-orifice voltage scanning methods and precursor ion scanning generated ions that are specific for the carbohydrate moieties of interest. These techniques facilitate the location of the glycopeptides in the CZE-nESMS analysis of proteolytic digests.

The combination of CZE with online tandem mass spectrometry generated structural information restricted to the oligosaccharides appended to the peptide backbone. By promoting the formation of first generation fragment ions in the orifice/skimmer region, peptide sequence analysis could be obtained by conducting tandem mass spectrometric experiments on the fragment ion corresponding to [peptide+GlcNAc]. The combination of these experiments enabled characterization of both carbohydrate and peptide structures. Identification of glycopeptides and characterization of site heterogeneity were described for a number of N-linked and O-linked glycoproteins and provided valuable structural information using low picomole sample loadings.

Further sensitivity for the analysis of protein digests was demonstrated using PC-CZE-nESMS. This method permitted the analysis of a protein digest at the fmol/μL level, generating data of sufficient quality for reliable database searching. Glycoprotein analysis using PC-CZE-nESMS is expected to be enhanced through the use of an affinity-based stationary phase, such as an immobilzed lectin. These techniques should provide a

powerful tool for the structural analysis of glycoproteins, particularly in instances where sample availability is limited.

Chapter 6

6.0 Summary

The utility of capillary zone electrophoresis-electrospray mass spectrometry as a tool for the analysis of biomolecules, especially proteins and glycoproteins, has been limited due to the technique's inherently poor concentration detection limits. The development of a nanoelectrospray interface and a chromatographic preconcentration technique for CZE described in this work permits the analysis of these molecules at concentration levels well below standard CZE-UV and CZE-ESMS detection limits. The analysis of glycoproteins using the nanoelectrospray interface permitted the development of novel scanning methods for the identification of glycopeptides and their structures at the femtomole level.

The nanoelectrospray interface uses tapered and metallized tips that are butted to the separation capillary. This interface was fully optimized with respect to tip geometry and capillary coating. Control of the tip i.d. was crucial to the stable operation of the interface as well as to the flowrate generated by the separation. The novel coating agent developed

for this work prevented loss of analyte on the fused silica surface while providing a compatible eof for stable nanoelectrospray and enhanced separations relative to previously described coating agents.

Future developments of the nanoelectrospray interface would involve the development of an interface that does not rely on metallized tips. Such an interface would reduce the time and effort involved in constructing the interface. One possible method would be to use a conductive ferrule in the butt connector. Voltage applied to the metal body of the connector would then reach the liquid at the junction of the tip and the capillary. This liquid junction would serve to complete the electrophoretic circuit as well as permit the application of electrospray voltage.

The characterization of chromatographic preconcentration for CZE revealed both strengths and weaknesses for this technique. This method was optimized with respect to stationary phase and elution protocol. Large volumes of elution solvent degraded the separation to an unacceptable level, and smaller volumes did not allow for complete recovery of the trapped sample. This fact was used as an advantage, and a "single-injection/multiple-elution" protocol was developed for the analysis of a single injection of sample. The preconcentrator on-line with the nanoelectrospray interface permitted the routine analysis of peptides from a protein digest at the fmol/μL level. Such data were of sufficient quality for database searching of protein libraries.

An exciting potential development of the preconcentration technique is the use of affinity-based phases for the selective enrichment of analytes. This would involve the development of separation conditions that are compatible with such a phase as well as with mass spectrometric detection, and will no doubt be a challenge. One such application would be the use of immobilized lectins for the selective enrichment of partially glycosylated peptides from digests of glycoproteins.

The use of CZE for the analysis of glycoprotein digests provided resolution of protein glycoforms not typically available with HPLC. This resolution, in conjunction with the sensitivity provided by the nanoelectrospray interface provided information on the distribution of these N-linked glycoforms. Low levels of partially glycosylated peptide were identified in the presence of non-glycosylated peptides for the O-linked glycoprotein studied. The pitfalls of mixed scanning to selectively identify glycopeptides were addressed through the use of multiple oxonium ion monitoring to eliminate the possibility of falsely identifying a peptide as a glycopeptide. Tandem mass spectrometry was used to provide structural information on the oligosaccharide appended to the peptide backbone. More significantly, tandem mass spectrometry of ions generated by collisional induced dissociation in the orifice/skimmer region of the mass spectrometer provided peptide sequence ions not usually obtained with the low energy collisions typical for triple quadrupole mass spectrometers. These methods were applied to both N- and O-linked glycoproteins.

Further study of O-linked glycopeptides may lead to the development of conditions that permit the unequivocal identification of the site of carbohydrate attachment. Under the conditions used, the labile nature of the peptide (Ser or Thr) to carbohydrate linkage does not produce fragment ions with this bond intact. Careful control of the collision energy may generate such ions in favorable cases. Chemical cleavage or endogylcanases that remove O-linked oligosaccharides while producing glycosylation site tags could also be used to determine linkage sites. The study of glycoproteins using the preconcentrator with an immobilized lectin, as mentioned above, is also an interesting prospect.

REFERENCES

1 J.W. Jorgenson and K.D. Lukas, *Anal. Chem.*, 53 (1981) 1298.

2 D.R. Salomon and J. Romano, *J. Chromatogr.*, 602 (1992) 219.

3 K.A. Hargadon and B.R. McCord, *J. Chromatogr.*, 602 (1992) 241.

4 V.C. Trenerry, R.J. Wells and J. Robertson, *J. Chromatogr. Sci.*, 32 (1994) 1.

5 B.F. Kenney, *J. Chromatogr.*, 546 (1991) 423.

6 R.M. McCormick, *Anal. Chem.*, 60 (1988) 2322.

7 D.N. Heiger, A.S. Cohen and B.L. Karger, *J. Chromatogr.*, 516 (1990) 33.

8 A.E. Vorndran, P.J. Oefner, H. Scherz and G.K. Bonn, *Chromatographia*, 33 (1992) 163.

9 N. Matsubara and S. Terabe, *J. Chromatogr.*, 680 (1994) 311.

10 P. Thibault, S. Pleasance and M.V. Laycock, *J. Chromatogr.*, 542 (1991) 483.

11 J. Romano, P. Jandik, W.R. Jones and P.E. Jackson, *J. Chromatogr.*, 546 (1991) 411.

12 G. Schomburg, D. Belder, M. Gilges and S. Motsch, *J. Cap. Elec.*, 1 (1994) 219.

13 J.R. Mazzeo and I.S. Krull, *BioTechniques*, 10 (1991) 638.

14 K.P. Bateman, P. Thibault, D.J. Douglas and R.L. White, *J. Chromatogr.*, 712 (1995) 253-268.

15 K.A. Cobb, V. Dolnik and M. Novotny, *J. Chromatogr.*, 62 (1990) 2478.

16 K.P. Bateman, R.L. White, M. Yaguchi and P. Thibault, *J. Chromatogr.*, submitted for publication.

17 K.P. Bateman, S.J. Locke and D.A. Volmer, *J. Mass Spectrom.*, 32 (1997) 297.

18 T. Tsuda, J.V. Sweedler and R.N. Zare, *Anal. Chem.*, 62 (1990) 2149.

19 G.J.M. Bruin, G. Stegeman, A.C. Van Asten, X. Xu, J.C. Kraak and H. Poppe, *J. Chromatogr.*, 559 (1991) 163.

20 X. Xi and E.S. Yeung, *Appl. Spectrosc.*, 45 (1991) 1199.

21 L. Hernandez, J. Escalona, N. Joshi and N. Guzman, *J. Chromatogr.*, 559 (1991) 183.

22 X.C. Huang, M.A. Quesada and R.A. Mathies, *Anal. Chem.*, 64 (1992) 967.

23 Y.F. Cheng and N.J. Dovichi, *Science*, 242 (1988) 562.

24 S. Wu and N.J. Dovichi, J. *Chromatogr.*, 481 (1989) 141.

25 Y.F. Cheng, S. Wu, D.Y. Chen and N.J. Dovichi, *Anal. Chem.*, 62 (1990) 496.

26 Y.H. Lee, R.G. Maus, B.W. Smith and J.D. Winefordner, *Anal. Chem.*, 66 (1994) 4142.

27 B.B. Haab and R.A. Mathies, *Anal. Chem.*, 67 (1995) 3253.

28 M. Yu and N.J. Dovichi, *Anal. Chem.*, 61 (1989) 37.

29 K.C. Waldron and N.J. Dovichi, *Anal. Chem.*, 64 (1992) 1396.

30 R.D. Smith, J.A. Olivares, N.T. Nguyen and H.R. Udseth, *Anal. Chem.*, 60 (1988) 436.

31 R.D. Smith, H.R. Udseth, J.H. Wahl, D.R. Goodlett and S.A. Hofstadler, *Methods Enzymol.*, 271 (1996) 448.

32 K.P. Bateman, R.L. White and P. Thibault, *Rapid Commun. Mass Spectrom.*, 11 (1997) 307.

33 J.F. Kelly, L. Ramaley and P. Thibault, *Anal. Chem.*, 67 (1997) 51.

34 D. Figeys, I. van Oostveen, A. Ducret and R. Aebersold, *Anal. Chem.*, 68 (1996) 1822.

35 M.S. Kriger, K.D. Cook and R.S. Ramsey, *Anal. Chem.*, 67 (1995) 385.

36 R.L. Chien and D.S. Burgi, *Anal. Chem.*, 64 (1992) 1046.

37 D.S. Burgi and R.L. Chien, *Anal. Chem.*, 63 (1991) 2042.

38 R.L. Chien and D.S. Burgi, *Anal. Chem.*, 64 (1992) 489A.

39 M. Mazereeuw, U.R. Tjaden and N.J. Reinhoud, *J. Chromatogr. Sc.*, 33 (1995) 686.

40 A.J. Tomlinson, N.A. Guzman and S. Naylor, *J. Cap. Elect.*, 6 (1995) 247.

41 A.J. Tomlinson and S. Naylor, *J. Cap. Elect.*, 5 (1995) 225.

42 M.A. Strausbauch, J.P. Landers and P.J. Wettstein, *Anal. Chem.*, 68 (1996) 306.

43 A.J. Tomlinson, L.M. Benson, S. Jameson, D.H. Johnson and S. Naylor, *J. Am. Soc. Mass Spectrom.*, 8 (1997) 15.

44 D. Figeys, A. Ducret and R. Aebersold, *J. Chromatogr.*, 763 (1997) 295.

45 H.E. Duckworth, R.C. Barber and V.S. Venkatasubramanian, *Mass Spectrometry second edition*, Cambridge University Press, New York (1990) 124-126.

46 C.M. Whitehouse, R.N. Dreyer, M. Yamashita and J.B. Fenn, *Anal. Chem.*, 57 (1985) 675.

47 A.P. Bruins, T.R. Covey and J.D. Henion, *Anal. Chem.*, 59 (1987) 2642.

48 J.B. Fenn, M. Mann, C.K. Meng, S.F. Wong and C.M. Whitehouse, *Science*, 246 (1989) 64.

49 A.P. Bruins, *Mass Spectrom. Rev.*, 10 (1991) 53.

50 J.V. Iribarne and B.A. Thomson, *J. Chem. Phys.*, 71 (1979) 4451.

51 P. Kebarle and L. Tang, *Anal. Chem.*, 65 (1993) 972A.

52 G. Siuzdak, *Proc. Natl. Acad. Sci.*, 91 (1994) 11290.

53 M.S. Wilm and M. Mann, *Int. J. Mass.Spectrom. Ion Processes*, 136 (1994) 167.

54 G.A. Valaskovic, N.L. Kelleher, D.P. Little, D.J. Aaserud and F.W. McLafferty, *Anal. Chem.*, 67 (1995) 3802.

55 M. Wilm and M. Mann, *Anal. Chem.*, 68 (1996) 1.

56 A. Shevchenko, M. Wilm, O. Vorm and M. Mann, *Anal. Chem.*, 68 (1996) 850.

57 M. Wilm, A. Shevchenko, T. Houthaeve, S. Breit, L. Schweigerer, T. Fotsis and M. Mann, *Nature*, 379 (1996) 466.

58 S. Pleasance, P. Thibault and J. Kelly, *J. Chromatogr.*, 591 (1992) 325.

59 E.D. Lee, W. Muck, J.D. Henion and T.R. Covey, *Biomed. Environ. Mass Spectrom.*, 18 (1989) 844.

60 I.M. Johansson, E.C. Huang, J.D. Henion and J. Zweigenbaum, *J. Chromatogr.*, 544 (1991) 311.

61 F. Garcia and J.D. Henion, *Anal. Chem.*, 64 (1992) 985.

62 J.H. Wahl, D.C. Gale and R.D. Smith, *J. Chromatogr.*, 659 (1994) 217.

63 R.S. Ramsey and S.A. McLuckey, *J. Microcol. Sep.*, 7 (1995) 461.

64 J.C. Severs, A.C. Harms and R.D. Smith, *Rapid Commun. Mass Spectrom.*, 10 (1996) 1175.

65 D.F. Hunt, J.R. Yates III, J. Shabanowitz, S. Winston and C.R. Hauer, *Proc. Natl. Acad. Sci. USA*, 83 (1986) 6233.

66 M. Mann and M. Wilm, *Anal. Chem.*, 66 (1994) 4390.

67 J.K. Eng, A.L. McCormack and J.R. Yates III, *J. Am. Soc. Mass Spectrom.*, 5 (1994) 976.

68 J.R. Yates III, J.K. Eng, A.L. McCormack and D. Schieltz, *Anal. Chem.*, 67 (1995) 1426.

69 M. Mann, P. Højrup and P. Roepstorff, *Biol. Mass Spectrom.*, 22 (1993) 338.

70 W.J. Henzel, T.M. Billeci, J.T. Stults and S.C. Wong, *Proc. Natl. Acad. Sci. USA*, 90 (1993) 5011.

71 D.J.C. Pappin, P. Højrup and A.J. Bleasby, *Curr. Biol.*, 3 (1993) 327.

72 P. James, M. Quadroni, E. Carafoli and G. Gonnet, *Biochem. Biophys. Res. Commun.*, 195 (1993) 58.

73 J.R. Yates III, S. Speicher, P.R. Griffin and T. Huntkapiller, *Anal. Biochem.*, 214 (1993) 397.

74 R. Bonner and B. Shushan, *Rapid Commun. Mass Spectrom.*, 9 (1995) 1067.

75 R. Bonner and B. Shushan, *Rapid Commun. Mass Spectrom.*, 9 (1995) 1077.

76 R.A. Dwek, *Chem. Rev.*, 96 (1996) 683.

77 R.B. Parekh, A.G.D. Tse, R.A. Dwek, A.F. Williams and T.W. Rademacher, *EMBO J.*, 6 (1987) 1233.

78 C.F. Goochee, M.J. Gramer, D.C. Andersen, J.B. Bahr and J.R. Rasmussen, in P. Todd, K. Sikdar and M. Bier (Eds.) Frontiers in Bioprocessing II, American Chemical Society, Washington DC, 1992, pp. 199-240.

79 R. Kornfeld and S. Kornfeld, *Ann. Rev. Biochem.*, 54 (1985) 631.

80 H.A. Kaplan, J.K. Welply and W.J. Lennarz, *Biochim. Biophys. Acta*, 906 (1987) 161.

81 R.D. Marshall, *Biochem. Soc. Symp.*, 40 (1974) 17.

82 Y. Gavel and G. von Heijne, *Protein Eng.*, 3 (1990) 433.

83 S.H. Shakin-Eshleman, S.L. Spitalnik and L. Kasturi, *J. Biol. Chem.*, 271 (1996) 6363.

84 K. Nehrke, F.K. Hagen and L.A. Tabak, *J. Biol. Chem.*, 271 (1996) 7061.

85 Volume 230 of Methods in Enzymology is dedicated to techniques in Glycobiology.

86 V.N. Reinhold, B.B. Reinhold and S. Chan, *Methods Enzymol.*, 271 (1996) 377.

87 W.J. Richter, D.R. Müller and B. Domon, *Methods Enzymol.*, 193 (1990) 607.

88 R.B. Parekh, *Methods Enzymol.*, 230 (1994) 340.

89 S.A. Carr, J.R. Barr, G.D. Roberts, K.R. Anumula and P.B. Taylor, *Methods Enzymol.*, 193 (1990) 501.

90 M.J. Huddleston, M.F. Bean and S.A. Carr, *Anal. Chem.*, 65 (1993) 877.

91 S.A. Carr, M.J. Huddleston and M.F. Bean, *Protein Sci.*, 2 (1993) 183.

92 J.F. Kelly, S.J. Locke, L. Ramaley and P. Thibault, *J. Chromatogr. A*, 720 (1996) 409.

93 C.A. Zittle and J.H. Custer, *J. Dairy Sci.*, 46 (1963) 1183.

94 M.A. Moseley, L.J. Deterding, K.B. Tomer and J.W. Jorgenson, *Anal. Chem.*, 63 (1991) 109.

95 J.E. Wiktorowicz and J.C. Colburn, *Electrophoresis*, 11 (1990) 769.

96 J.H. Beattie, R. Self and M.P. Richards, *Electrophoresis*, 16 (1995) 322.

97 M.E. Swartz and M.J. Merion, *J. Chromatogr.*, 632 (1993) 209.

98 M.A. Strausbauch, B.J. Madden, P.J. Wettstein and J.P. Landers, *Electrophoresis*, 16 (1995) 541.

99 G. Hopfgartner, K. Bean, J. Henion and R. Henry, *J. Chromatogr.*, 647 (1993) 51.

100 R.M. McCormick, *Anal. Chem.*, 60 (1988) 2322.

101 X.W. Yao, D. Wu and F.E. Regnier, *J. Chromatogr.*, 636 (1993) 21.

102 D.R. Goodlett, J.H. Wahl, H.R. Udseth and R.D. Smith, *J. Microcol. Sep.*, 5 (1993) 57.

103 J.R. Perkins and K.B. Tomer, *Anal. Chem.*, 66 (1994) 2835.

104 A.J. Tomlinson, L.M. Benson, N.A. Guzman and S. Naylor, *J. Chromatogr.*, 744 (1996) 3.

105 M.A. Strausbauch, J.P. Landers and P.J. Wettstein, *Anal. Chem.*, 68 (1996) 306.

106 A.J. Tomlinson, L.M. Benson, S. Naylor, *LC•GC*, 12 (1994) 122.

107 H. Lis and N. Sharon, *Annu. Rev. Biochem.*, 55 (1986) 35.

108 I.E. Liener, N. Sharon and I. Goldstein, eds., *The Lectins: Properties, Functions and Applications in Biology and Medicine*, Academic Press, Orlando, FL, 1986.

109 D.A. Ashford, R.A. Dwek, T.W. Rademacher, H. Lis and N. Sharon, *Carbohyd. Res.*, 213 (1991) 215.

110 N.M. Young, D.C. Watson, M. Yaguchi, R. Adars, R. Arango, E. Rodriguez-Arango, N. Sharon, P.K.S. Blay and P. Thibault, *J. Biol. Chem.*, 270 (1995) 2563.

111 L.M. Hoffman and D.D. Donaldson, *EMBO J.*, 4 (1985) 883.

112 L. Dorland, H. van Halbeek, J.F.G. Vliegenthart, H. Lis and N. Sharon, J. *Biol. Chem.*, 256 (1981) 7708.

113 A.J. Kalb, *Biochim. Biophys. Acta*, 168 (1968) 532.

114 S. Blumberg, J. Hildesherim, J. Yariv and K.J. Wilson, *Biochim. Biophys. Acta*, 264 (1972) 171.

115 Y. Konami, K. Yamamoto and T. Osawa, *FEBS Letts.*, 268 (1990) 281.

116 M. Wilm, G. Neubauer and M. Mann, *Anal. Chem.*, 68 (1996) 527.

117 J.J. Conboy and J.D. Henion, *J. Am. Soc. Mass Spectrom.*, 3 (1992) 804.

118 J. Liu, K.J. Volk, E.H. Kerns, S.E. Klohr, M.S. Lee and I.E. Rosenberg, *J. Chromatogr.*, 632 (1993) 45.

119 A.A. Gooley, B.J. Classon, R. Marschalek and K.L. Williams, Biochem. *Biophys. Res. Commun.*, 178 (1991) 1194.

120 A. Pisano, N.H. Packer, J.W. Redmond, K.L. Williams and A.A. Gooley, *Glycobiology*, 4 (1994) 837.

121 A.L. Burlingame, *Curr. Opin. Biotech.*, 7 (1996) 4.

122 S.C. Hall, D.M. Smith, K.R. Clauser, L.E. Andrews, F.C. Walls, J.W. Webb, H.M. Tran, L.B. Epstein and A.L. Burlingame, in *Mass Spectrometry in the Biological Sciences*, A.L. Burlingame and S.A. Carr, eds., Humana Press, Totowa, NJ, (1996) 171.

123 A.L. McCormack, D.M. Schieltz, B. Goode, S. Yang, G. Barnes, D. Drubin and J.R. Yates III, *Anal. Chem.*, 69 (1997) 767.

124 R.D. Cummings, *Methods. Enzymol.*, 230 (1994) 66.

125 I. West and O. Goldring, *Appl. Biochem. Biotech. B: Mol. Biotech.*, 2 (1994) 147.

126 K. Yamamoto, T. Tsuji and T. Osawa, *Appl. Biochem. Biotech. B: Mol. Biotech.*, 3 (1995) 25.

127 A. Kobata, *Biochem. Soc. Trans.*, 22 (1994) 360.

IMAGE EVALUATION TEST TARGET (QA-3)

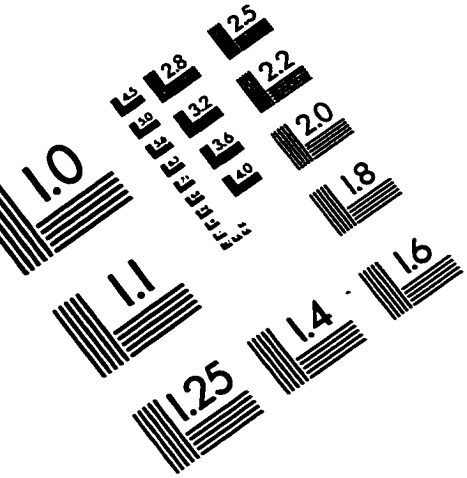

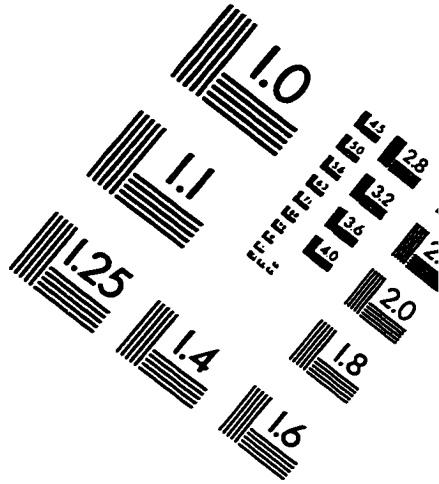

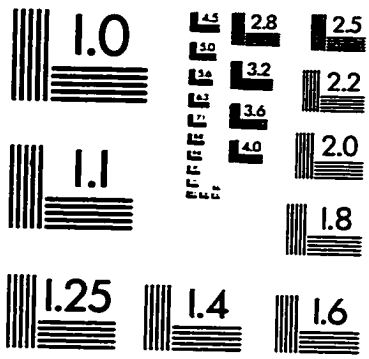

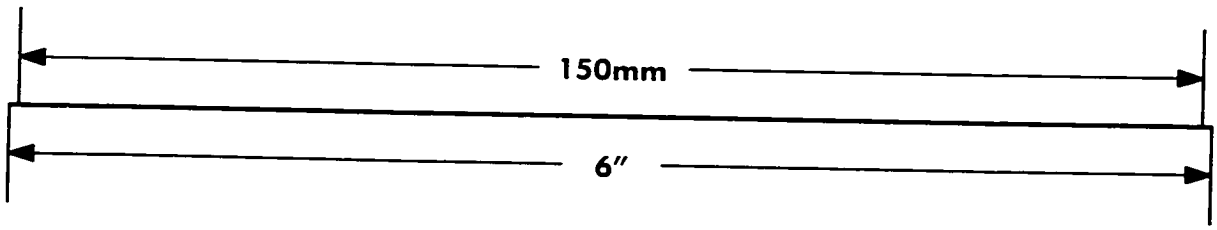

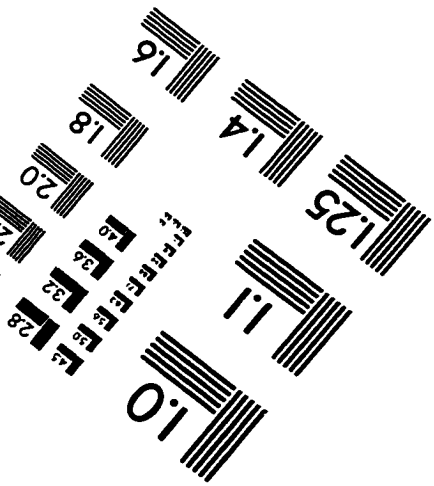

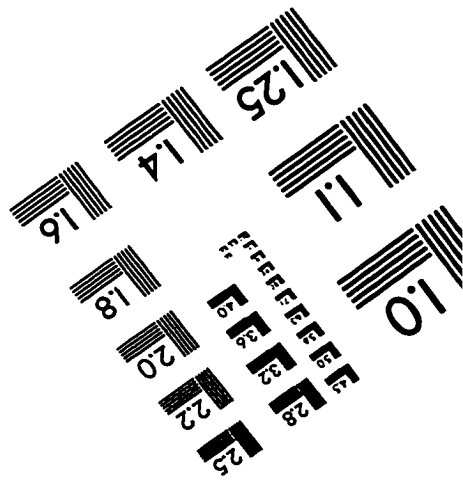

APPLIED IMAGE, Inc
1653 East Main Street
Rochester, NY 14609 USA
Phone: 716/482-0300
Fax: 716/288-5989